1998-10-01

The Development and Characterisation of a Red-sensitised Photopolymer Holographic Recording Material

Clodagh Feely
Technological University Dublin

THE DEVELOPMENT AND CHARACTERISATION OF A RED-SENSITISED PHOTOPOLYMER HOLOGRAPHIC RECORDING MATERIAL.

by

Clodagh A. Feely B.Sc. (App. Sc.)

A thesis submitted for the degree of Doctor of Philosophy

to the Department of Pure and Applied Physics

University of Dublin

School of Physics,

Dublin Institute of Technology

October 1998

Declaration

- This thesis has not been submitted as an exercise for a degree at any other university.
- Apart from the assistance mentioned in the acknowledgements, the work is entirely my own.
- I agree that Trinity College Library may lend or copy this thesis upon request.

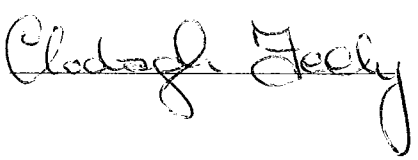

Acknowledgements

I would like to take this opportunity to mention a number of people who have helped me in many different ways towards the submission of this work.

I would like to thank my supervisor, Dr. Vincent Toal for his continual advice and encouragement throughout the time it has taken me to finish this thesis.

Particular thanks are due to Dr. Suzanne Martin who not only helped me to make sense of it all but has also lent me a shoulder many times in the last couple of years. Thanks to Dr. Sean Sheridan for his assistance with all things Laplacian and to Dr. Hugh Byrne for burning the midnight oil in the Raman Spectroscopy lab.

There are a number of people in Trinity College whom I would like to acknowledge. I would like to thank Prof. Werner Blau for welcoming me into his research group. I would also like to thank Dr. Andy Davey, Prof. Vincent Mc Brierty and Dr. John O'Brien for their advice and practical help with the work involving NMR. Thanks also to Dr. Fiona Coyle and Dr. Miriam Mc Carthy.

I would also like to specially thank all the Kevin Street gang:
The postgraduates, past and present, particularly those in my own research group for the happy times divided between the canteen, Whelans and Devitts. Sergio for reading the thesis for me, I just know he enjoyed it and the staff of the Schools of Physics and Chemistry for their practical help and advice.

Professor Antonio Fimia and his research group in Alicante University, Spain merit a special mention for allowing me the opportunity to study with them in their holographic laboratories. Thanks are also due to Mairead Connolly for being solely responsible for my career choice, many years ago.

These acknowledgements would not be complete without mentioning my collective source of constant support and encouragement: Mam and Dad, Fionnuala, Declan, Mercedes and Breege.

Finally, true to tradition I've saved *my* best 'til last; thank you to Stephen for just about everything.

Contents

For my Mam and Dad

The development and characterisation of a red-sensitised photopolymer holographic recording material.

by

Clodagh A. Feely

Abstract

The development and characterisation of a photopolymerisable photopolymer holographic recording material, for red sensitisation is described. The material comprises dye (methylene blue), an electron donor (triethanolamine) and monomer (acrylamide and methylene-bis-acrylamide). A binder is also included (poly(vinylalcohol) to allow recording in dry layer format. One of the main advantages of the material is its ability to self-develop, which makes it highly suitable for a range of applications which includes the fabrication of Holographic Optical Elements (HOEs).

The optimisation of the material formula for red-sensitisation using holographic techniques is described. Diffraction efficiencies of over 70% were obtained in 25 seconds with the optimised material. Sensitivity was improved considerably from approx. 650mJ/cm^2 at the start of the optimisation study to approx. 130mJ/cm^2. The chemical characterisation of the material was conducted using spectroscopic techniques. Results have shown that no chemical interaction occurs between the material components prior to exposure at the desired wavelength. The holographic characterisation was also described in terms of optimum layer thickness, beam intensity and ratio and spatial frequency response, for efficient recording.

Some of the physical processes that occur during holographic recording were investigated. Through the study of amplitude gratings recorded in the material and the application of a mathematical model, it has been proven that the diffusion of dye molecules is the main contributing factor leading to the decay of this type of grating. The dependence of the rate of diffusion of dye on the molecular weight of the binder has also been demonstrated. This has lead to ideas on how to improve the spatial frequency response of the material.

Aspects of the material's physical and holographic recording characteristics, which are relevant to the recording of HOEs as well as practical limitations of elements recorded in this material, are discussed. It is shown that the material can tolerate a slant angle of up to 40^0 without significant loss of diffraction efficiency. The results obtained for on and off-axis focusing elements are presented as well as some work on stacked elements.

Summary

Chapter 1 begins by introducing some of the different types of photopolymerisable photopolymer recording materials, which have been developed. Both liquid and dry layer formats are discussed, along with some of the commercially available materials. The material, which is described in this thesis and its associated photochemical processes, are also introduced.

Chapter 2 examines the chemical structures and properties of each of the material components. Spectroscopic techniques are employed to analyse the material and to ensure that no chemical interaction occurs between the components prior to exposure at the desired wavelength.

Chapter 3 introduces the fundamentals of holographic recording. The optimisation of the material formula is described. The characterisation of the material is also described in terms of optimum layer thickness, recording beam intensity and ratio and spatial frequency. Kogelnik's coupled wave theory is used to calculate typical refractive index modulation values for gratings recorded under various experimental conditions.

Chapter 4 is a more detailed study of the physical processes that occur within the material during holographic recording. A mathematical model is formulated to study diffusion of dye in transient amplitude gratings. It is shown that diffusion of dye is the main contributor to the transient nature of these gratings under normal conditions. The influence of the physical properties of the binder on the rate of diffusion of dye molecules is also discussed here.

Chapter 5 describes the practical application of the material to the recording of Holographic Optical Elements (HOEs). The advantages and limitations of the material are discussed with relevance to this application. The results obtained for the recording of on and off-axis focussing HOEs and stacked on-axis HOEs are reported.

Chapter 6 presents a discussion of the main conclusions of the thesis.

1. Photopolymer recording materials: a brief history.

1.1 Holography

When Denis Gabor[1] presented "a new microscopic principle" in *Nature* (May, 1948), the imaging world suddenly became three-dimensional. He called the new principle "holography", indicating that a "whole" image could be recorded. After its initial discovery, the lack of a coherent light source restricted the work conducted on holography until July 1960, when an equally historic discovery was presented. Theodore Maiman [2] announced the discovery of "stimulated optical radiation in ruby masers" which marked the advent of coherent light emission and a long-awaited source for holographic recording. The era of holography started in earnest in the early 1960s when Leith and Upatneiks[3-5] published a series of reports demonstrating that holography had practical use with the laser playing an essential role.

Since those early years, the use of holography has become interdisciplinary and has been explored for a wide range of applications. The diversity of these applications includes the use of holographic non-destructive testing techniques [6,7] in the engineering field. The study of polymer aging[8], optical information processing[9] are other successful exploitations of holography. The production of holographic optical elements (HOEs)[10-12] for various applications is becoming increasingly popular as the

advantages of these devices become more apparent. The advantages of HOEs will be discussed in greater detail in Chapter 5.

1.2 Suitable materials

The most widely used materials for holographic recording in the past have been silver halide[13] and dichromated gelatin[14] but one of the most limiting properties of these materials was the need for wet chemical post-processing. For applications such as holographic interferometry, which involves the exact superposition of two wavefronts, this was a severe limitation. It meant that the first hologram had to be processed and replaced *exactly* in the same position. Any shrinkage or deformation from the processing of the hologram introduced spurious fringes at best.

For another application of holography, the fabrication of holographic optical elements, (HOEs) high angular selectivity[15] of the recording material is a pre-requisite. Volume materials have an intrinsically high angular selectivity, which make them ideal for this application. (The properties of volume materials are discussed in Chapter 3).

For the wide and diverse range of applications to which holography seemed suitable, it became clear that some flexibility was required from recording media. The

development of self-processing recording materials was a logical progression to allow holographic applications to be fully exploited.

Many varieties of holographic recording materials[16-23], have been developed throughout the years, each with its own unique characteristics. However since the focus of this thesis is a photopolymerisable photopolymer material, the discussion that follows will be limited to such. In order to convey the variety of this particular type of photopolymer material that has been developed, some liquid and dry systems will be discussed.

1.3 Introduction to photopolymers

Photopolymers can be generally classed as liquid or dry chemical compositions, the difference being the inclusion of a polymer binder for dry layer format. Photopolymerisable photopolymers are a subset of photopolymer materials. Other subsets include photocrosslinking materials that react to incident light by making or breaking a polymer bond and absorption materials, which comprise dye in a polymer binder. The photopolymerisable systems described here usually comprise a photosensitiser (usually a dye), an electron donor (to produce free radicals), and monomer, the binder being optional. When a photopolymer is exposed to light of the appropriate wavelength, the sensitiser and electron donor react to form free radicals, which initiate a polymerisation process. Given the correct recording conditions, this

polymerisation can ultimately lead to the recording of a hologram. A detailed description of the photochemical processes the material studied in this thesis undergoes, is given later. Holographic recording is described in Chapter 3.

Before commencing with the next section, some of the terms used need to be briefly explained. *Diffraction efficiency* is the efficiency with which a hologram will diffract light. *Exposure energy* is the energy needed to record a hologram and depends on the recording power and the recording time. *Sensitivity* is related to both the diffraction efficiency and exposure energy of a hologram and high sensitivity is usual desirable in holography. More precise definitions of these terms can be found in Chapter 3.

1.3.1 Liquid photopolymers

Layers comprising liquid photopolymer material are usually fabricated by enclosing the liquid between two transparent substrates that are uniformly separated by metal foil (which is commercially available in a variety of thickness). These types of material are self-developing but can be messy to prepare and handle. Some of the liquid photopolymer systems that have been investigated are described below.

Dye-sensitised photopolymerisation reactions have been investigated for a number of years, from as early as the 1950s. The most prominent of those investigators were Oster and Oster[24-26], who in 1962 in conjunction with a group of scientists from the

Hughes Research Laboratories[27] showed that a dye-sensitised acrylamide system could be used to record ruby laser pulses as "buttons" of polymer gel.

From these initial studies, a photopolymer system based on the monomer, barium acrylate, was later refined and investigated by Close[28] (1969). The material was sensitised by methylene blue and sodium salts of *p*-toluene sulfinic acid and nitrophenyl acetic acid as photocatalysts for recording at 694nm with a ruby laser. The exposure energy needed for 45% diffraction efficiency was approximately 300mJ/cm^2. The holograms were fixed by 30 seconds of exposure to a 200W mercury arc lamp, which bleached any remaining dye. However, the scattering produced by the polymer particles in the liquid reduced the signal to noise ratio. The material had a short shelf-life but became the first commercially available photopolymer holographic recording material, manufactured by Newport Research Corporation.

Further work on this system was carried out by Jenney (1970)[29] who discovered that the inclusion of acrylamide with the acrylate monomers improved hologram sensitivity. This combination of monomers also reduced the scattering noise. Sensitivities as high as 0.6mJ/cm^2 were reported for Helium-Neon laser light but the maximum attainable diffraction efficiencies remained low at approximately 35%. The actual mechanism by which holograms were stored in the medium was also discussed with experimental evidence of surface height modulation in low spatial frequency gratings.

Van Renesse (1972)[30] reported improvements to this acrylamide system by the inclusion of N,N-methylene-bis-acrylamide which served as a crosslinker to the main polymer network. In this way more stable holograms were recorded. However, the drawbacks of this system included lack of adhesion to the substrate and surface crystallisation of chemicals on the layers.

Sugawara et al (1975)[31] also worked on an acrylamide/bisacrylamide only system using t-butyl hydrogen peroxide as the electron donor and ferric ammonium citrate for sensitisation in the green region of the visible spectrum. Their reasoning for working on this specific system was that holograms recorded in acrylic-based materials degraded rapidly and exhibited low diffraction efficiency (45%). The system Sugawara used yielded holograms with 80% diffraction efficiency with a sensitivity of 20mJ/cm^2.

More recently, Lougnot and Turck[32,33] (1992) have reported a liquid system based on a multifunctional acrylate monomer, an amine electron donor and different xanthene dyes for sensitisation. Using different combinations of additives[34] (1993) holograms, which exhibited diffraction efficiencies as high as 86%, were reported, for exposure energies of typically 150mJ/cm^2. Holograms recorded using this system did not lose diffraction efficiency over a period of 12 months.

Fimia[35-37] (1993, 1995, 1997) et al have published work on applications for both liquid and dry layer systems having red and green sensitisation. One of the most interesting is a paper[38], (1993) which is concerned with the elimination of *inhibition time* for liquid layer exposure. Inhibition time is the time it takes inhibiting species, such as oxygen, in the system to react after which free-radical polymerisation takes place. It is an inherent feature in most liquid systems as the layers are more permeable than dry layer formats and are open to attack from oxygen in the atmosphere. Any oxygen present is highly reactive with triplet dye states (refer to Section 1.4.1) and will react preferentially with the dye until all oxygen is used up. This raises the exposure energy needed to record a hologram and can lead to lower diffraction efficiency than would otherwise be obtained.

Fimia proposed a liquid system containing a mixture of two sensitising dyes, one for red the other for green. For red sensitisation the layer is pre-exposed to green light which does not use up the red dye molecules but allows any oxygen present to react with green dye excited states. The oxygen is then converted into a form, which is unreactive to dye molecules used for actual recording. Diffraction efficiencies of 50% with exposure energy of 10mJ/cm^2 have been observed in the pre-exposed systems. Gratings with spatial frequency of up to 2800 lines/mm have been recorded with the system.

It can be concluded from the discussion of some of the liquid systems mentioned, that instability of recorded holograms can be a problem. The inhibition period, which is also a feature of most liquid systems, can also affect the quality of holograms by lowering the maximum diffraction efficiency that can be obtained.

The inclusion of a polymer binder to photopolymer systems can help to address these problems. It also makes the format more user-friendly and storage of recorded holograms is easier. Some systems based on acrylamide monomer are described in the next section.

1.3.2 Acrylamide-based dry compositions

Jeudy and Robillard (1975)[39] reported an interesting version of the liquid Sugawara system which included a reversible photochrome (indolino-spiropyran), as sensitiser and poly(vinyl alcohol) as binder. The photochrome, which was fully transparent in visible light, could be activated by ultra-violet (UV) light shifting its absorption band to facilitate recording at 633nm. When recording was completed the UV was switched off and the photochrome was rendered inactive resulting in a highly transparent, stable hologram of typically 90% diffraction efficiency with an exposure energy of 100mJ/cm^2.

Sadlej and Smolinska (1975)[40] improved the original system proposed by Jenney by including a binder. In this way the shelf-life of the original material was greatly improved, proving that a binder can improve the stability of recorded holograms. Spatial frequencies of up to 4700 lines/mm could be recorded. However, one of the major drawbacks with this system was the extremely low diffraction efficiency reported, only 4.5%.

The system that has been developed in our laboratories is based on one that was first presented by Calixto[41] (1987). The material originally contained acrylamide monomer, triethanolamine as electron donor, methylene blue dye and PVA as binder. Although exposure energy was low at approximately 94 mJ/cm^2, the maximum diffraction efficiencies reported were low at 10%.

So it seemed that apart from the Jeudy and Robbillard system described, which is quite different to the others, the addition of a binder to acrylamide photopolymers improved the stability but not without loss of diffraction efficiency. However, the advantages of dry layer format warranted further study into improving this type of system.

1.4 Commercially produced systems

Among a number of commercially available dry-layer format technologies[42-52] to emerge over the years, those that are the most widely known are of DuPont™ and Polaroid™. For this reason, a brief review of the systems associated with both companies will be given.

1.4.1 Du Pont photopolymers

Du Pont has been one of the major contributors in the development and production of photopolymers for holography for over 25 years. In 1971, Colburn and Haines[53] published a paper on a theory of volume hologram formation in a photopolymer developed by DuPont[54]. The material was based on a liquid acrylic monomer and a cellulosic binder with a photoinitiator system. The actual individual components were not named. Characterisation studies carried out by the authors revealed diffraction efficiencies of approximately 10% could be achieved with exposure energy of 50mJ/cm^2.

Later, (1975) another photopolymer[55] produced by DuPont was reported to achieve diffraction efficiency of approximately 100% with only 40mJ/cm^2. In order to achieve this high diffraction efficiency, post-exposure processing was required. This system was the second system to be commercially produced.

In 1990, Smothers and co-workers[56] reported a new family of photopolymer recording materials, which later became known as the Omnidex series. Although based on the original materials, other components such as surfactants or plasticisers were added to make the material suitable for specific applications[57]. Production of holograms in the Omnidex series involved three steps: (1) holographic exposure of typically 5-100mJ/cm^2 over a range of wavelengths ranging from UV to near-IR, (2) UV exposure of typically 100mJ/cm^2 and (3) heat treatment with time duration of 2-120 minutes at 100-160°C. Diffraction efficiencies of approximately 100% can be obtained with some of the materials (HRF-700X015-20). Others have been specifically formulated to record reflection holograms (HRF-600) so high spatial frequencies may be recorded.

Although the holograms do not need any wet chemical processing, the heat treatment can take up to two hours to produce very high diffraction efficiencies.

Monroe[58, 59] and co-workers have carried out interesting studies on different monomer and binder combinations for DuPont. It was reported that maximum refractive index modulation in a material during recording can be achieved when the difference in the initial refractive indices of monomer and binder is maximum.

1.4.2 Polaroid photopolymers

Ingwall and Troll[60-62] have carried out extensive research on a photopolymer based on acrylic monomers for the Polaroid Corporation. The material is known commercially as DMP-128 and is a mixture of lithium acrylate, acrylic acid and methylene bisacrylamide in a polymer binder. Ingwall and Fielding[63] initially presented the photopolymer formula in 1985. It is sensitive in both the red and green regions of the visible spectrum. A typical exposure energy of $5mJ/cm^2$ will produce transmission holograms of 80-95% diffraction efficiency. Reflection holography is also possible. However, wet chemical processing is needed to achieve these values of diffraction efficiency as initial exposure produces a latent image of only 1% diffraction efficiency.

1.5 The material

Several conclusions may be drawn from the description of all the materials mentioned to date. It has already been shown that the inclusion of a binder improved some characteristics of a photopolymer material but limited the diffraction efficiency somewhat. This issue needed to be addressed to maximise the diffraction efficiency.

For holographic applications, liquid systems can be quite messy to handle so again, dry layer format is a better option. Although commercially produced photopolymers can exhibit very high diffraction efficiencies, post-exposure is usually needed.

The material which is the subject of this thesis was initially developed by Martin (1995) [64] for sensitisation in the 514nm region. The material formulation was improved by adding a crosslinking monomer which improved the overall stability of the material.[65] Diffraction efficiencies of approximately 100% were obtained and exposure energy required of the material has been as little as 50 mJ/cm^2. The material has been used for various holographic applications with excellent results.[66] One drawback to date, has been the inability of the material to record reflection holograms. Reflection holography requires a recording medium capable of spatial frequencies in the region of 5000 lines/mm. The limiting spatial frequency of the material is approximately 3000 lines/mm.

The work presented in this thesis concerns the development of a red-sensitised version of the material for use in the 633nm region. The fact that Helium-Neon lasers are relatively inexpensive, more compact and more readily available than "green" lasers are the underlying reasons for this development. However, they also have much less lasing power. The material needed to be adapted to record holograms with high diffraction efficiencies at a relatively low exposure energy. The characteristics of the material for red-sensitisation were also studied to determine any difference between the red and green versions of the material leading to a better understanding of the internal processes that drive material efficiency.

1.6 Photochemical processes

It is now appropriate to describe the photochemical processes that are induced in the material under the influence of light of the appropriate sensitising wavelength. For the moment the discussion will be limited to the chemical interactions only in order to outline the interdependence of each component. The principles of the actual holographic recording process, which occurs simultaneously are described in chapter 3, section 3.1.

1.6.1 Photosensitisation

The photosensitisation of the material depends on the dye and the electron donor. The reaction between these components produces free radicals, which are vital for the onset of the polymerisation process. The following is a description of the chemical processes leading to the production of free radicals.

When the photosensitive dye (methylene blue, MB) is exposed to light of a compatible wavelength a primary photoprocess ensues. The dye absorbs a photon of the light and enters into an excited singlet state.[67]

(1) $\mathbf{MB + h\nu \rightarrow {}^1MB^*}$

This may either revert to the ground state by emission of a photon (fluorescence) or by radiationless transfer to another molecule e.g. the electron donor, **ED** (fluorescence quenching).

(2) $^1MB^* \rightarrow MB + h\nu$ (fluorescence)

(3) $^1MB^* + ED \rightarrow MB + ED$ (fluorescence quenching)

or it may cross over to the more stable and long lived ,triplet state (inter system crossing).

(4) $^1MB^* \rightarrow {}^3MB^*$ (intersystem crossing)

Methylene blue has a higher oxidation potential in the triplet state, so the dye molecule can undergo a redox reaction with the electron donor to form the leuco (transparent) form of the dye, by the abstraction of 2 hydrogens. It may also revert to the ground state by radiationless transfer (triplet quenching) or by emission of delayed fluorescence or phosphorescence. At high dye concentrations, concentration quenching can occur, whereby an excited dye molecule is deactivated by collision with another dye molecule.

(5) $^3MB^* + MB = 2MB$ (concentration quenching of triplet state)

Oxygen quenching is also a significant process[68] leading to the reduction of triplet and singlet state quantum yields. This causes an 'inhibition period' at the beginning of the polymerisation, during which the oxygen and other inhibitors are used up and no polymerisation is initiated. The inhibition period is usually identified with liquid photopolymers as it is easier for inhibitors to enter the material in this form.

(6) $^3MB^* + {}^3O_2 = MB + {}^1O_2^*$ (oxygen quenching)

(7) $^1MB^* + {}^3O_2 = MB + {}^1O_2^*$ (oxygen quenching)

Zakrezewski and Neckers[69], studied the reaction of a xanthene dye, rose bengal under reducing conditions with triethanolamine, $(HOCH_2CH_2)_3N$:, as the electron donor. Both xanthene and thiazine dyes undergo reduction when illuminated with the appropriate sensitising wavelength so the process detailed below can equally be applied to methylene blue.[70]

The triethanolamine donates an electron to the excited triplet state of the dye molecule leaving the latter with one unpaired electron and an overall negative charge.

(8) $^3MB^* + (HOCH_2CH_2)_3N: \rightarrow MB^{\bullet -} + (HOCH_2CH_2)_3N^{\bullet +}$

The triethanolamine radical cation then loses a proton and becomes an uncharged free radical.

(9) $(HOCH_2CH_2)_3N^{\bullet +} \rightarrow (HOCH_2CH_2)_2NCH^{\bullet}CH_2OH + H^+$

In the presence of the acrylamide monomer a triethanolamine radical can follow either of two pathways:

It can react with a monomer molecule to initiate free radical polymerisation. The free radical formed in (9) above is denoted by $TEA^{\bullet +}$ in (10) below, which shows the reaction with a molecule of acrylamide (denoted ACR). This is the initiation stage of polymerisation.

(10) $TEA^{\bullet +} + ACR = H^+ + TEA\text{-}ACR^{\bullet}$ (initiation)

It can also react with dye to cause dye bleaching. In order for bleaching to occur, the dye radical formed in step (8) abstracts a hydrogen from the triethanolamine radical to form the dihydro dye (transparent) and an unstable triethanolamine intermediate containing a carbon - carbon double bond.

(11) $(HOCH_2CH_2)_2NCH^{\bullet}CH_2OH + H^+ + MB^{\bullet -}$

$\rightarrow (HOCH_2CH_2)_2NCH=CHOH + H_2MB$

The unstable intermediate rearranges to a more stable product shown below:

(12) $(HOCH_2CH_2)_2NCH=CHOH \rightarrow (HOCH_2CH_2)_2NCH_2CHO$

So in order to form the transparent form of the thiazine dye, two hydrogens are abstracted from the triethanolamine molecule. Although hydrogen abstraction from the PVA binder is possible in the absence of electron donor due to the presence of labile hydrogens, this process is inefficient. The presence of the electron donor allows the process to be more efficient for the production of free radicals. Bleaching any remaining dye after holographic recording is an important process as it ensures final hologram transparency. The polymerisation process is now described below.

1.6.2 The polymerisation process

The polymerisation process initiated by free radicals is essentially the production of poly(acrylamide) from acrylamide and methylene-bis-acrylamide. In general polymerisation[71] processes can take various forms but poly(acrylamide) [72] is produced by free radical polymerisation, which is the only type considered here. There are three distinct stages in free radical polymerisation initiation, propagation and termination, each of which is outlined below.

In this process the initiating molecule is a free radical, a highly reactive molecule possessing an unpaired electron. The radical attacks the carbon—carbon double bond (the vinyl group) on the monomer and links itself to the monomer molecule. This reaction is shown in step (10) above. This causes the monomer itself to become a free

radical, which will attack another monomer molecule and repeat the process. A chain reaction ensues which creates a growing polymer chain which will only terminate when a step occurs which consumes a radical but does not produce one.

The first step of the polymerisation process in the material involves the initiating radical attaching itself to the monomer molecule by addition across the carbon-carbon double bond.

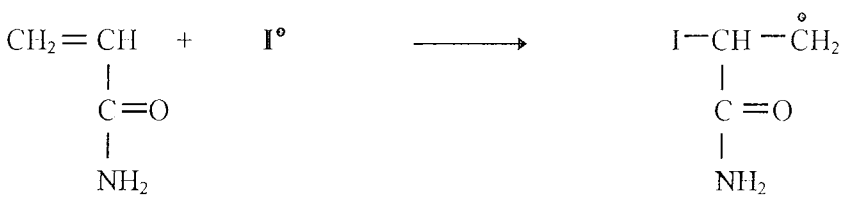

In doing this the free radical uses its odd electron and one of the π electrons from the carbon carbon double bond. The other carbon is left with an odd electron and thus the monomer molecule becomes a free radical.

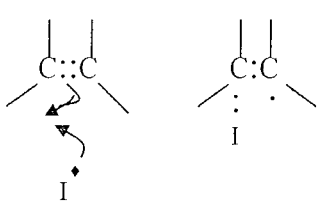

This radical will attack another monomer in the same way, again creating a new free radical.

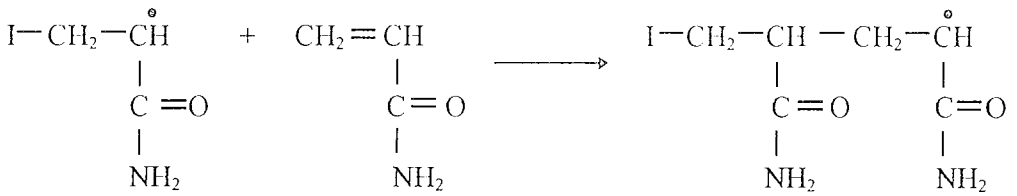

The chain will propagate in this way, growing by one monomer link each time the process is repeated, until finally termination occurs. This can be either by combination or disproportionation. Combination occurs when two radicals meet and the chains join to form one long polymer chain

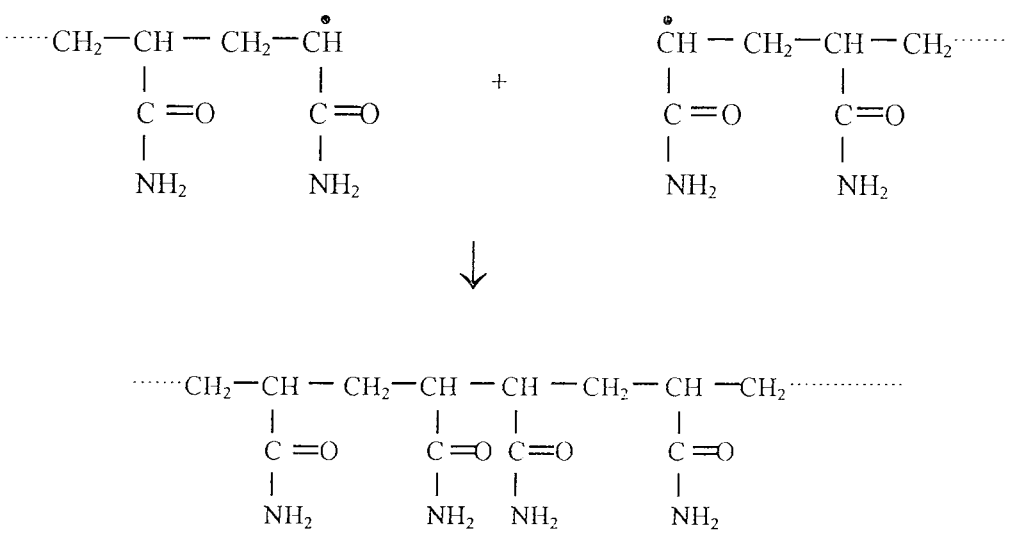

When the chain reaction terminates by disproportionation a hydrogen atom is abstracted from one growing chain to the other and the double bond reforms. The result is two separate chains.

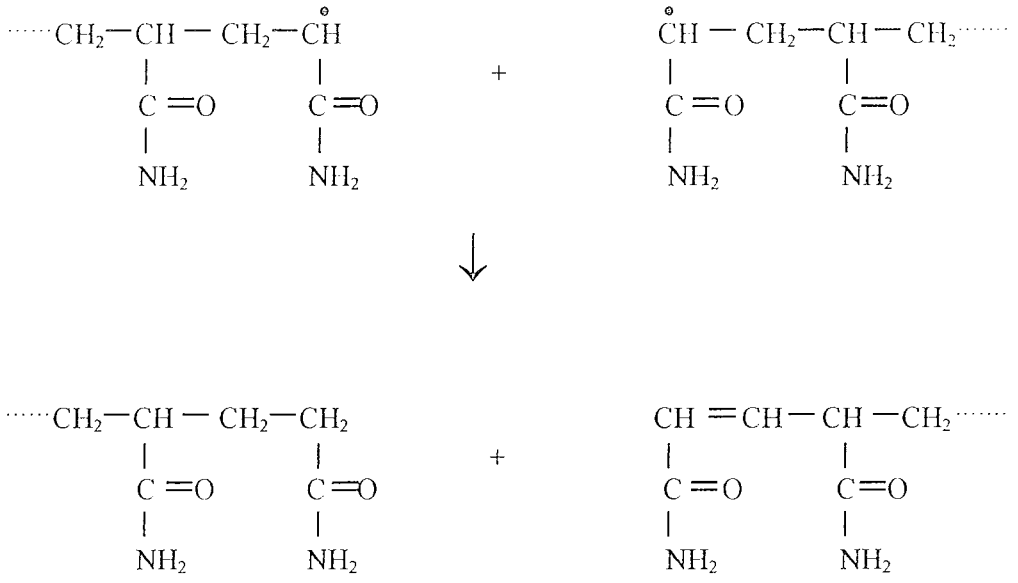

As the polymerisation process proceeds, the optical properties of polymer produced are different to those of the monomer. On polymerisation, each double bond is replaced by two single bonds, lowering the molar refractivity of the material and by contribution, subsequently its refractive index. However, this is usually accompanied by a large increase in density (10-15%) due to the polymer chains so the overall refractive index is higher in the polymer than the monomer. The main outcome of this type of reaction in a hologram is that a refractive index modulation is induced between light exposed and unexposed areas. This type of hologram is known as a phase hologram and will be discussed in detail in Chapter 3.

The final diffraction efficiency of a phase hologram depends on the extent of the refractive index modulation. It in turn depends on the rate of polymerisation within the material. By ensuring that there is a balance of component concentration in the material, the speed of response of the material to light can be optimised. The next chapter is concerned with the optimisation of the chemical formula with a view to improving the overall efficiency of the material. The characterisation of the material is also reported.

1.7 Conclusion

A review of some photopolymers in both liquid and dry layer formats for use as holographic recording materials has been presented. It was demonstrated that there are many different types available, each with their own unique properties. The systems developed commercially by Du Pont and Polaroid have been described and whilst these materials have advantages, time consuming post-exposure is needed to exploit these systems fully.

The material, which has been developed in our laboratory, was introduced along with some of its characteristics to date. The importance of developing an efficient, red-sensitive version of the material was also outlined.

The photochemical processes that ensue under illumination by the correct wavelength, were presented to show the inter-dependence of the various chemical

components to the overall recording process. In addition, several conclusions can be drawn from the description of the photochemical processes. The production of free radicals is vital to the polymerisation process so the concentrations of dye and electron donor must be optimised to allow efficient polymerisation of monomer to occur. The mobility of the reacting species should not be too restricted as initiation may be restricted nor should the binder be so permeable as to allow inhibitors, such as oxygen to enter. Chapter 3 explores the optimisation and characterisation studies that were conducted on the material.

The object of this thesis is to further investigate the chemical and physical processes that occur in the material, with a view to a fully optimised red-sensitive system. This will be achieved through use of various holographic techniques.[73] Chapter 2 is concerned with examining each of the components individually, then in combination. The chemical structure of each of the components in the material is outlined and the techniques used to examine each are briefly explained.

2. Chemical characterisation

Photopolymerisable photopolymer recording materials, in both liquid and dry layer formats were described in Chapter 1. The material that is the focus of this work was introduced and the importance of developing an efficient red-sensitive material in particular was discussed.

This chapter describes the chemical structure and relevant properties of each of the material components. Nuclear Magnetic Resonance[74] (NMR) was used to obtain spectra for each of the components and the material mixture, to verify that no significant chemical interaction takes place prior to material exposure. Raman spectroscopy[75] was also employed to observe monomer reaction.

However, it must be stressed that although analytical techniques have been used in order to examine the role of each component, the main theme of the thesis is the development of the material for use in holography and related applications. Conditions within the material during holographic recording are unique in that there can be dramatic variations in reaction rates and component concentrations over very small distances (of the order of microns). Holographic techniques are the most suitable way to study the material as they involve the recording of actual holograms. In addition the quality of the holograms can be potentially improved, as the response of the material to variations in the recording

conditions is improved. The holographic techniques employed to study various aspects of the material are described in subsequent chapters.

2.1 Chemical characterisation techniques

The following describes the spectroscopic methods used to analyse the material.

2.1.1 Nuclear magnetic resonance (NMR)

The theory of NMR is highly complex and there are many different ways in which the technique can be employed for chemical analysis[76]. In its simplest form, it is the study of the properties of molecules containing magnetic nuclei by applying a magnetic field and observing the frequency at which the molecules come into resonance. The nuclei in question are those of the hydrogen atom (or proton) and the carbon –13 isotope.

The study of a molecule by NMR spectroscopy enables the elucidation of its structure by establishing the different types of chemical environment present in the molecule and the atoms present on neighbouring groups. The same nuclei in different chemical environments give rise to what is known as the *chemical shift* (δ). The chemical shift of a nucleus is the difference between its resonance frequency and that of a reference standard (the solvents used here are D_2O and $CDCl_3$ depending on the component being analysed). The separation of the resonance of a particular group of nuclei from the standard increases with the strength of the applied magnetic field. This is because the field that is

induced, due to the magnetic properties of the nuclei (local magnetic field), is proportional to the applied field.

Chemical shifts are calculated using the δ scale, which is defined as

$$\delta(ppm) = \frac{\nu - \nu^{\circ}}{\nu^{\circ}} \times 10^{6} \qquad (2.1)$$

where ν° is the resonance frequency of the standard and ν the frequency of the applied field.

The existence of chemical shift can be used to explain the spectrum for ethanol (CH_3CH_2OH) which is shown in Figure 2.1. The CH_3 protons form one group of nuclei with a chemical shift value of δ=1. The CH_2 protons, being in a different part of the ethanol molecule, experience a different local magnetic field and resonate at δ=3. The OH proton resonates at δ=4. The relative intensities of the signals (areas under the absorption lines) can also be used to distinguish which signal belongs to which group of nuclei. In the case of ethanol, the intensities are in the ratio 3:2:1 according to the number of protons in each group.

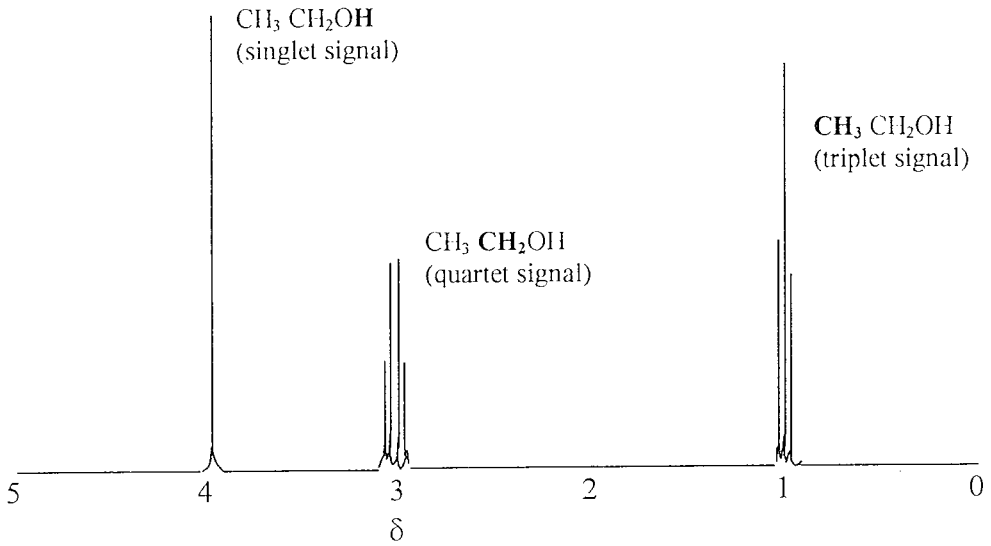

Figure 2.1 A simple spectrum of ethanol. The bold print denotes the proton to which the signal corresponds.

The splitting of resonances into individual lines, (shown in Figure 2.1), is called the fine structure of the spectrum. The individual lines occur as a result of the contribution of each magnetic nucleus to the local field experienced by other nuclei. The strength of the resulting interaction is expressed in terms of the *spin-spin coupling constant* (*J/Hz*).

In Figure 2.1, for example, the three protons of the CH_3 group split the single resonance of the CH_2 protons into a quartet. The two protons of the CH_2 group also split the single resonance of the CH_3 group into a triplet signal. To calculate J for the triplet signal, for example, the δ value for the outer absorption lines are subtracted from the δ value for the

middle line and an average δ value obtained. This average is then multiplied by the applied magnetic field* to yield J for that particular triplet.

The format for all results obtained for the material components is shown in Figure 2.2 for proton NMR (^{1}H NMR). The chemical shift value (δ) for each relevant proton/carbon (underlined) is quoted with spin-spin coupling constant (J) where necessary. The same format applies for carbon-13 NMR (^{13}C NMR) where carbon groups in different chemical environments within the material components are analysed.

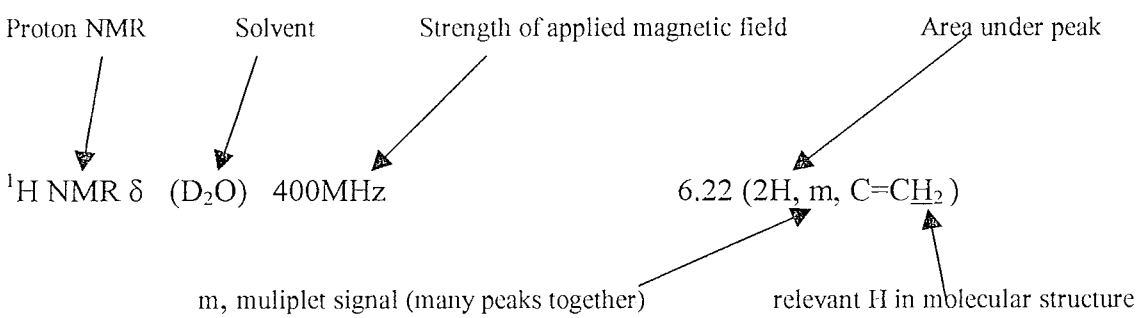

Figure 2.2 Format of results

* The value of the applied magnetic field depends on the individual spectrometer, in this case it was 400MHz.

2.1.2 Raman Spectroscopy

When monochromatic radiation of wavenumber ϖ_0 is incident on a chemical system, most of it will be transmitted or scattered elastically. However, some inelastic scattering of the radiation is observed. On analysis, the frequency content of this scattered radiation is found to contain not only the wavenumber of the incident radiation but new components of the type $\varpi' = \varpi_0 \pm \varpi_m$.

These new components, ϖ_m are associated with transitions between the rotational, vibrational and electronic levels in molecular systems. The intensity of scattered radiation, Raman scattering, with its associated frequency shift, may be plotted as a Raman spectrum. The elastic scattering of incident radiation, by a system, without any change in frequency is known as Rayleigh scattering. The intensity of Rayleigh scattering is generally 10^3 of the intensity of the incident radiation. The intensity of strong Raman bands is generally about 10^{-6} of the intensity of Rayleigh scattering.

There are many applications of Raman Spectroscopy[77], one of which is the identification of chemical species using Raman spectra. It is used here to observe the monomer reaction *in-situ*. There are some advantages in using this technique to study the material. Water is an ideal solvent for the technique as it has a single band at 3654 cm^{-1}. No sample preparation is required, so spectra may be obtained directly from the material as it is used for holographic recording.

The following sections are structured so that all relevant information and results obtained for a specific component are contained within that section. The first component that will be considered is the binder.

2.2 The binder.

A binder is generally included in recording materials to create a matrix-like structure through which the active components may move and react.[78] The role of the binder will be discussed in later chapters where it will be shown that its physical properties can influence the behaviour of other components in the material. For now, the following discussion is limited to the general properties of PVA. In order to examine any influence the binder may have on the physical properties of the recording material, it is useful to have some knowledge of its structure and physical properties.

2.2.1 Chemical structure

PVA (shown in Figure 2.3.) is a vinyl polymer with an asymmetric structure due to the presence of the alcohol (OH) group, which is oriented randomly on either side of the carbon plane.

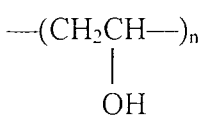

Figure 2.3 Structure of PVA where n indicates repeating units of the "monomer".

This type of polymer structure is classed as atactic which means that PVA is never perfectly ordered or *crystalline*. However, it may contain regions that exhibit an ordered structure depending on the manufacturing process.

There are two main factors that govern the mechanical properties of a polymer.[79] The average molecular size, which is determined by the degree of polymerisation (n), which is a function of the manufacturing process where n indicates the number of repeating units in a polymer molecule, is the first. The second factor is the shape and molecular regularity of the polymer. The presence of side branching on a polymer chain can cause significant changes in the mechanical properties of the polymer. Both of these factors depend on the duration and the conditions of the polymer manufacturing process, which is briefly described below.

2.2.2 Manufacturing process

PVA is prepared by a process called alcoholysis where Poly(vinylacetate) (PVAc) is reacted with methanol or ethanol to form PVA.[80] This process is more commonly known as hydrolysis and the polymer is usually partly characterised by the degree of hydrolysis it attains during the manufacturing process. Effectively, (ignoring any traces of reacting agent or catalyst in the end product), 80% hydrolysed PVA contains 20% PVAc by weight. This degree of hydrolysis is important, as a mixture of two polymers will usually be less structurally ordered than a pure polymer. For our purposes, it may also influence the rate at which migrating molecules can move through a polymer film.

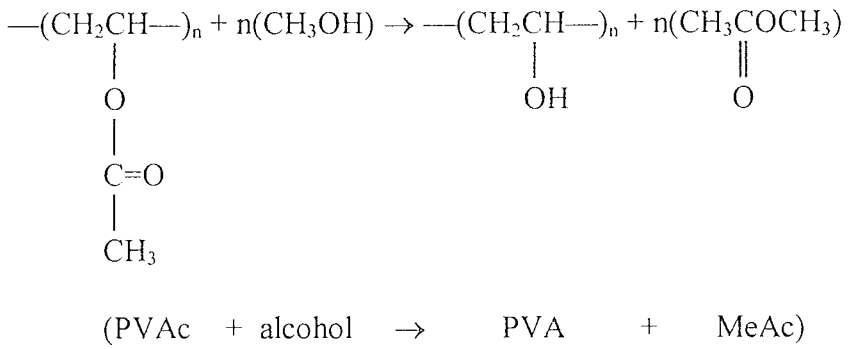

Figure 2.4 Manufacturing process for PVA

2.2.3 Plasticisers

Plasticisers are substances that are usually added to polymers to reduce overall structural rigidity.[81] They have a significant effect on the mechanical properties since the interchain forces within the polymer are reduced. Plasticisation is usually restricted to amorphous polymers or polymers with a low degree of crystallinity because of the limited compatibility of plasticisers with highly crystalline polymers.

For our purposes, the term plasticiser will be applied to any substance which, when added to the polymer binder, renders it more pliable or permeable.

2.2.5 NMR results

Two samples of PVA were analysed, one with only 80% hydrolysis and one with an unknown degree of hydrolysis. The two samples will be referred to as PVA A and PVA F respectively, for cross-reference with Chapter 5.

From the description of NMR in Section 2.1.1, a proton spectrum of the PVA structure alone (Figure 2.4) would contain 2 peaks, one triplet peak assigned to the CH group and the other doublet peak from the CH_2 group. This was indeed the case, as reported in Table 2.1 below.

^{1}H NMR δ (D_2O) 400MHz	**^{13}C NMR ppm (D_2O) *(PVA F)***	**^{13}C NMR ppm (D_2O)*(PVA A)***
1.63 (2H, d, J=4.9 Hz, $C\underline{H}_2$),	44.55 ($\underline{C}H_2$),	20.29 ($\underline{C}H_3$)
4.01 (1H, t, J=4.9 Hz, $C\underline{H}$)	66.28 (CO$\underline{C}$H)	43.77 ($\underline{C}H_2$)
		65.92 (CO$\underline{C}$H)

Table 2.1 proton and ^{13}carbon NMR results for the binder

Referring to columns 2 and 3, the extra signal for the carbon-13 spectrum of PVA A is due to the methyl carbons on the acetate group, (Figure 2.4) as the PVA A contains 20% poly(vinylacetate) from the manufacturing process. This would suggest that by comparison, the PVA F contains a negligible amount of PVAc and is theoretically 100% hydrolysed.

2.2.6 Approximate determination of hydrolysis-Raman spectroscopy

PVA F, which is normally used as the binder in the material has a molecular weight range of 30-200*10^3 and is supplied by Reidel de Haen chemicals. The degree of hydrolysis was already found to be 100% by experiment using NMR. To verify this characterisation was carried out using Raman spectroscopy.

A number of PVA samples with different chemical characteristics were tested for a comparative study. Spectra were obtained for each of the PVA types and the peak at approximately 1750 cm^{-1}, indicated by the arrow in Figure 2.5, was identified as the actetate group. Comparison to the other PVA types lead to the conclusion that PVA F was 99% hydrolysed, indicating a negligible presence of PVAc repeat units. The spectrum for PVA F is at the fore of the spectra shown in Figure 2.5.

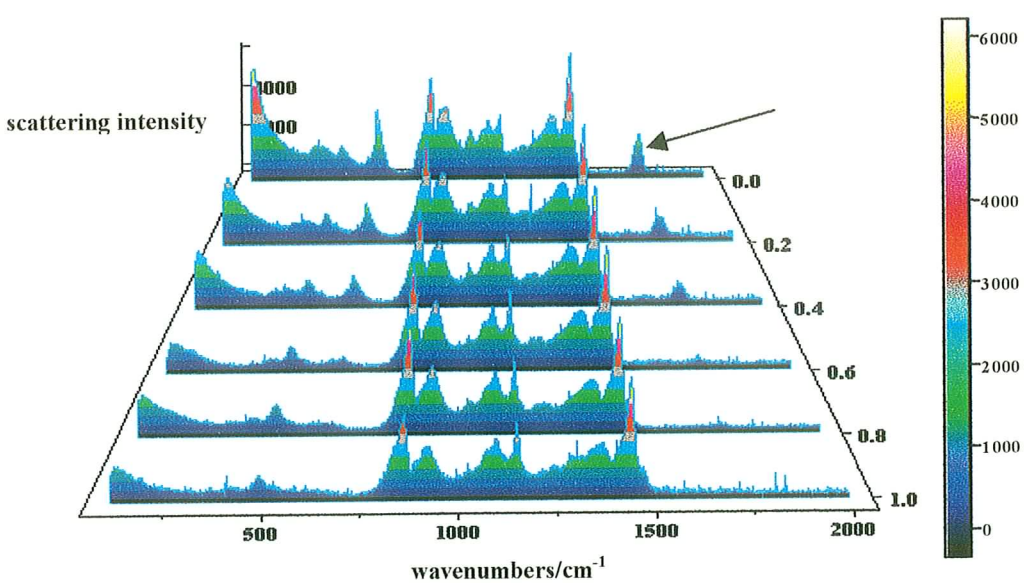

Figure 2.5 PVA spectra. The arrow indicates the actetate peak. The spectrum for PVA F is at the fore of the spectra.

2.3 The Monomers

There are two monomers in the material. The first is acrylamide, which forms the main polymer chains in illuminated areas during holographic recording. The second monomer, is N,N-methylenebisacrylamide which with polymerisation, acts as a crosslinker between the main polymer chains. The result is a stable polymer network within the light exposed areas of the hologram.

2.3.1 Monomers-NMR results

The molecular structure of acrylamide is shown below in Figure 2.6. There are 4 different proton environments present in the monomer. However, the spectrum yielded only two signals, one doublet corresponding to the proton on the COCH group and two overlapping quartets for the $C=C\underline{H}_2$ group (see Table 2.2). The third proton due to the NH_2 group was not visible due to ion exchange with the solvent (D_2O).

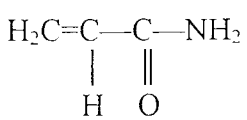

Figure 2.6 Molecular structure of acrylamide

^{1}H NMR δ (D_2O) 400MHz	^{13}C NMR ppm (D_2O) 400MHz
5.80 (1H, d, J=9.2 Hz COC<u>H</u>),	128.04 (C=C<u>H</u>$_2$), 129(CO<u>C</u>H),
6.22 (2H, m, C=C<u>H</u>$_2$)	170.52 (C=O)

Table 2.2 NMR results for acrylamide.

The structure for N,N-Methylenebisacrylamide is shown below in Figure 2.7. The molecule has some degree of symmetry with a methyl group in the centre between two acrylamide groups. This is shown in Figure 2.7 with a broken line indicating the plane of symmetry.

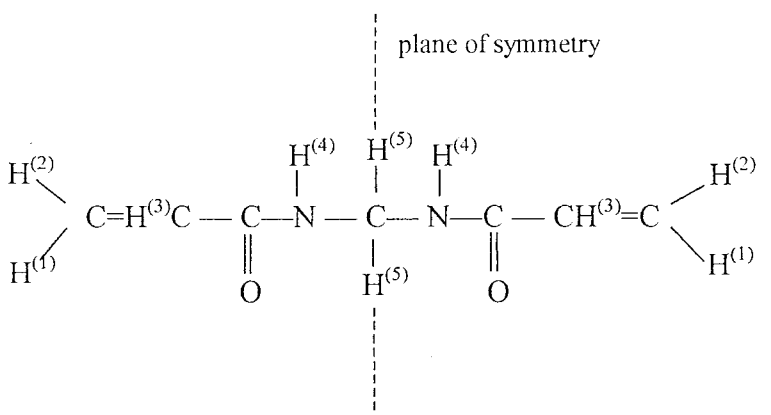

Figure 2.7 Molecular structure of N,N-Methylenebisacrylamide

Because of this degree of symmetry, only 5 different proton environments are evident from the NMR spectrum, each approximately double the intensity accounting for the two acrylamide groups. However, the protons attached to the bridging methyl group are not in the same magnetic environment. This leads to each of the protons attached to the

central methyl group splitting the other into doublet signals. The doublet signals are overlapped, which leads to what appears to be a triplet signal on the spectrum.

The results are shown below for the monomer dissolved in $CDCl_3$. For practical reasons, the protons on N,N-Methylenebisacrylamide have been numbered so that the spin-spin coupling (J) between protons can be shown. This coupling will be denoted by ($J_{x,y}$) where x and y are the assigned numbers of the interacting protons, shown in Figure 2.7.

^{1}H NMR δ ($CDCl_3$) 400MHz
6.32 (2H, d, J= 17Hz ($J_{1,3}$))
5.71 (2H, d, J= 10Hz ($J_{2,3}$))
6.15 (2H, dd, J= 10Hz ($J_{3,2}$)), J= 17Hz ($J_{1,3}$),
7.13 (2H, s)
4.79 (2H, dd, J= 6.5Hz ($J_{5,5}$))

Table 2.3 Proton NMR results for crosslinking monomer.

2.3.3 Experimental observation of monomer reaction

An interesting study to observe the polymerisation of monomer *in-situ* was conducted using Raman spectroscopy. The material was exposed at intervals using the spectrometer light source with an appropriate filter, to obtain a series of spectra (Figure 2.8) detailing

the gradual polymerisation of monomer. The peaks due to double bonds are indicated. The spectrum indicated by the arrow was obtained before exposure took place.

This study was made possible by the existence of a spectral region at approximately 1600cm^{-1}, which can be attributed only to the monomer double bonds. As the material is polymerised, the peaks due to the double bonds can be seen to decrease in intensity.

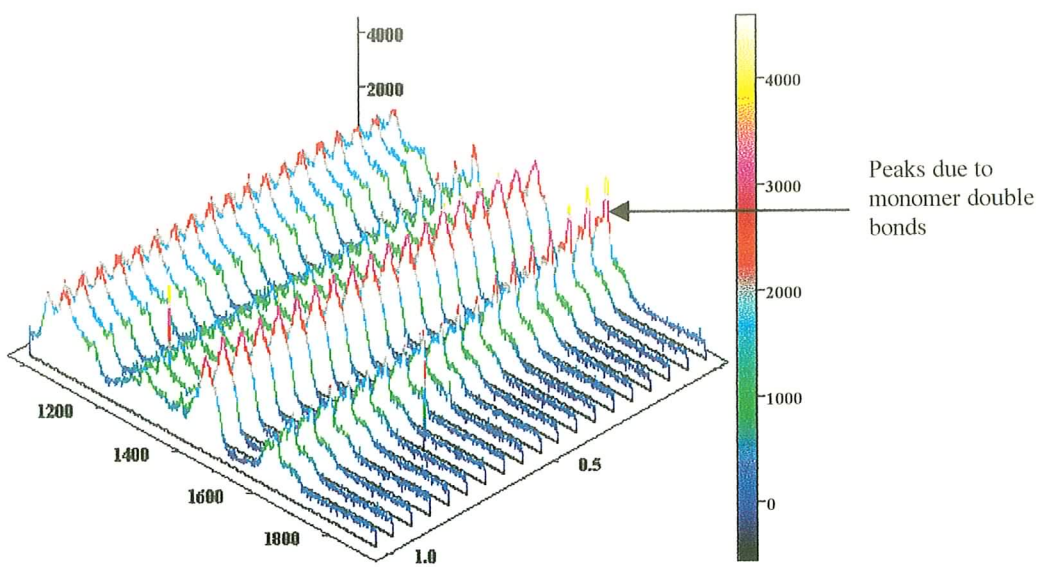

Figure 2.8 A series of spectra obtained for polymerisation of the material as a function of exposure time. The peaks representing the double bonds of the monomer are indicated by the arrow.

2.4 The Dye.

Methylene blue dye is classed as a thiazine[82] dye. The structure of thiazine dyes centres around the presence of three aromatic (ringed) sites, to which protons are attached. A diagram of an expanded aromatic structure is shown in Figure 2.9. Note that one proton is attached to each of the carbons in the ring. This is a basic aromatic structure but other groups may be attached to the carbons in place of protons.

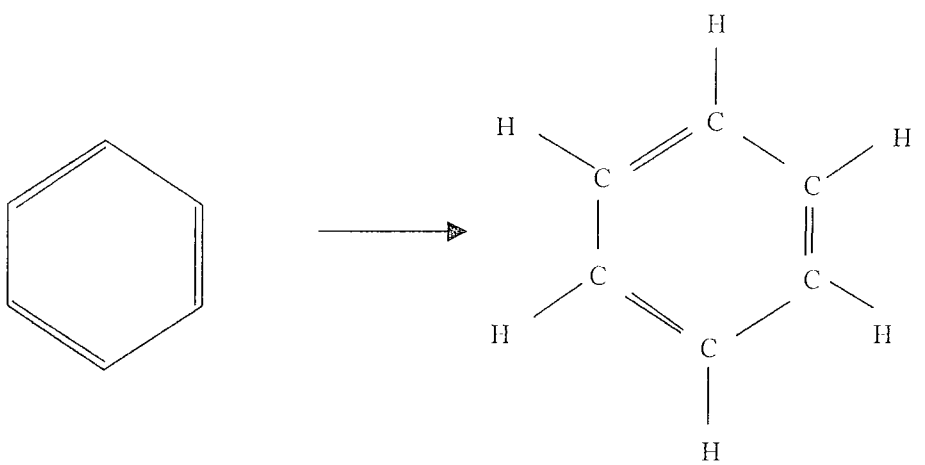

Figure 2.9 Basic aromatic structure.

The structure of a molecule of methylene blue is shown below in Figure 2.10. The expanded structure has not been shown. The groups associated with each edge of the structure have each been assigned a number commencing with Sulphur being assigned 1 and continuing anticlockwise. The numbering system allows interactions between particular groups to be easily recognised. The carbons in the molecule are also numbered in the same way.

Because of the degree of symmetry (discussed above for N,N-Methylenebiscrylamide) present only 7 signals were observed on the NMR spectra. Six of these signals are associated with the aromatic sites and the seventh with the side groups ($N(CH_3)_2$). The results are presented below in Table 2.4.

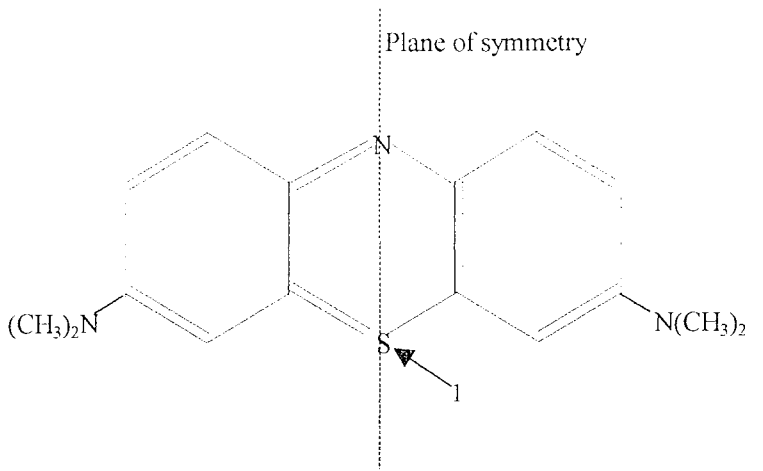

Figure 2.10. The structure of a methylene blue dye molecule. Each group on the structure is numbered anticlockwise starting with the proton associated with the Sulphur atom indicated above.

^{1}H NMR δ (D_2O) 400MHz	**^{13}C NMR ppm (D_2O) 400MHz**
3.02 (12H, s, $C\underline{H}_3$)	40.10 (CH_3)
6.69(2H, s, H-3, H-13)	105.48, 120.32 (C-5, C-6, C-10, C-11)
6.87 (2H, d, J=9.4Hz, ($J_{5,11}$))	133.22, 133.07 (C-2, C-7, C-9, C-14)
7.10 (2H, d, J=9.4Hz, ($J_{3,10}$))	135.77 (C-3, C-13,) 152.48 (C-4, C-13)

Table 2.4 NMR results for the sensitising dye.

2.5 The electron donor

The structure of TEA is outlined below in Figure 2.11. It is classed as a tertiary amine, which is formed when the basic amine structure of NH_3 undergoes hydrogen replacement from other reacting groups.[83] In this case the replacement group is ethanol (C_2H_5OH). TEA acts as a highly efficient electron donor due to its lone pair of electrons associated with Nitrogen. The solvent used to dissolve the TEA was D_20 which underwent proton exchange with the OH so this signal was not present on the ^{1}H-NMR spectrum.

$$N(CH_2CH_2OH)_3$$

Figure 2.11 Molecular structure of Triethanolamine

As a result the proton NMR spectrum yielded only two triplet signals due to the CH_2 groups which are situated in different chemical environments. The signals were of a high intensity due to the fact that the 3 ethanol chains were equivalent. The ^{13}C spectrum yielded 2 peaks as expected corresponding to the carbons in different environments. The results are presented below in Table 2.5.

^{1}H NMR δ (D_2O) 400MHz	^{13}C NMR ppm (D_2O) 400MHz
2.68 (6H, t, J=6.2Hz $C\underline{H}_2OH$)	55.31 ($\underline{C}H_2OH$)
3.62 (6H, t, J=6.2Hz N-$C\underline{H}_2$)	58.51 ($N\underline{C}H_2$)

Table 2.5 NMR results for the electron donor.

2.6 The material

Having analysed the individual components, the material as it is used for recording was also examined. Both liquid and dry formats of the material were analysed using the NMR technique. However, due to the difference in solubility between the two versions of the material, D_2O was used to dissolve the liquid material and $CDCl_3$ was the solvent used for the dry material format. The results are presented below in Table 2.6 for liquid and solid composition. The main peaks for each of the components are noted.

Component	^{1}H NMR δ (D_2O) 400MHz (Liquid format)	^{1}H NMR δ ($CDCl_3$) 400MHz (Dry format)
TEA	2.7 (6H, t, J=6.2Hz $C\underline{H}_2OH$)	2.65 (6H, t, J=6.2Hz $C\underline{H}_2OH$)
	3.6 (6H, t, J=6.2Hz N-$C\underline{H}_2$)	3.65 (6H, t, J=6.2Hz N-$C\underline{H}_2$)
Acrylamide (aa)and	5.7-6.28 (m)	5.7-6.34 (m)
Bisacrylamide (ba)	(4 peaks aa, 2 peaks ba)	(4 peaks aa, 2 peaks ba)
PVA	1.63 (2H, d, J=4.9 Hz, $C\underline{H}_2$),	1.44 (2H, d, J=4.9 Hz, $C\underline{H}_2$),
	4.01 (1H, t, J=4.9 Hz, $C\underline{H}$)	3.4(1H, t, J=4.9 Hz, $C\underline{H}$)

Table 2.6 NMR results for liquid and dry formats of the material.

When the individual results were compared to the results obtained for the material a number of observations were noted.

1. A broad peak at approximately 4.7 ppm was assigned to water in both the liquid and dry material spectra.
2. The difference in the assigned peaks for PVA in liquid and dry format was attributed to solvent shift due to D_2O.
3. The methylene blue dye signal was not evident in either of the spectra of the material mixture. The reason for this was due to the fact that each of the components was added to the sample in the same ratio of concentrations that is used for preparing holographic layers. The other components were present in larger quantities, which gave rise to a small signal for the dye.

The results indicated that there was no direct evidence of any interaction between the material components other than that due to the solvent.

2.7 Conclusion

The material components have been analysed in terms of structure. It was also verified by NMR and Raman spectroscopy that no reaction seems to take place in the material prior to exposure. This observation is limited to the time taken for the NMR tests to be completed, which was approximately 3 weeks for the material samples.

The following chapter outlines the chemical optimisation. It also details the characterisation of the material that serves to further improve its overall performance. Both optimisation and characterisation are carried out using holographic methods that will be described in detail.

3. Holographic Optimisation and Characterisation of the material.

Having completed the chemical characterisation stage and outlined the role of each of the individual components of the material, the next stage in its development was to optimise the chemical composition for holographic applications. This was performed in an attempt to balance the concentration of each component to quantitatively optimise the efficiency of the material. A detailed optimisation and characterisation had previously been conducted for recording in the 514nm region of the visible spectrum using an Argon ion laser[64]. It was essential, for a number of reasons that a separate study was conducted for recording in the 633nm region.

1. A new class of dye was needed for red-sensitisation. The new dye concentration had to be optimised in relation to the other components.
2. The physical parameters of the binder were not previously investigated in terms of influence on the material.
3. Commercially available Helium Neon lasers are generally of limited power compared to the Argon ion laser. A study had to be conducted in order to determine how the material responded to relatively low powers.

The characterisation study is also vital, as it is important that the limitations of the material are known. A systematic study of material response under varying recording

conditions can yield greater understanding of the processes in the material. Kogelnik's [84] coupled wave theory is useful in describing the theoretical behaviour of a hologram recorded under specific experimental conditions. The refractive index modulation produced during holographic recording can be easily determined using the theory which relates diffraction efficiency, grating thickness and recording wavelength.

In this chapter, the optimisation of the material will be described, followed by an introduction to the principles of holographic recording. The characterisation study of the material is then presented.

3.1 Optimisation

The photochemical processes that take place under the appropriate sensitising illumination were discussed in Chapter 2. The free-radical polymerisation process leading to refractive index modulation in the material was seen to have three distinct stages: initiation, propagation and termination. Efficiency of initiation depends on the dye and electron donor. A high rate of polymer chain growth is desirable to maximise polymerisation of the monomers leading to a high refractive index modulation. It is clear that in order to fully realise the potential of the material for holographic recording the correct balance between the quantities of all components must be achieved. In this respect, miscibility of components is also extremely important to produce homogeneous layers with a high surface quality.

A simple optimisation of the material was carried out by varying the concentration of each of the components in turn whilst the others remained constant. The method used for preparing the layers for holographic recording is outlined below.

3.1.1 Layer preparation for optimisation.

PVA 1: molecular weight (MW) 70-100*10^3	(SIGMA chemicals)
PVA 2: molecular weight 18-200*10^3	(REIDEL-de-HAEN)
PVA 3: molecular weight 30-70*10^3	(SIGMA)
Methylene blue dye	
Triethanolamine (TEA)	
Acrylamide (electrophoresis grade)	
Methylene-bis-acrylamide	

Solution 1:

PVA(10g)
Water(100mls)

Solution 1 was prepared for each type of PVA used. The composition of solution 2 varied as the concentration of each component was changed in turn for optimisation.

Solution 2:

TEA(2mls-6mls) mixed with 3mls of water
Methylene blue dye(2mg-8mg)
Crosslinking monomer(0.15g-0.35g)

Monomer(0.45g-1.05g)

Solution 1(approx. 18mls)

Total volume of the final solution was approximately 25mls.

Samples were prepared by mixing 1ml of total solution with 1ml of water and depositing on clean glass substrates that were previously placed on a level surface to ensure layers were of uniform thickness. The edges of the photopolymer layers are always slightly thicker than the centre due to the drying process but since only the central part was used at all times this was not a problem. The variation in thickness in the central region of the layers was approximately 10%. In an effort to produce thinner layers, a number were prepared using lower %/w PVA solutions as binder. Layers containing less than 6%/w PVA were non-uniform as the high water content resulted in a high amount of evaporation and the normal amount of coating solution was inadequate to cover the substrates completely. This meant that higher amounts of coating solution were needed to produce useful layers. The layers were allowed to dry for approximately 20 hours by evaporation. When attempts were made to transfer the layers to a dessicator after this drying period in order to dry out further, precipitation was evident on the layer surface. This meant that if thinner layers were required, a lower percentage weight PVA binder solution was used or normal drying time was increased to ensure that any excess water had completely evaporated. 20 hours was usually sufficient to completely dry standard layers for recording. Laboratory conditions were maintained at approximately $70 \pm 5\%$ relative humidity and $25 \pm 3^{\circ}C$ throughout sample preparation for optimisation studies.

3.1.2 Experimental set-up

Diffraction gratings were recorded using the experimental set-up illustrated in Figure 3.1. The inter-beam recording angle was kept constant to produce gratings with a constant spatial frequency of 1,000 lines/mm. A Newport 845 shutter (shutter 1) was placed in front of the 35mW Spectraphysics 127 laser (beam was spatially filtered and collimated) and was used to control the recording time. A second shutter (shutter 2) was positioned in the pathway of one of the recording beams (beam 1). Shutter 2 was programmed to remain open for most of the duration of the recording process but to close periodically in order to allow diffraction of the second recording beam (beam 2) through the developing grating. The diffracted light was monitored by a Newport 835 optical power meter, which was placed behind the grating, directly in the path of beam 1. In this way the growth of the diffraction efficiency of a grating during exposure could be monitored. Diffraction efficiency is usually calculated as the percentage of the incident light which is diffracted into the first order direction by the grating. If the incident light on the grating is denoted as I_1 and the light diffracted as I_D then the diffraction efficiency of the grating at any instant is defined as I_D / I_1.

This set-up was designed to eliminate problems associated with measuring the diffraction efficiency of gratings at the Bragg angle. Since the recording wavelength is the same as that which is used to continuously monitor the diffraction efficiency, this means that all readings are taken at the Bragg angle. Care was taken to ensure that

the diffraction efficiency measurement times are minimised during the recording process so that no grating damage occurred due to over-exposure to a uniform beam. Data from the photodetector was passed through an acquisition unit connected to a PC.

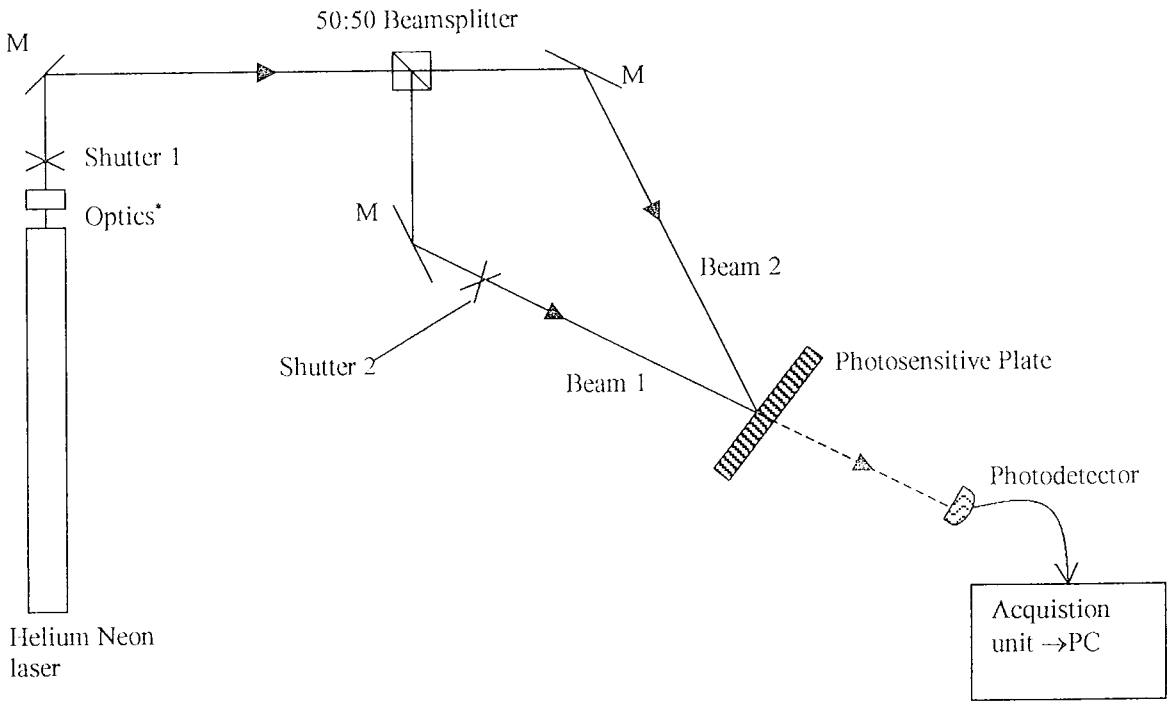

Figure 3.1. Diagram of experimental set-up. Optics denotes the spatial filter and collimating lens. M, denotes mirror.*

3.2 Results: Optimisation

Graphs were plotted of the growth in diffraction efficiency with time for each different parameter under investigation. Transmission curves were also obtained by blocking beam 2 so that only one beam was used to bleach the material. The increase in light intensity penetrating directly through the sample is monitored in this way.

3.2.1 Efficiency of material using different PVA binders

Three PVA binders of different molecular weight ranges were used in this study. It was important also to vary the monomer content. This was to determine not only which binder produced the best layers but also which one contained the monomer sufficiently without the appearance of precipitate on dry layers, prior to exposure. The precipitate has been identified as monomer by infra-red spectroscopy in previous work.[85]

PVA 1

This binder produced good optical quality dry layers containing relatively high amounts of total monomer. However, there appeared to be a maximum amount of monomer which could be dissolved in solution before saturation occurred. Evidence of this can be seen in Figure 3.2. When concentrations higher than Concentration no.4 (0.9g monomer, 0.3g crosslinker) were used, diffraction efficiency decreased. This is because the surfaces of the resulting dry layers were coated with a fine white

precipitate which hindered the recording of a grating through the layer. This concentration worked well at the relatively high humidity at which the optimisation study was carried out. However, at lower humidity it was found that a further reduction in monomer concentration to that of Concentration no. 2 was necessary as the precipitate problem recurred at this lower humidity with Concentration 4.

PVA 2

This PVA type had the highest molecular weight range and it could contain higher amounts of monomer than the other two types with little or no decrease in diffraction efficiency. This indicated that the sample layers prepared with PVA 2 would be more stable than those prepared with the other types.

PVA 3

This sample had the lowest molecular weight range tested in this particular study. Although layers containing PVA 3 binder were used to record high diffraction efficiencies, the optical quality of the layers was poor. Small bubbles were trapped within the dry layers making it difficult to obtain consistent results. As in the case of PVA 1 there was a maximum monomer concentration that could be contained in the dry layers.

The apparent differences in results indicated that the role of the binder could be more influential than was originally thought. The role of the binder is discussed in more detail in the following chapters.

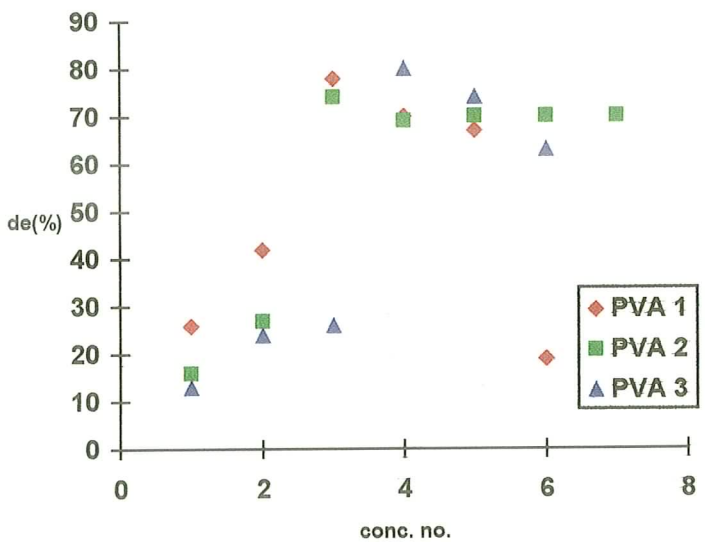

Figure 3.2. Graph of diffraction efficiency (%) vs concentration number of the amount of monomer in total sample solution. The ratio of monomer to crosslinker is 3:1. Total weight: (1)0.6g, (2)0.8g, (3)1g, (4)1.2g, (5)1.4g, (6)1.6g, (7)1.8g

3.2.2 Optimisation of monomer

The total monomer concentration was varied in all three PVA types. Concentration 2 was chosen as optimum concentration as at higher concentrations some precipitation occurred around the edges of the dry layers. Although when recording, the centre of a

layer was usually exposed, it was thought that the appearance of the precipitate was an indication of instability.

A number of ratios of monomer to crosslinker were tested, nine in total. When the crosslinking monomer was at a higher ratio to the monomer, solvation did not occur and therefore suitable layers could not be produced. At 1:1 solvation did occur but only after a long period of time and resulting layers were coated with precipitate of monomer. To a lesser extent the same result was obtained with a ratio of 2:1 monomer to crosslinker. A ratio of 3:1 monomer to crosslinker produced the best results in terms of the highest diffraction efficiencies obtained. (Figure 3.3).

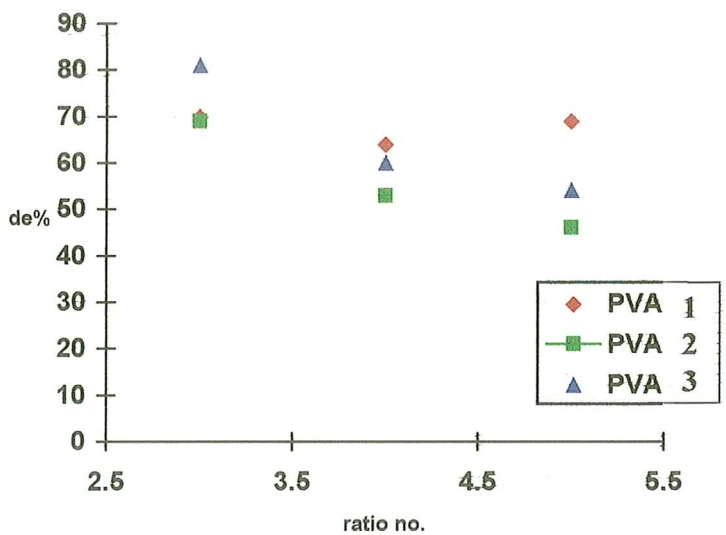

Figure 3.3. Graph of diffraction efficiency (%) vs ratio no. of monomer(m) to crosslinking monomer(c). 3; 3:1, 4, 4:1, 5; 5:1

3.2.3 Optimisation of electron donor and dye

These two components constitute the photosensitisation part of the material so the optimisation process is described for each in this section.

TEA-electron donor

The TEA constitutes a large percentage of the volume of a typical dry layer (approximately 50%) and as a consequence the amount used must be carefully considered. In addition to its primary role as electron donor the TEA seems to aid the binder in holding the other components effectively.[65] The effect of TEA on the binder is examined in further detail later.

The growth curves plotted for gratings recorded from layers containing varying amounts of TEA are shown in Figure 3.4. As the concentration of TEA is increased the maximum diffraction efficiency decreases. However as it is present is such high quantities, a small increase in TEA content produces a larger decrease in the relative amounts of the other components in the layer so careful control must be exercised to keep them at the same ratio. Note that using 1ml TEA, the diffraction efficiency growth of the grating is very rapid. Unfortunately, the optical quality of layers containing only 1ml of TEA was found to be poor. This was due to the appearance of monomer precipitate on the surface of the layers. The optimised amount of TEA

needed to produce good quality layers was 2mls approx./25mls of total coating solution.

If the TEA content is increased with no corresponding increase in the other component concentrations, the effectiveness of the binder is reduced. This opens the way for inhibitors such as oxygen to reduce the efficiency of the layers. This phenomenon has been mentioned in section 2.7.1. Although a dry layer is still produced, an inhibition time is evident before polymerisation may occur (Figure 3.5).

Figure 3.5 shows the growth curves obtained with gratings that have varying dye concentration but a relatively large concentration of TEA. The grating growth does not begin for at least 30 seconds after recording has commenced for each dye concentration indicating that it is preferable to use TEA in lower quantities.

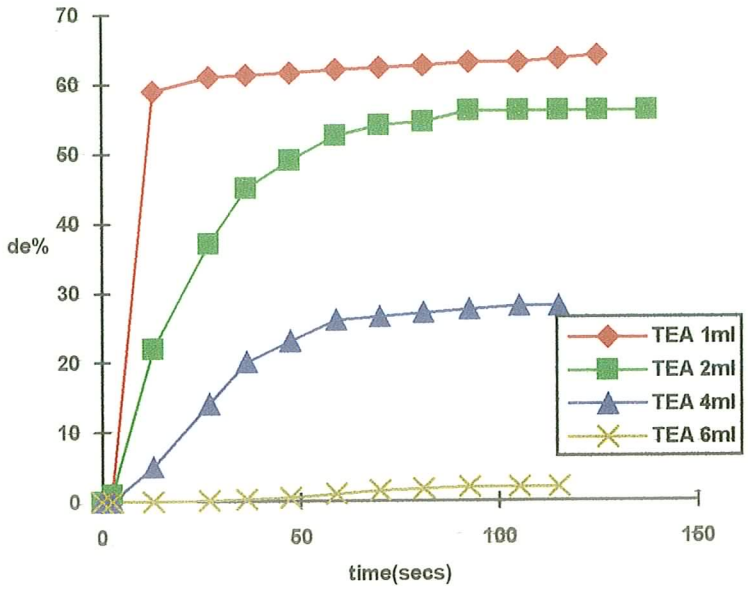

Figure 3.4 Graph of the effect on diffraction efficiency when the amount of TEA used is increased beyond the optimum conc. Dye; 2mg/total sample solution for this set of data.

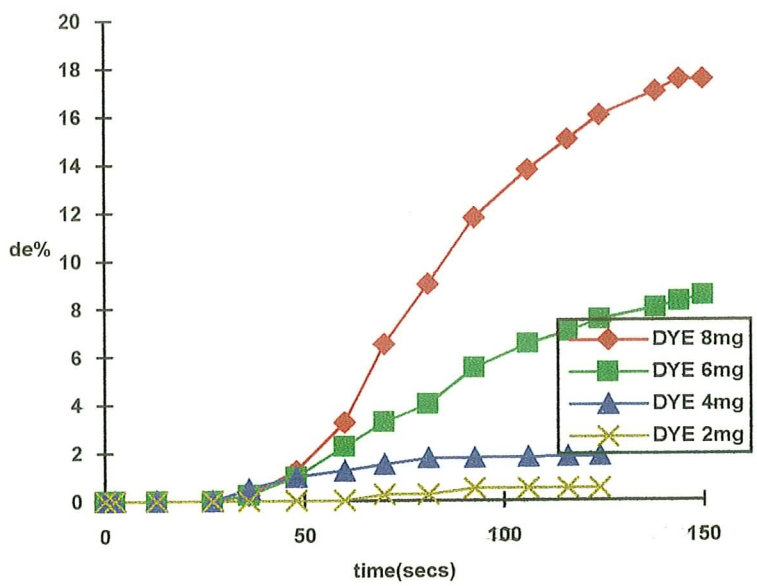

Figure 3.5 Graph illustrating evidence of an inhibition time. TEA; 6ml/total sample solution

Dye studies

Figure 3.6 shows the transmission curves for layers containing varying concentrations of dye. Note that for the layer containing the lowest concentration of dye initial transmission of incident light is 65%. At 200 seconds the layer is completely bleached even though the transmission maximum reads only 75%. This can be attributed in part, to losses due to reflection at the surfaces. As the concentration of dye continues to increase the initial transmission gets progressively smaller as expected. At the highest dye concentration, at 0 seconds only 25% of the incident light has penetrated the layer. After 200 seconds the transmission is 62%.

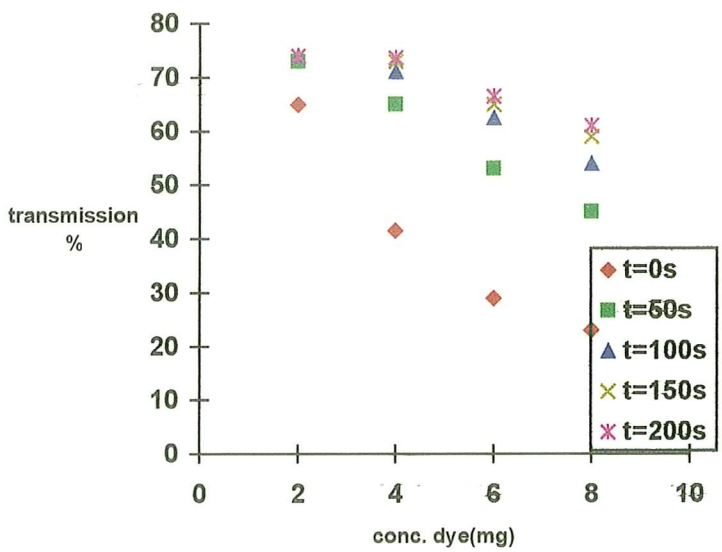

Figure 3.6 Graph illustrating the decrease in light transmission when dye content is increased. TEA;1ml/total sample solution for this set of data.

The layers comprising the optimised formula produced gratings with 70% diffraction efficiency in 25 seconds at a total beam power of 5.5mW/cm^2. Thus sensitivity was

approximately 130mJ/cm^2 (Figure 3.7). The grating growth rate is approximately 2.8% per second for the most linear part of the graph. The optimum dye concentration was identified as being 4mls in 25 mls of sample solution. (The results for 2mls were less consistently good than for the higher concentration).

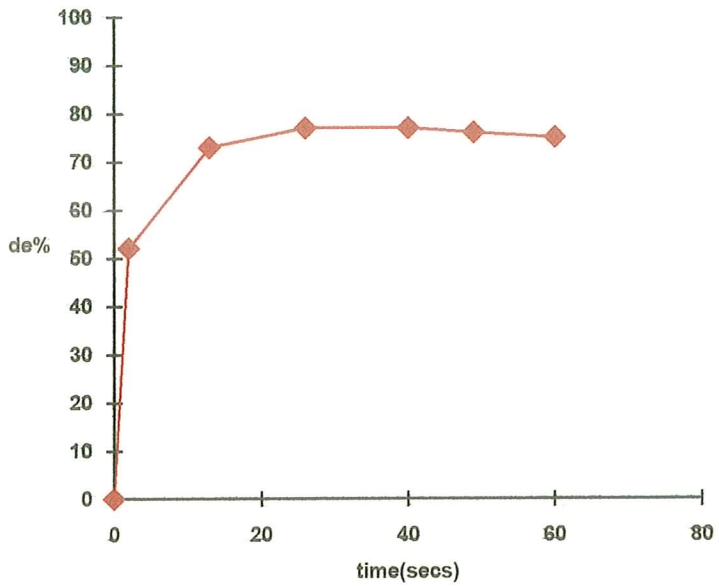

Figure 3.7 Growth curve illustrating the maximum diffraction efficiency obtained using the optimised formula.

The optimised formula is shown in Table 3.1. Holograms recorded with the optimised formula were shown to need relatively low exposure energy (120mJ/cm^2) to produce high diffraction efficiencies of 70%.

It has also been shown that the permeability of the binder can be affected if the balance between the material components is not correct. This is particularly true of

TEA as this component is present in high concentrations within a dry layer. Further study into the roles of both TEA and binder can be found in subsequent chapters.

Component	*Concentration/25mls*
Acryamide	0.6g
M/bis-acrylamide	0.2g
Triethanolamine	2ml
Methylene blue	4mg
Poly(vinyl)alcohol	10% solution, 18mls of

Table 3.1 Optimised red-sensitive formula

Now that optimisation of the material is complete, it is now appropriate to introduce the principles of holographic recording.

3.3 Introduction to Holography

In conventional photography, when the image of an object is recorded in a suitable medium, only the intensity of light from each point on the object is recorded. The information contained in the light waves from the object, concerning the relative spatial position of each point on it is lost. This information is necessary to give the

appearance of depth and perspective to the image, in other words to make it three-dimensional.

Holography is a technique which preserves all the relevant information contained in the light waves from an object, in order to reconstruct a three dimensional image of that object.

3.3.1 Holographic recording

A typical set-up for holographic recording is shown in Figure 3.8. Highly coherent, collimated light from the laser is divided so as to produce a reference wave and to illuminate the object, creating an object wave. In the plane of the photosensitive medium the two waves interfere producing a highly complex interference pattern. After development of some type has occurred, the result is a hologram. Figure 3.9 shows the reconstruction stage, where the original reference wave is used to illuminate the hologram and is diffracted by the recorded interference pattern so as to form an image of the object. The process may be explained mathematically in simple terms as follows[88].

The object wave is represented as

$$a(x,y)\ \exp[j\phi(x,y)] \tag{3.1}$$

where a(x,y) is the wave amplitude and $\phi(x,y)$ is its phase. The reference wave is represented by

$$b \exp[-jky\sin\theta] \tag{3.2}$$

travelling at an angle θ to the normal to the photosensitive plate, which is positioned so that the object and reference waves overlap in its plane.

The total field distribution in the plane of the medium due to interference of the two waves is represented by

$$a^2 + b^2 + ab \exp[j(\phi(x,y)) + ky\sin\theta] + ab \exp[-j(\phi(x,y)) + ky\sin\theta] \tag{3.3}$$

If the plate is processed so that the *amplitude transmittance* is proportional to the original illuminating intensity distribution then illumination of the resulting amplitude hologram with the reference beam will yield an expression for the output light amplitude given in Equation 3.4.

$$b(a^2 + b^2) \exp[-jky\sin\theta] + b^2\, a(x,y) \exp[j(\phi(x,y))] +$$

$$b^2\, a(x,y) \exp[-j(\phi(x,y) + 2ky\sin\theta)] \tag{3.4}$$

The first term is directly proportional to the reference wave and constitutes the zero order wave. The second term is directly proportional to the complex amplitude of the scattered wave from the original object. It contains the phase information, thus it is responsible for the reconstruction of a three-dimensional virtual image of the object, known as the orthoscopic image (Figure 3.9). The third term represents a conjugate version of the original object wave. If a wave conjugate to the original reference wave illuminates the hologram then a conjugate version of the original object is produced, represented by

$$b^2\, a(x,y) \exp\,[-j(\phi(x,y)] \tag{3.5}$$

Thus a real image of the object is produced in front of the holographic plate, known as the pseudoscopic or conjugate image.

The above treatment describes the production of an amplitude hologram where the amplitude transmittance of the hologram is proportional to the original illuminating intensity distribution. In the absence of monomer, the material described in this work can be used to record amplitude holograms. When monomer is included in the formulation, a refractive index modulation results, which is proportional to the intensity distribution thus producing permanent, phase holograms.

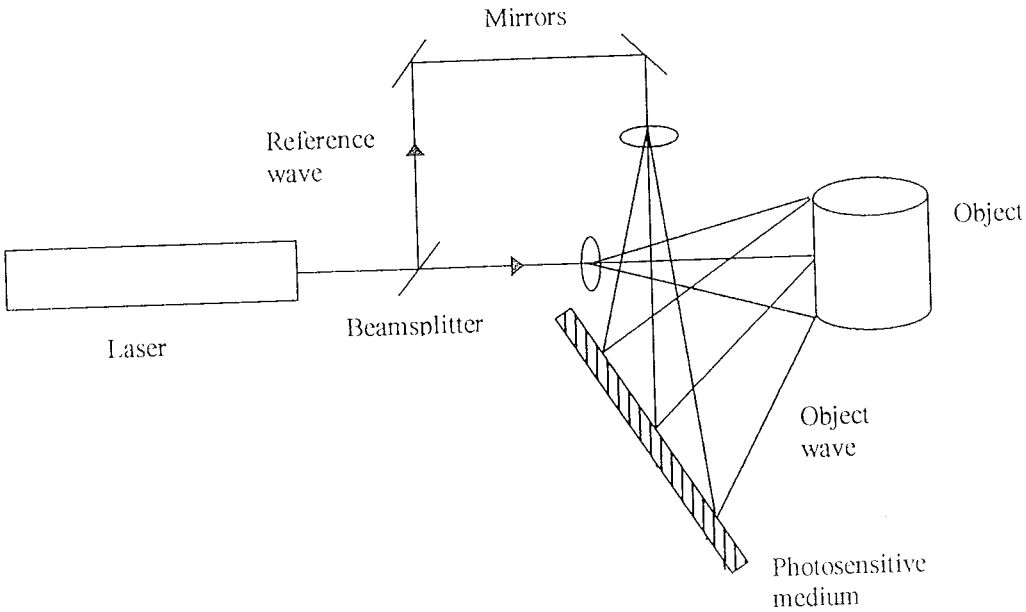

Figure 3.8. Experimental set-up for recording a transmission hologram

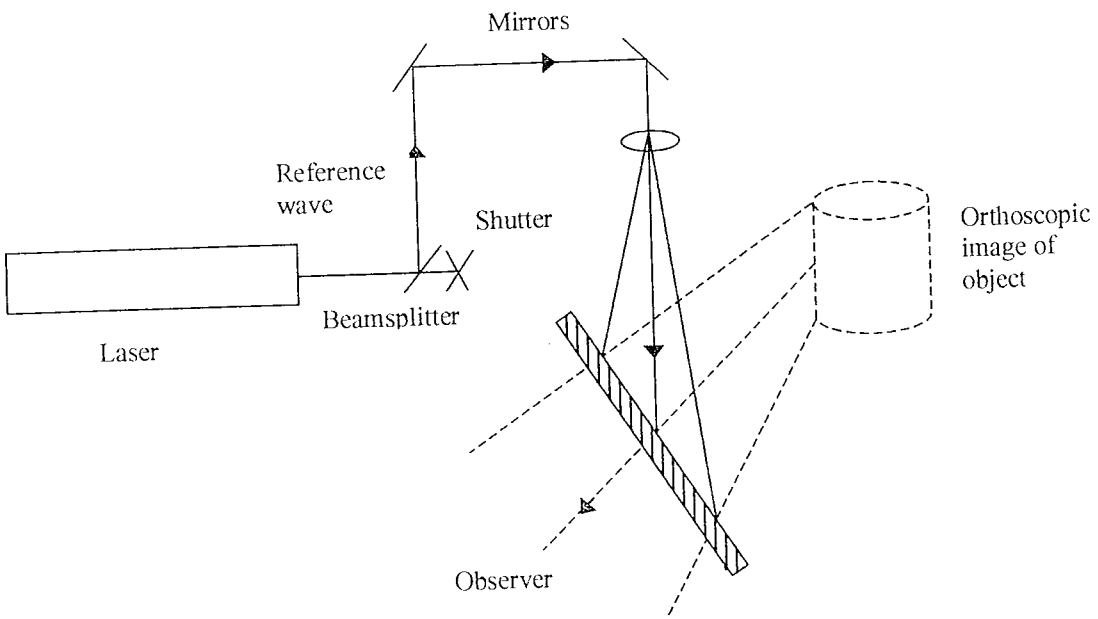

Figure 3.9 Reconstruction requires the illumination of the recorded hologram with the reference beam to produce an image of the object. An observer sees an image of the object through the hologram

3.3.2 Volume holography

In most experimental studies of holographic recording materials, the sample is exposed to an interference fringe pattern having a single spatial frequency of up to several thousand lines per millimetre (l/mm), producing a diffraction grating. Diffraction gratings are simple both to record and analyse as the light emitted in the diffraction orders is easily measured. For these reasons, the efficiency with which the gratings diffract incident light is a parameter that is used in a number of holographic techniques to provide valuable information for both optimisation and characterisation of the material. However, the actual physical thickness of a grating is important to quantify, as the reconstruction conditions of volume (thick) gratings are more stringent than those for the plane (thin) grating.

Figure 3.10(a) shows a reference beam incident on a plane grating. The object beam is also shown as a dashed line. The output is a diffracted wave produced in the direction of the object beam, where Y is an integer, in accordance with

$$\sin i + \sin \delta = Y \frac{\lambda}{\Lambda} \tag{3.5}$$

which is the well known grating equation[87]. According to equation (3.5) the light amplitude diffracted by each period of the plane grating adds in phase, to produce a maximum diffracted wave. Even if the wavelength of light incident on the grating is different to that used for recording it will be diffracted. It is also evident that the

larger the spatial period, the greater the number of diffracted orders that will result. However, the grating equation only produces information about the number of diffraction orders present and their spatial frequency.

The conditions for reconstruction of a volume grating are collectively known as Bragg's law

$$2\Lambda(\sin\theta) = Y\lambda \qquad (3.6)$$

This situation is shown in Figure 3.10(b).

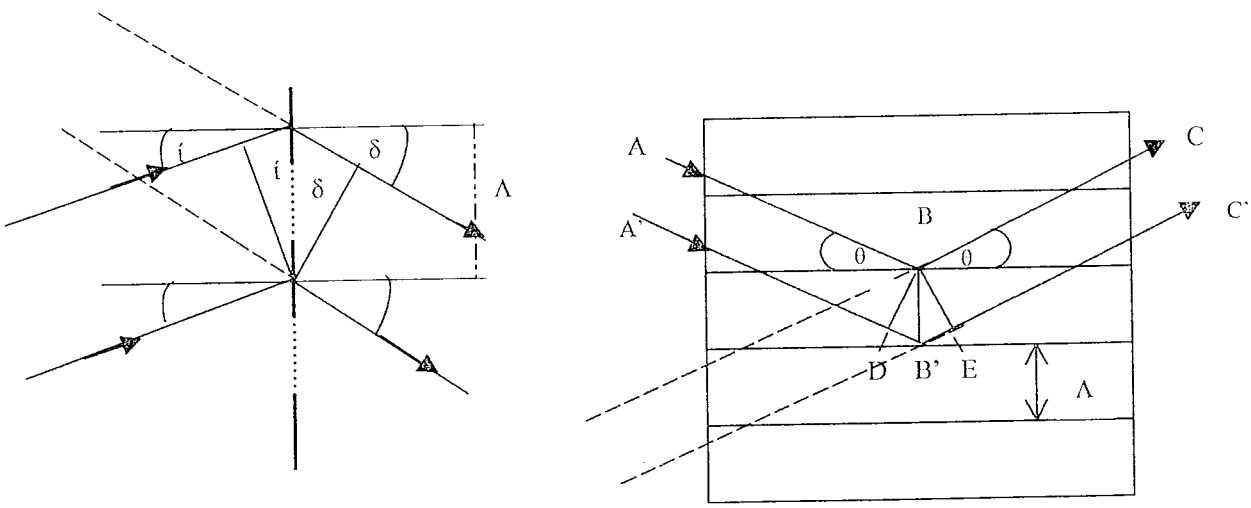

Figure 3.10(a) Grating equation: sin i + sin δ= Yλ/Λ *(b) Braggs law: DB' + B'E = 2Λsinθ =Yλ*

Gratings illuminated with one beam only. Dashed line indicates the second recording beam.

This condition is stricter than the grating equation. For any input angle, the grating equation predicts the existence of many diffraction orders over a wide range of output angles. If the wavelength of light incident on a holographically recorded volume

grating with fixed fringe width, is different to that used in recording, the angle of incidence of the reconstructing beam must be altered to satisfy Bragg's law. How the law may actually be applied in order to obtain information in the analysis of volume holograms is discussed in more detail in section 3.3.

The parameter Q[88] is frequently used to approximately distinguish between thick and thin gratings where

$$Q= (2\pi\lambda_{air}d)/n\Lambda^2 \qquad (3.7)$$

n is the refractive index of the medium, λ_{air} is the recording wavelength in air, d is the thickness of the medium and Λ is the fringe width of the grating. When $Q\leq 1$ a hologram can be regarded as thin, for $Q\geq 10$, thick hologram theory is appropriate. For all of the holograms recorded throughout this work, thick hologram theory was appropriate.

3.3.3 Coupled wave theory

As we have seen the record of the holographic interference pattern usually takes the form of a spatial modulation of the absorption constant or the refractive index of the medium, or both. Kogelnik's coupled wave theory[84] considers the properties of all these types of holograms. Of particular interest, is the efficiency with which thick

holograms can diffract incident light and the angular dependence of this diffraction efficiency as the incident light deviates from the Bragg angle.

The theory is based on a number of assumptions. The total field inside a thick grating can be described by two waves travelling through the grating, the reference and signal (diffracted) waves. Therefore, the higher orders produced by the grating are negligible. Energy is coupled slowly back and forth between these two waves as they travel through the grating, so that any second derivatives produced in the theory may be considered negligible also. Based on these assumptions, the theory yields a pair of coupled differential equations, which may be solved by applying appropriate boundary conditions. The boundary conditions differ according to the type of grating recorded.

The theory yields equations, which may be used to relate the diffraction efficiency of the grating to a number of parameters that may be experimentally determined. In the case of an unslanted, phase transmission grating it can be shown that the diffraction efficiency, η, can be expressed as

$$\eta = \sin^2\left(\frac{d\pi n_1}{\cos\theta_0 \lambda_a}\right) \tag{3.7}$$

where d, represents grating thickness, n_1, the refractive index modulation produced in the grating, θ_0, the angle of incidence and λ_a, wavelength of incident light in air.

This expression describes the diffraction efficiency of the grating when it is illuminated at the Bragg angle. However, the 'off-Bragg' parameter, ξ may be introduced which determines the diffraction efficiency of the grating in terms of angular deviation from the Bragg condition.

$$\eta = \frac{\sin^2(\nu^2 + \xi^2)^{\frac{1}{2}}}{(1 + \frac{\xi^2}{\nu^2})} \tag{3.8}$$

where $\nu = d\pi n_1/\cos\theta_0\lambda_a$

and $\xi = \frac{d\pi}{\Lambda \cos\theta_0}(\phi_1 - \theta_0)$

ϕ_1 represents the slant angle. (It is evident that when $\xi = 0$, Equation (3.8) becomes Equation (3.7).) Diffraction efficiency may be plotted as a function of the off-Bragg parameter in order to predict the angular response of a grating for small deviations from θ_0, for specific values of ν.

Figure 3.11 illustrates the angular response of a grating, with a diffraction efficiency of unity, (at the Bragg angle) corresponding to $\nu = \pi/2$. When this value for ν is exceeded the grating is said to be overmodulated, in terms of its refractive index, with the result that the power in the diffracted wave is coupled back into the reference wave. As the diffraction efficiency is a measure of the light in the diffracted beam this results in a decrease in the central peak and an increase in the side-lobes. Further over-modulation shows that the diffraction efficiency for the central peak drops to zero. The response of a grating with maximum modulation then subsequent over-modulation is illustrated in Figures 3.11(a), (b), (c) and (d), for varying values of ν.

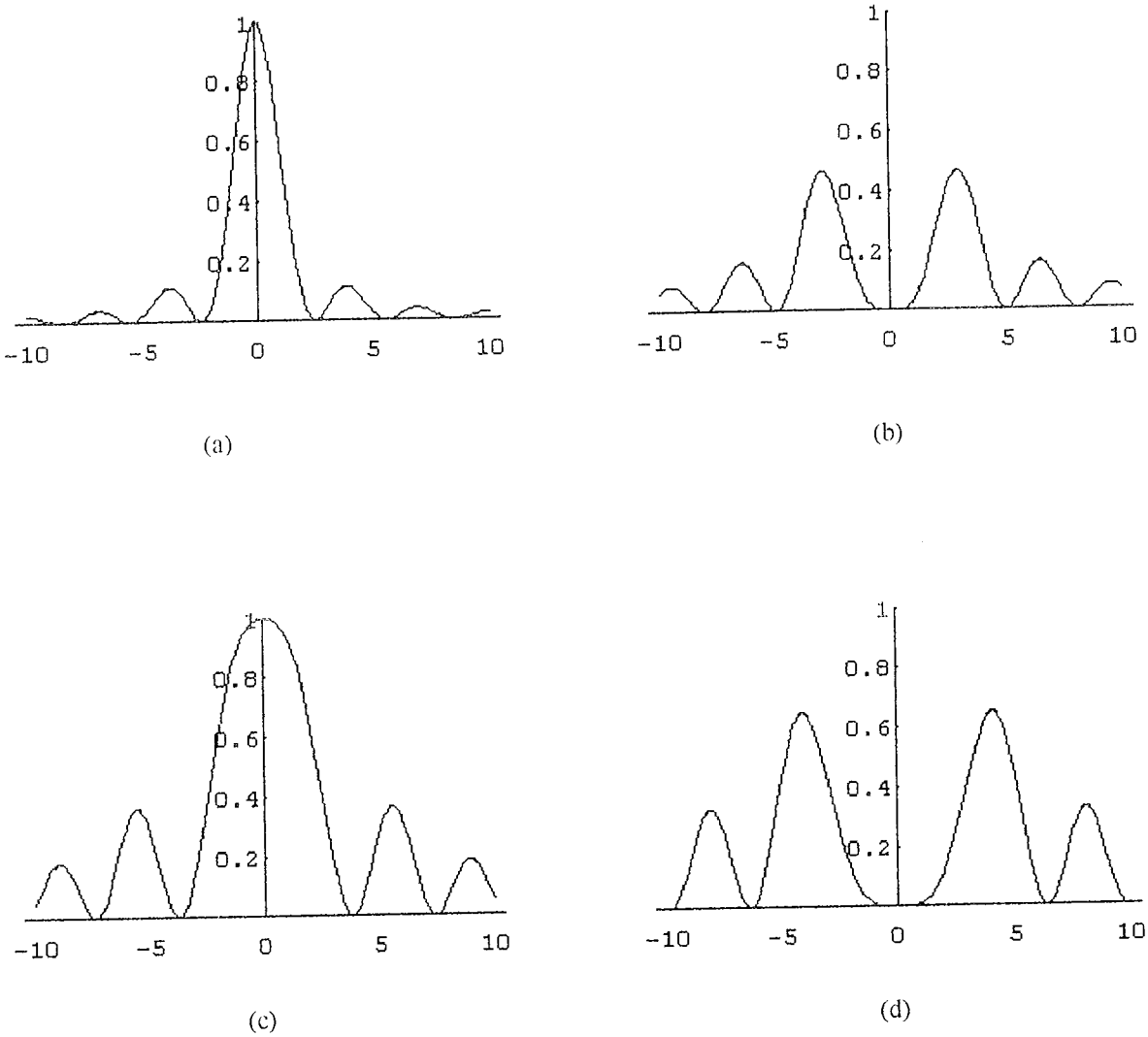

Figure 3.11 Theoretical curves illustrating effect of varying v parameter: (a) Maximum modulation at $v=\pi/2$. (b) Overmodulation at $v=\pi$. (c) $v=2\pi$. (d) $v=3\pi/2$.

Kogelnik's theory is particularly suited to the gratings recorded in this material because as the gratings are thick, the resulting diffraction efficiencies often approach unity. The usefulness of the theory for the prediction of the angular response of gratings to incident light has already been demonstrated.

The refractive index modulation for phase gratings can be easily determined under varying experimental conditions using equation 3.7, which relates diffraction efficiency, grating thickness, recording wavelength and the on-Bragg reconstruction angle. The characterisation study of the material, which is described next, involved the variation of the physical state of the photosensitive layers and recording conditions in order to determine the negative and positive attributes, as well as leading to further improvement of, the material.

3.4 Characterisation studies

In order to ascertain the practical value of a real recording material it is useful to compare it to an ideal, so that any limitations will become apparent. For this reason an outline of the behaviour of an ideal material will be given before presenting the results obtained with this material. Collier, Burckhardt and Lin[11] have outlined the characteristics required for an ideal recording material and the following studies are based on these characteristics.

3.4.1 Exposure and Sensitivity

For comparison, one holographic recording material is more *sensitive* than another if, for fixed illumination conditions, less exposure is required to produce a hologram of specified diffraction efficiency.

For practical purposes, the exposure of a material is usually defined as

$$E' = Pt_eA \tag{3.9}$$

where P is the recording power incident on the recording area, t_e is the recording time and A is the area of the photosensitive plate which is being exposed.

The sensitivity (S) of a recording material is related to the exposure by the expression

$$\sqrt{\eta} = S\,E'\,V \tag{3.10}$$

It is easy to see that for an ideal recording material, a graph of $\sqrt{\eta}$ vs V with E' as the variable should be perfectly linear. A plot of $\sqrt{\eta}$ vs E' with V as the variable should yield a similiar response. Figures 3.12 and 3.13 show the graphs expected for the ideal recording material. For real materials the range of beam ratio for which hologram recording is linear is indicated by the extent of the linear section of their $\sqrt{\eta}$ vs V curve. For a constant beam ratio the sensitivity required in order to obtain a specific diffraction efficiency can be obtained from the plot of $\sqrt{\eta}$ vs E'.

Departure from linearity of response is an inherent drawback in most real recording materials. Most will only exhibit linearity up to a certain point, which is usually for quite low diffraction efficiencies. The response of our recording material has been

studied in relation to the parameters contained in equation 3.7. as well as other physical aspects of the material.

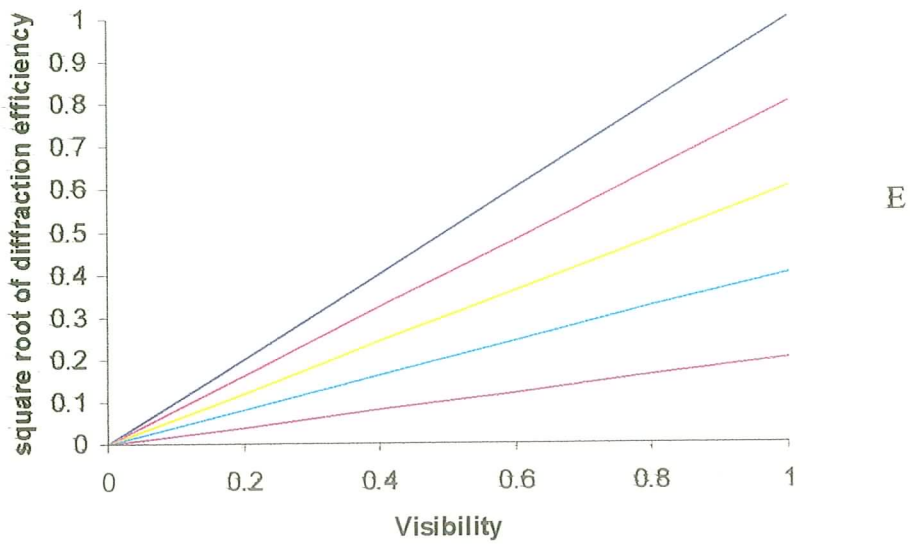

Figure 3.12. A plot of $\sqrt{\eta}$ *vs V with* E' *as the parameter for the ideal holographic recording material.*

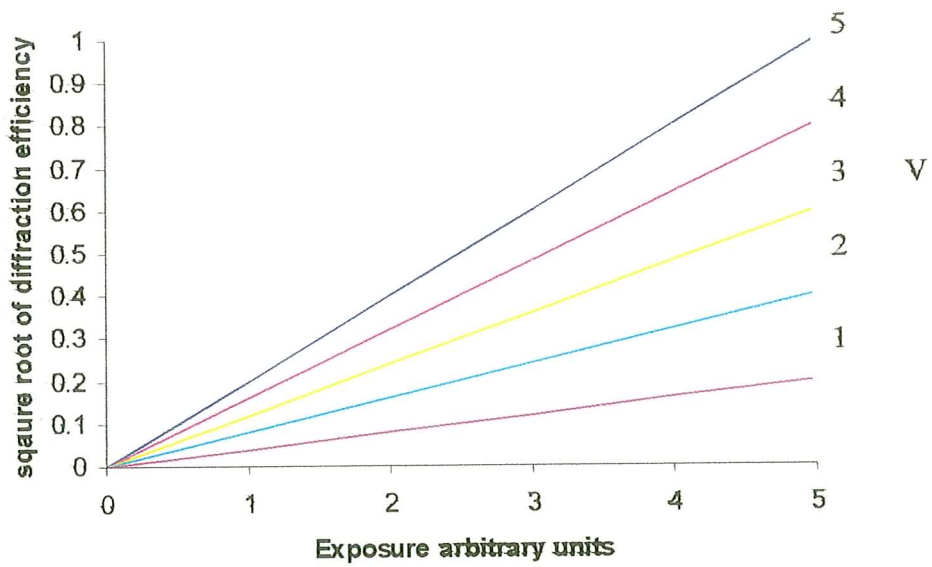

Figure 3.13 A plot of $\sqrt{\eta}$ *vs* E' *with V as the parameter for the ideal recording material.*

3.5 Experimental

Gratings were recorded and the rate of growth in diffraction efficiency obtained for each using the technique described in section 3.3.2. The angular response of each grating to incident light, shown as a variation of its diffraction efficiency (Bragg curves) was generated using a specifically designed program written in Microsoft Excel, which was based on Kogelnik's theory.[89] Theoretical and experimental Bragg curves were generated using the program for each grating. The experimental response is the blue line.

3.5.1 Set-up for analysis

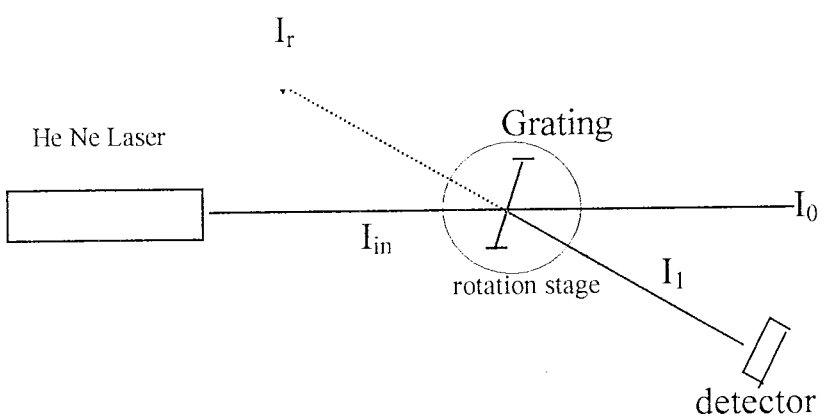

Figure 3.14. Set-up for angular response of grating to incident light.

To experimentally measure angular response, a grating was positioned on a calibrated rotation stage so that the incident probe beam was satisfying the Bragg condition. The

incident power, I_{in}, the light in the zero and first orders, I_0 and I_1 and the reflected light from each grating were then measured using the photodetector which was placed at the first order position.

Experimental parameters were varied systematically, the optimum value in each case being retained as standard. For all experiments spatial frequency was set at 870lines/mm (fringe width 1.15μm) except when the parameter under investigation was spatial frequency response.

3.6 Results

For each set of gratings recorded, growth curves or diffraction efficiency measurements were obtained. Kogelniks theory was used to calculate refractive index modulation corresponding to each set of experimental parameters.

3.6.1 Layer thickness

The first characterisation study was carried out by varying layer thickness. This is an important factor as if a layer is too thick an incomplete recording of a grating may result, which will lower the resulting diffraction efficiency. The experimental layers for this study were prepared using the optimised coating solution described in section 3.2.3. The amount of coating solution used varied from 0.6ml to 3.0ml to give layers of different thickness. A graph of maximum diffraction efficiency versus amount of

coating solution is shown in Figure 3.15. It is evident from the scatter of points on the graph that some error is introduced by the method used to deposit material on substrates. The maximum error is usually approximately 10% and in most cases much less than this. Experiments are always repeated to ensure validity of results as an added precaution.

2mls per glass slide (2 x 21/2 inches) generated the highest diffraction efficiency. This value corresponded to a dry layer thickness of 60μm.

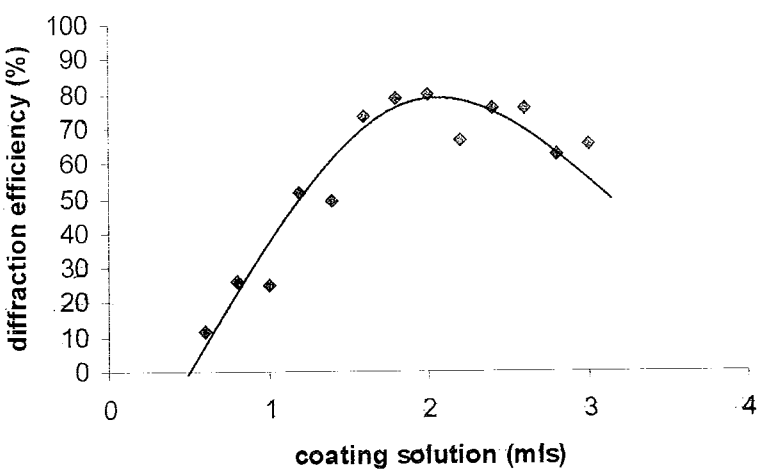

Figure 3.15. Maximum diffraction efficiency obtained with varying layer thickness

The Bragg curve for a grating recorded in a dry layer of the optimum layer thickness of 60μm is shown in Figure 3.16. Note how the maximum diffraction efficiency of 65% drops by half with less than one degree deviation from the Bragg angle. This

demonstrates the angular selectivity of the grating. The experimental curve is in good agreement with the theoretical curve.

For comparison, Figure 3.17 is shown which is a plot of the angular response of a grating of 21μm thickness and fringe spacing of 1.15μm to incident light. The angular response is quite broad due to the comparatively thin nature of the layer so light is distributed into higher diffraction orders. This results in the maximum diffraction efficiency observed in the first order being very low at 12%. At approximately 4 degrees rotation the value of the diffraction efficiency has only dropped by half its maximum value.

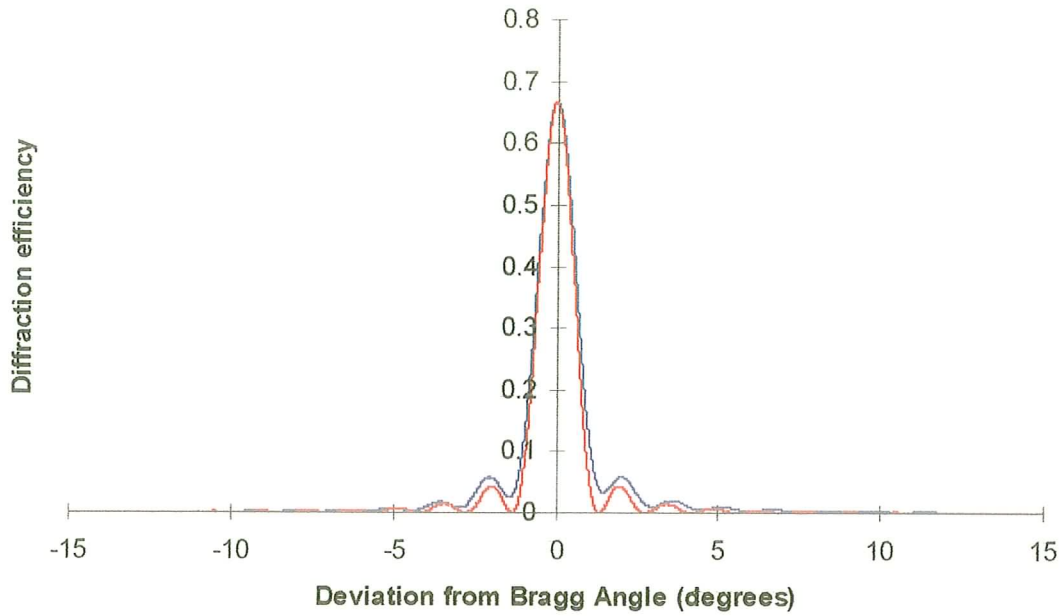

Figure 3.16 The angular response of a grating of 60μm thickness to incident light.

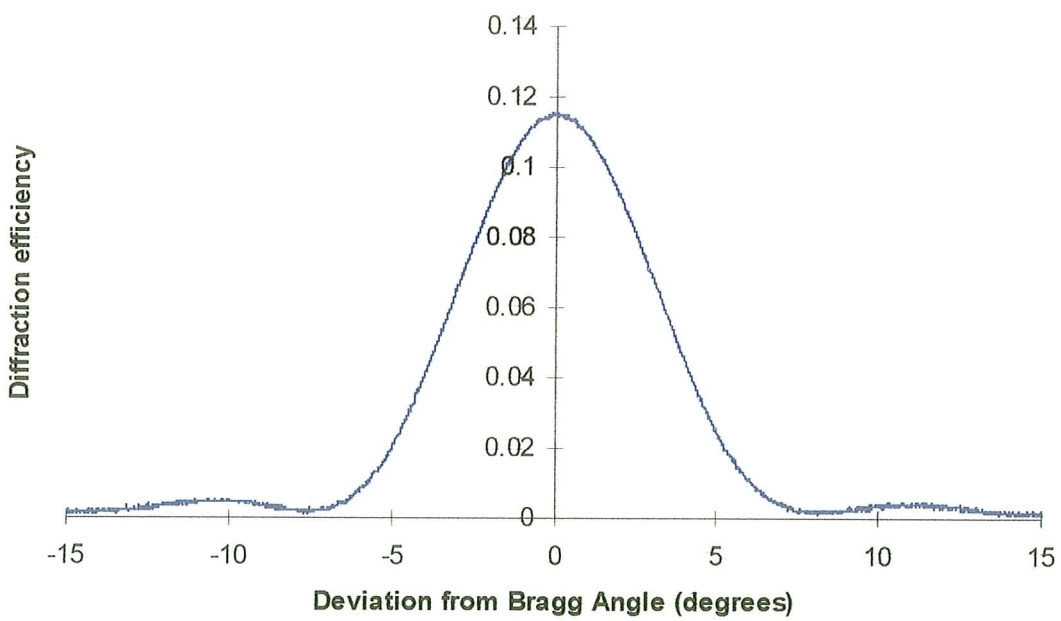

Figure 3.17 The angular response of a grating of 21μm thickness to incident light.

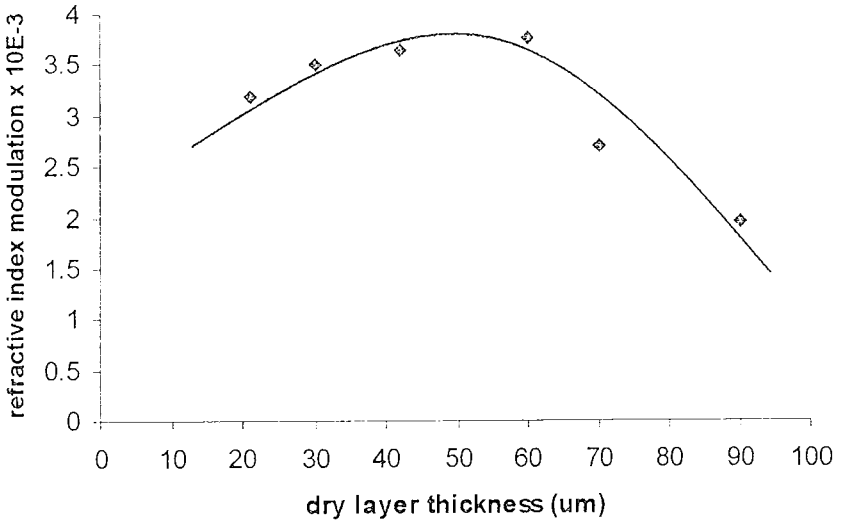

Figure 3.18 Refractive index modulation for varying dry layer thickness

Figure 3.18 indicates that the calculated refractive index modulation decreases as the layer thickness is increased. This can be explained by the incomplete recording of gratings as the recording beams are increasingly attenuated before they can penetrate through the entire layer depth.

It was concluded from this study that 60μm was the optimum layer thickness for recording and subsequent layers were prepared at this thickness.

3.6.2 Beam Intensity

In practice, the rate of growth in diffraction efficiency is used to monitor the materials response to different experimental parameters, as it is readily obtained during grating recording. Materials may also be characterised by their exposure energy. Both diffraction efficiency growth curves and exposure energy values are shown below for

varying beam intensities. This study was conducted in order to examine the material response to relatively low levels of light. A Helium-Neon laser typically operates at low power unlike Argon or pulsed Ruby lasers.[90] The material does respond well to low powers but some degree of compromise is needed between exposure time and diffraction efficiency.

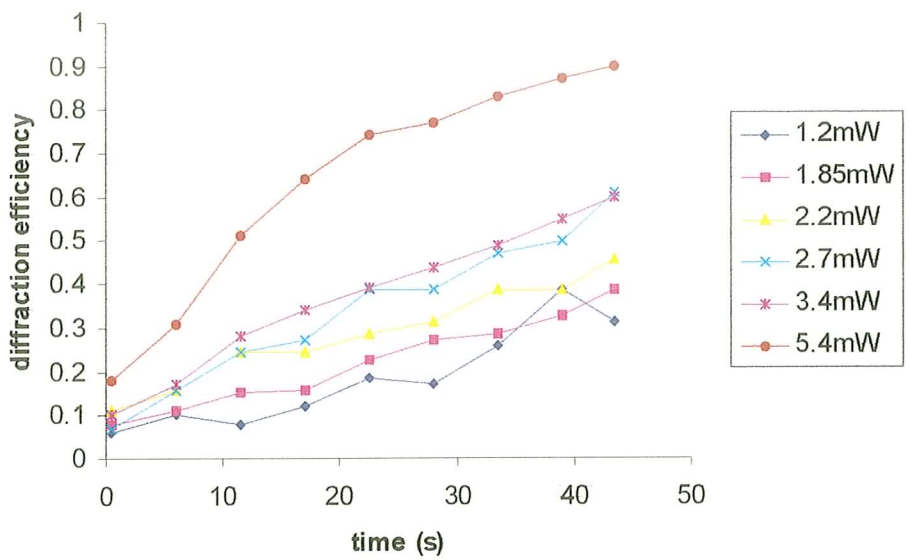

Figure 3.19 Growth curves shown for varying beam intensity.

Figure 3.19 shows the growth of diffraction efficiency as a function of time for gratings that have been recorded with different combined beam powers. As expected, the highest combined recording power has produced the highest diffraction efficiency. However, the results also indicate that even at relatively low powers, (see the growth

curve for combined power of 1.85mW/cm^2 in Figure 3.19), the response of the material is good although the final diffraction efficiency is only approximately 30%.

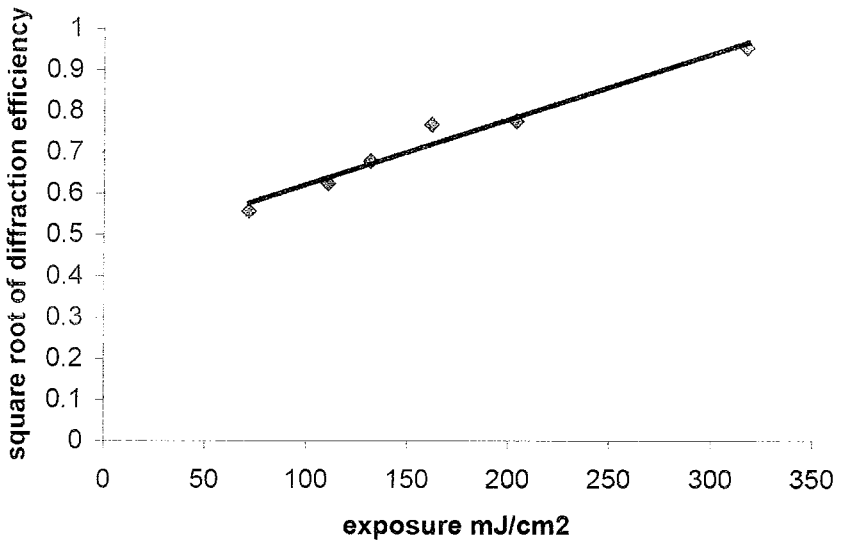

Figure 3.20. Graph of $\sqrt{\eta}$ - E' for V of 1. (Exposure values were calculated using the intensity values represented in Figure 3.19 for a constant exposure time of 60 seconds). Spatial frequency is 400 lines/mm.

Figure 3.20 represents the materials response at a spatial frequency of only 400 lines/mm. The diffraction efficiencies which were obtained for gratings recorded at this low spatial frequency were surprisingly high. The linearity of response is also good compared with that for the ideal recording material at V =1 in Figure 3.13.

It has been shown that the material responds well even at low beam intensity. Even though the highest beam intensity (5.4mW) produced the best response it is unusual that it would be this high in practice. A short collimating lens which limits the beam

diameter, was used in the set-up to produce this high intensity. The next highest intensity of 3.4mW still produced a good response and as it is a more realistic practical value, it was used in subsequent studies.

3.6.3 Beam ratio

High contrast or large modulation depth between fringes in an interference pattern implies that the amplitude of the spatially varying cosine term is large in comparison with the spatially constant term. High contrast in the interference pattern implies bright images. Contrast is specified by the parameter V where

$$V=\frac{2\sqrt{R}}{1+R} \tag{3.11}$$

and R is the ratio of intensities of the two beams measured in the plane of the interference pattern. It is therefore essential to ensure that the recording conditions are optimised to produce a high contrast interference pattern.

Figure 3.21 shows the diffraction efficiencies obtained when the beam ratio was varied. Note that at a beam ratio of unity the value of diffraction efficiency is lower than predicted. One would expect that as the fringes in the interference pattern are at maximum contrast, the diffraction efficiency would be approximately 100%. When the angular response of the grating in question was obtained, it became obvious that

over-modulation of the grating during recording had caused the spurious result. The angular response of the grating, is shown below in Figure 3.22.

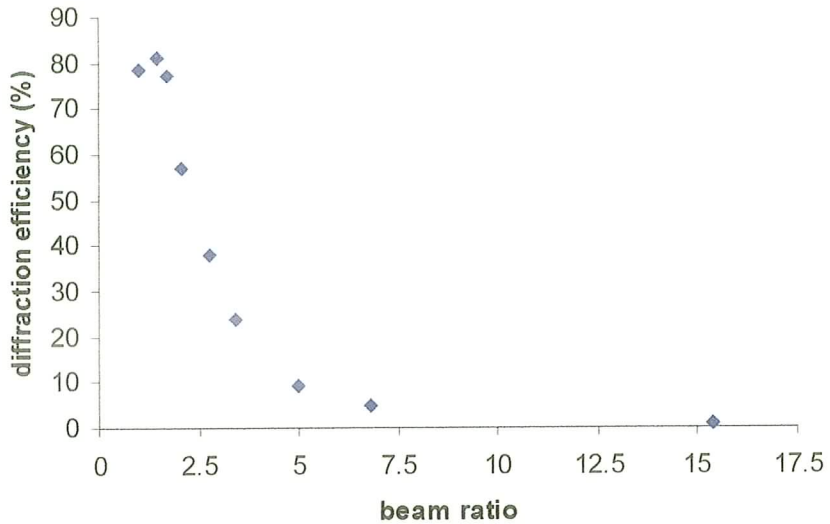

Figure 3.21 Maximum diffraction efficiency for varying beam ratio

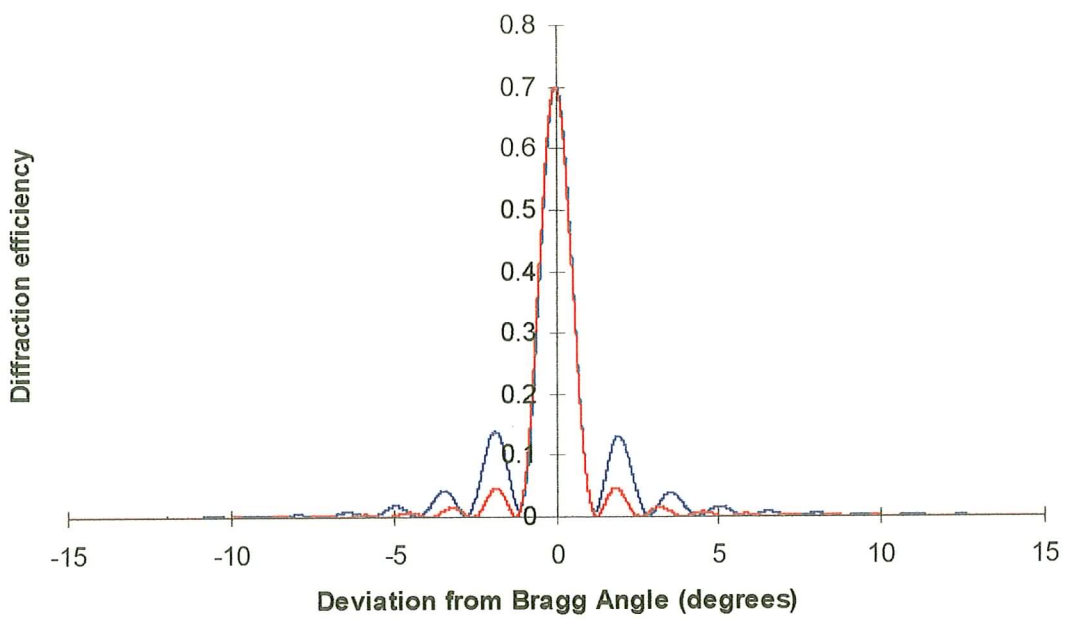

Figure 3.22 Angular response of over-modulated grating at a beam ratio of 1:1

Recall that the red line represents the theoretical response whilst the blue line is the experimental one. A clear indication that over-modulation has occurred is the characteristic elevation of the side lobes relative to the central peak as described in section 3.3.4. The results plotted in Figure 3.21 were converted to square root of diffraction efficiency and visibility values in order to test linearity of response. As can be seen in Figure 3.23 the relationship between the two parameters is linear over a broad range.

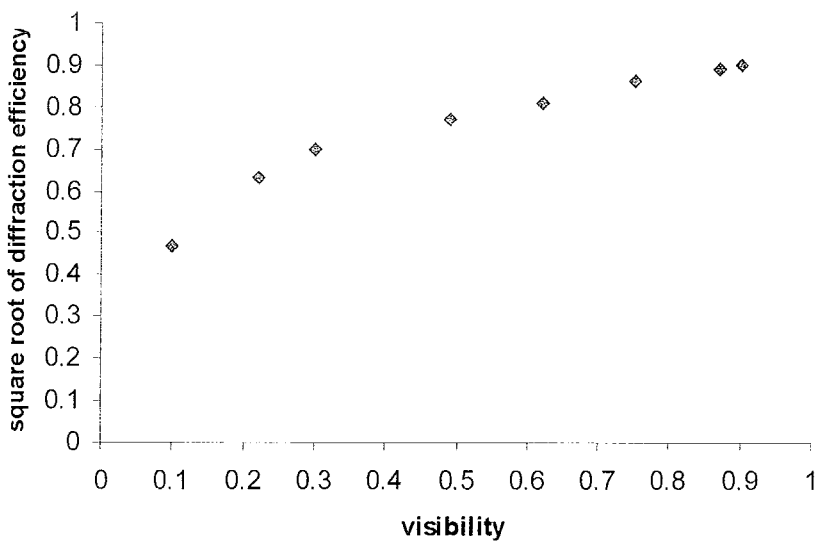

Figure 3.23. Square root of diffraction efficiency plotted as a function of the visibility parameter.

It may be concluded from this section that when recording holograms the ideal beam ratio is approaching unity.

3.6.4 Spatial frequency response.

For accurate reconstruction of holographic images an ideal recording material should respond equally to all spatial frequencies in the interference pattern. High spatial frequency gratings are desirable for high dispersion of light but a wide spatial frequency range is particularly important for holographic applications such as Holographic Optical Elements (HOEs) which incorporate many. For most real materials a graph of diffraction efficiency versus spatial frequency of the recorded grating will show that the response is essentially constant up to a certain cut-off spatial frequency above which the material response decreases rapidly. This cut-off is usually quoted as the maximum resolution of the material.

In order to determine the spatial frequency range of this material, gratings were recorded for a range of inter-beam angles and the resulting diffraction efficiencies noted. The maximum diffraction efficiency of each grating was dependent on its spatial frequency as expected for a real recording material. An exposure of 200mJ/cm^2 (60s x 3.4mW) was used and the spatial frequency was varied from 300 lines/mm up to 2500 lines/mm. As can be seen from Figure 3.24 the optimum response is at about 400 lines /mm with the diffraction efficiency dropping to half the maximum value at 350 lines/mm and 1200 lines/mm.

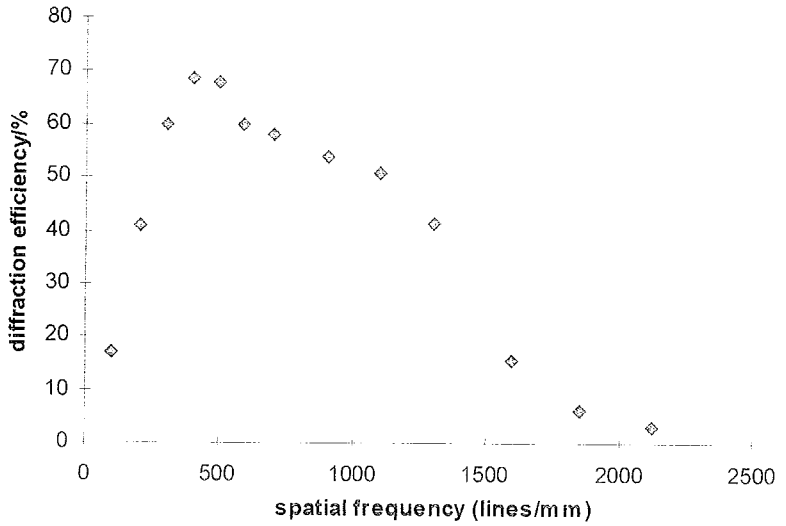

Figure 3.24 Diffraction efficiency as a function of spatial frequency

When the spatial frequency range was compared with that for the green-sensitised version of the material it was found that the maximum resolution attained was considerably different. For the green-sensitised version of this material the corresponding spatial frequency response curve indicates that the peak response of the material is between 1200 and 1400 lines/mm. At 500 lines/mm the diffraction efficiency is approximately 60%.

It has been seen that recording with higher beam intensity increases the overall diffraction efficiency so recording with the more powerful Argon ion laser could account for the higher diffraction efficiency attained with the green material.

However, this factor alone cannot account for the difference in the range of spatial response.

Essentially, the only difference between the two materials is the class of dye used for sensitisation. It is known that the molecular structure of xanthene dye molecules[91] is much bulkier than that of thiazine with additional aromatic sites. It is thought that one reason for the better response at low spatial frequency could be due to the smaller methylene blue molecules diffusing more rapidly over larger fringe widths to participate in the recording process, whilst the larger xanthene molecules would be slower to diffuse where they are needed. The following chapter describes the study that was carried out in an attempt to establish the occurrence of dye diffusion.

It was concluded that the optimum response of the red-sensitised material is approximately 400 lines /mm and the range of the material is somewhat limited, as the upper spatial frequency limit is only approximately 2000l/mm.

3.7 Conclusions

Optimisation of the material formulation was completed. Holograms were recorded with the optimised formula were shown to need relatively low exposure energy ($120mJ/cm^2$) to produce diffraction efficiencies of approximately 70%.

It has also been shown that the permeability of the binder can be affected by the concentration of TEA in the material formula. A more detailed study of binder permeability can be found in Chapter 4.

The suitability of Kogelnik's coupled wave theory for analysis of holographic gratings was demonstrated. The refractive index modulation of gratings recorded under different experimental conditions was seen to vary and optimised conditions could be determined as a result.

The material response was compared to that of an ideal recording material by varying parameters such as recording beam ratio. The spatial frequency response of the material for red-sensitisation was shown to vary from that of the green-sensitised material which has been already developed in the laboratory. A more detailed study into the possible diffusion of dye molecules is conducted in the next chapter. The binder is also studied to examine its role in more detail.

4. Diffusion studies

In the previous chapter it was explained how the material was optimised to improve its overall performance during holographic recording. The material has also been characterised. This chapter is concerned with a more detailed study of the physical processes that occur during holographic recording.

4.1 Introduction

Various hypotheses for explaining the mechanism of refractive index modulation in photopolymers during holographic recording have been proposed by several authors.[53,55, 92-94] The generally accepted basis of these theories, is that diffusion of monomer occurs from dark unexposed areas in a hologram to exposed areas during recording, resulting in a spatial density modulation. However, it is extremely difficult to monitor this process effectively as there are many components present to consider and the diffusion distance is typically small. If it were possible to establish evidence of diffusion of an isolated component, then this would aid in the understanding of the physical processes that occur in the material.

Normally this material responds to an optical interference pattern by changing both its absorption characteristics (as dye is bleached) and its refractive index (as polymerisation of the monomer occurs). In this way, amplitude gratings may be recorded even in the absence of monomer. If it can be shown that the absorbing dye

molecules are capable of diffusion over a fringe width, then it can be said that an amplitude grating (or transient grating) will disappear with time as the amplitude modulation decreases. A more detailed investigation of this observation is the main theme of this chapter.

In order to record transient gratings, the material was modified so that no monomer was present and a highly reduced amount of TEA was used. The work was carried out using the holographic grating relaxation technique (HGRT).

4.1.1 The Holographic Grating Relaxation Technique.

The holographic grating relaxation technique has become well known in recent years as a means to measure the slow translation diffusion coefficient of photoreactive organic dye molecules dissolved in amorphous solid-state polymer hosts.[95-97] The main advantage of the technique is that it shortens diffusion distance to the order of an optical wavelength thus decreasing the typically long measuring time associated with this type of experiment.

The period (Λ) of a grating induced at a recording angle (in air) of approximately 20^{o} with light of wavelength 633nm, is 0.9μm. Diffusion of molecules over distances shorter than $\Lambda/2$ can be detected, as movement of these molecules will decrease the amplitude modulation of the recorded grating and cause a decrease in diffraction efficiency. This decrease in diffraction efficiency can be directly measured and is a

function of how fast the molecules can diffuse through the medium. From this rate of decrease in diffraction efficiency the diffusion coefficient of the molecules can be calculated.

A model has been formulated based on the technique described above for the case of amplitude gratings recorded in this material. The model is based on Fick's laws of diffusion[98] and Kogelnik's description of the diffraction efficiency of amplitude gratings. It is described in Section 4.2.4.

4.1.2 Physical factors which may influence diffusion

From the brief description of amplitude gratings recorded in this material, it is clear that monitoring the subsequent post-recording decay is a highly suitable method of measuring the diffusion coefficient of the dye. However, the rate of transport of the dye molecules depends very much on the physical state of the medium through which they move. In the case of this material, the amount of TEA present and the physical state of the PVA binder would affect that rate. With this in mind, a study of both of these components was also conducted and is described later.

The current understanding of the behaviour of dye molecules, during the photochemical processes, both in the presence and absence of monomer has already been discussed in detail in Chapter 2, Section 2.7.1. Dye bleaching is briefly reviewed below, as it is the main mechanism involved in amplitude grating recording.

In the absence of monomer, the dye is converted to its leuco or colourless state by extracting 2 hydrogens from the TEA for each molecule of dye. This reaction is often called photobleaching. It is by this method that an amplitude grating can be recorded as the grating will have regions of high and low absorption of light in bleached and unbleached regions respectively. This is a transient process and when recording ends, the grating efficiency will immediately start to decrease. The decrease is thought to be primarily due to diffusion of the unreacted dye into the bleached areas, which effectively levels out the absorption modulation. The theory below contains a description of the recording of an amplitude grating.

4.2 Theory

The recording of an amplitude grating [11] is described briefly below before deriving the diffusion equation. A mathematical model based on the diffusion equation is then derived to produce an equation that may be applied to experimental results to prove diffusion of dye.

4.2.1 Amplitude gratings

Two coherent waves, with light intensities I_R and I_O respectively overlap in the plane of a photosensitive layer. Both are plane waves therefore the resulting interference pattern is a cosine modulation of intensity I (x) in the x-direction across the sample,

$$I(x) = (I_R + I_O)\left[1 + VCos\left(\frac{2\pi x}{\Lambda}\right)\right] \qquad (4.1)$$

where $V = 2\sqrt{I_R I_O} / I_R + I_O$

If the intensities of the beams are equal, then V equals unity and an interference pattern with maximum contrast between dark and bright fringe regions is generated.

If, as in the case of the material in this study, the sample contains molecules that are photochemically sensitive to the incident light, then the chemical properties of these molecules will change. This change manifests itself as an absorption modulation in the material, due to the presence of dye molecules. The dye molecules in the bright fringe regions lose their ability to absorb red light when the incident recording light causes them to be bleached. Therefore when a grating is recorded there is an absorption modulation created in the material between light and dark fringe regions produced by the interfering light beams. This type of grating is known as an amplitude grating as the amplitude of the light passing through it will be modulated due to the absorption modulation between light and dark fringe regions.

Kogelniks coupled wave theory describes the diffraction efficiency (η) of an unslanted absorption grating with thickness (d) as

$$\eta = \exp\left(-\frac{2\alpha d}{\cos\theta}\right) sh^2\left(\frac{\alpha_1 d}{2\cos\theta}\right) \qquad (4.2)$$

where α is the absorption constant and α_1 the amplitude modulation produced in the grating.

The diffracted amplitude increases with α_1, but since negative values of absorption are excluded, $\alpha_1 \leq \alpha$. and so the highest diffraction efficiency possible for an absorption grating is for the limiting case $\alpha_1=\alpha$.

If this maximum value of α_1 is used in Equation 4.2 and the diffraction efficiency of the grating is maximised with respect to $\alpha_1 d/\cos\theta$, then it has been shown that the maximum diffracted wave amplitude corresponds to a value of $\alpha_1 d/\cos\theta = \ln[3]$. Therefore, the maximum theoretical diffraction efficiency attainable in an amplitude grating is 3.7%.

4.2.3 The theory of diffusion

A transport property of a substance is its ability to transfer matter, energy or some other specified property from one place to another.[98] The hypothesis proposed here involves dye molecules within a polymer matrix diffusing down a concentration gradient induced by the recording of a holographic grating. They will continue to diffuse until uniform concentration is reached.

This diffusion is a transport property, which may be measured by its flux J, which is defined as the amount of that property, (in this case, the number of dye molecules) passing through unit area per unit time. For our case, the flux of matter J_x diffusing parallel to some axis x is proportional to the concentration gradient along that axis:

$$J_x \propto \frac{dN}{dx} \tag{4.5}$$

where N represents the number density of the molecules.

This relation is also known as Fick's first law of diffusion. If $J_x > 0$, the flux is towards increasing x, if $J_x < 0$ the flux is towards decreasing x. Matter flow will usually occur down a concentration gradient so if $dN/dx < 0$, J_x is positive as illustrated in Figure 4.1. This means that the constant of proportionality must be negative and is denoted -D. where D is referred to as the diffusion coefficient. Fick's first law then becomes

$$J_x = -D\frac{dN}{dx} \tag{4.6}$$

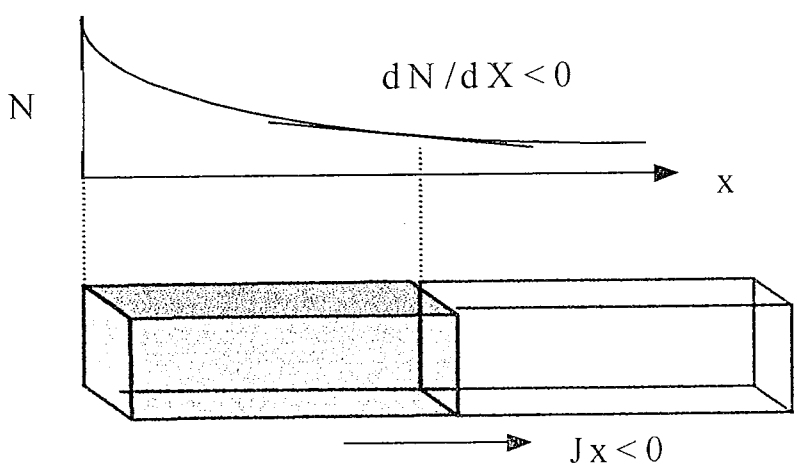

Figure 4.1 Diagram of increasing flux

Fick's law for particle flux in moles of molecules per unit area per unit time may be written as

$$J = -D\frac{dc}{dx} \tag{4.7}$$

where dc/dx represents the molar concentration gradient. This relation now must be expanded in order to take account of time-dependent diffusion processes. The aim of this is to obtain an expression that may be applied to the rate of change of the concentration of particles in an inhomogeneous region.

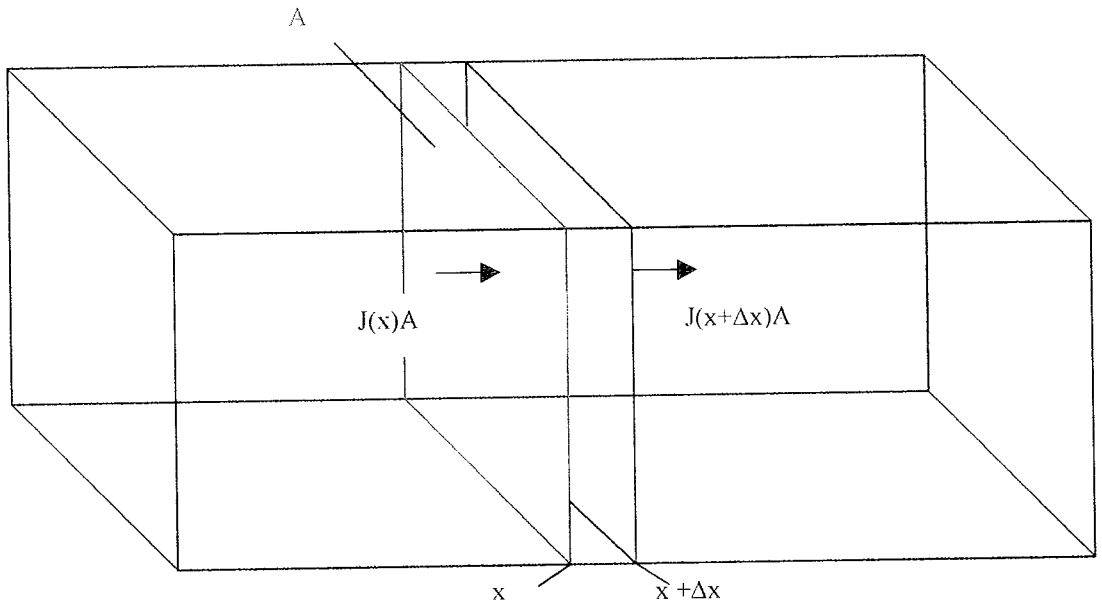

Figure 4.2. To illustrate flux for deriving the diffusion equation

Consider a thin slab of cross-sectional area A, extending a distance Δx, from x to x +Δx, as illustrated in Figure 4.2. Let the concentration at x be c at time t. The number of moles of particles entering the slab per unit time is J(x)A. The increase in concentration inside the slab with volume A(Δx)on account of the flux from the left is

$$\frac{dc}{dt} = \frac{JA}{A(\Delta x)} = \frac{J}{\Delta x} \text{ (in)}$$

There is also an outflow towards the right. This outflow is represented by J′ and can be represented by

$$\frac{dc'}{dt} = \frac{-J'A}{A(\Delta x)} = \frac{-J'}{(\Delta x)}_{(out)}$$

The net rate of change in concentration becomes

$$\frac{dc}{dt}(net) = \frac{J - J'}{\Delta x} \tag{4.8}$$

Each flux is proportional to the concentration gradient within the slab and so may be written in terms of Fick's first law

$$J - J' = -D\frac{dc}{dx} + D\frac{dc'}{dx}$$

$$= -D\frac{dc}{dx} + D\frac{d}{dx}\left\{c + \left(\frac{dc}{dx}\right)\Delta x\right\}$$

$$= D(\Delta x)\frac{d^2c}{dx^2} \tag{4.9}$$

Equation 4.9 now represents the change in flux. When this relation is substituted into the expression for the rate of change of concentration in the slab the general diffusion equation is obtained

$$\frac{dc}{dt} = D\frac{d^2c}{dx^2} \tag{4.10}$$

The concentration c, can now be recognised as a function of both distance x and time t.

4.2.4 Solution for transient gratings

Equation 4.10 must now be applied to the case of amplitude grating, which is decaying with time. An illustration of the fringe pattern of an amplitude grating that has just been recorded is shown in Figure 4.3. It can be seen that there are areas which are rich and replete in absorbing dye molecules. However, when recording beams are removed the grating will begin to decay and the concentration of dye in each of the fringe areas will change with time. A solution is needed which will account for this transient process.

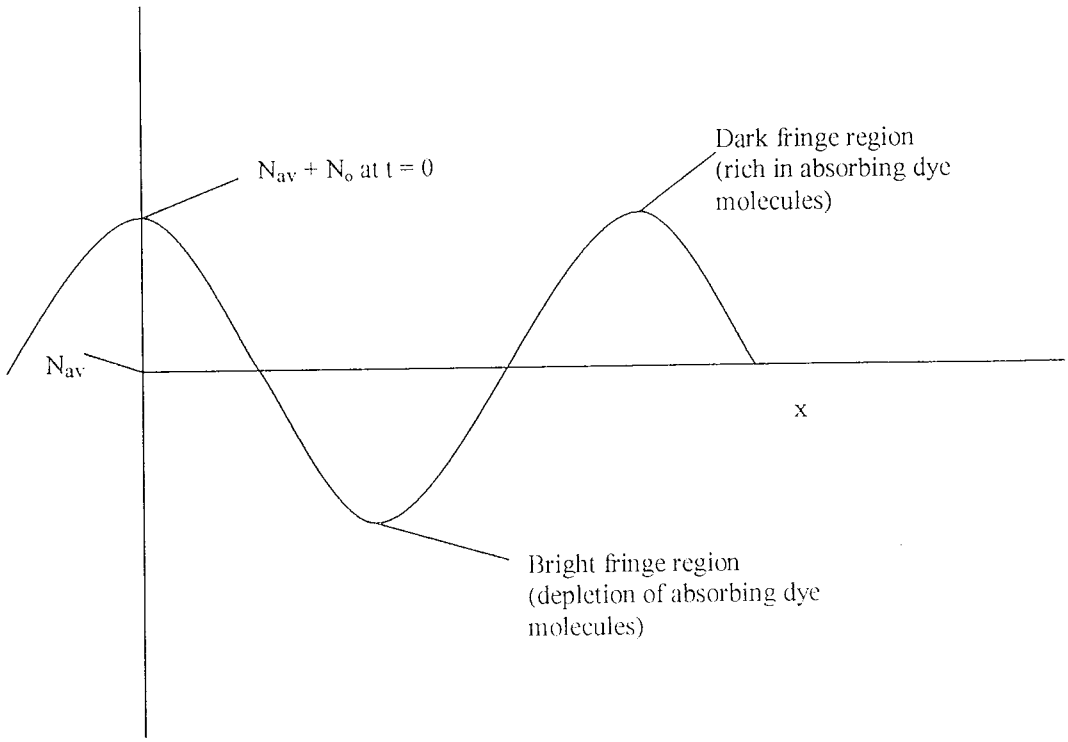

Figure 4.3 A recorded amplitude grating, to show the distribution of dye molecules.

The Laplace transform is an integral transform, which is often applied to engineering problems[100]. It will be used here to solve the diffusion equation specifically for the case stated here.

The Laplace transform (L) is defined as follows

$$L\{c(x,t)\} = \int_0^{\infty} c(x,t)e^{-st}dt = C(x,s)$$

or

$$L\left\{\frac{dc(x,t)}{dt}\right\} = sC(x,s) - c(x,0) \tag{4.11}$$

where s is the Laplace variable and c(x,0) represents the initial concentration, at t = 0 at all points in space. Applying 4.11, Equation 4.10 becomes:

$$sC(x,s) - c(x,0) = D\frac{d^2C(x,s)}{dx^2} \tag{4.12}$$

Rearranged this gives the linear second order inhomogeneous differential equation

$$\frac{d^2C(x,s)}{dx^2} - \frac{s}{D}C(x,s) = -\frac{c(x,0)}{D} \tag{4.13}$$

where in this case c(x, 0) acts as the driving function.

In order to apply Equation 4.13 more specifically, the following information may be noted:

At t = 0, an amplitude grating is recorded in the layer and the number of dye molecules has now been distributed spatially in the form of a cosine function. The initial concentration of dye molecules, c(x,0), within the exposed area when recording ends is fixed by the recording conditions (beam intensity, duration of exposure, and recording angle).

Referring to Figure 4.3, N_{AV} is the average number of absorbing dye molecules over x contained in the layer. N_0 is the amplitude of absorbing dye molecules distribution, generated during the recording time. Therefore, an absorption modulation has been induced, where the number of dye molecules at the centre of a dark fringe region is $N_{AV} + N_0$, while the number at the centre of a bright recording fringe is $N_{AV} - N_0$.

If Λ is the fringe spacing then the absorption modulation may be expressed as

$$c(x,0) = N_{AV} + N_0 \cos\left(\frac{2\pi}{\Lambda}x\right) \tag{4.14}$$

Substituting this into Equation (4.13) yields:

$$\frac{d^2C(x,s)}{dx^2} - \frac{s}{D}C(x,s) = -\frac{N_{AV}}{D} - \frac{N_0}{D}\cos\left(\frac{2\pi}{\Lambda}x\right) \tag{4.15}$$

Examining tables[101], the general solution of this equation is of the form:

$$C_G(x,s) = A(s)\exp\left[-\sqrt{s/D}\,x\right] + B(s)\exp\left[+\sqrt{s/D}\,x\right] \tag{4.16}$$

where *A(s)* and *B* (s) are constants in x. A particular solution must now be found by assigning values to A *(s)* and B (s) which are determined by the boundary conditions.

Examining tables, the particular solution of Equation (4.15) takes the form

$$C_p(x,s) = \frac{-N_{AV}/D}{-s/D} - \frac{-N_0/D}{-s/D-(2\pi/\Lambda)^2}\cos\left(\frac{2\pi}{\Lambda}x\right) \tag{4.17}$$

The full solution is then the sum of 4.16 and 4.17

$$A(s)\exp\left[-\sqrt{s/D}x\right] + B(s)\exp\left[+\sqrt{s/D}x\right] + \frac{N_{AV}}{s} - \frac{N_0}{s+D(2\pi/\Lambda)^2}\cos\left(\frac{2\pi}{\Lambda}x\right) \tag{4.18}$$

The Inverse Laplace Transform, denoted by $L^{-1}\{\text{-}\}$, is defined by

$$c(x,t) = L^{-1}\{C(x,s)\} = \int_0^\infty C(x,s)e^{-st}\,ds$$

Using tables, the time dependent solution is

$$\begin{aligned} c(x,t) = \; & L^{-1}\left\{A(s)\exp\left[-\sqrt{s/D}x\right]\right\} + L^{-1}\left\{B(s)\exp\left[+\sqrt{s/D}x\right]\right\} + L^{-1}\left\{\frac{N_{AV}}{s}\right\} \\ & - L^{-1}\left\{\frac{N_0}{s+D(2\pi/\Lambda)^2}\right\}\cos\left(\frac{2\pi}{\Lambda}x\right) \end{aligned} \tag{4.19}$$

The boundary conditions, which refer to the physical nature of the problem can now be applied to this solution to eliminate the constant coefficients.

The value of c(x,t) must be finite for all values of x and t. The same must also be true for C(x,s) for all values of x and s. In mathematical form:

$$\lim_{\substack{x\to\infty \\ t\to\infty}} c(x,t) < \infty, \quad \lim_{\substack{x\to\infty \\ s\to\infty}} C(x,s) < \infty \tag{4.20}$$

Since

$$\lim_{x\to\infty} \left\{ A(s)e^{-\sqrt{\frac{s}{D}}x} + B(s)e^{-\sqrt{\frac{s}{D}}x} \right\} \to \infty$$

unless B(s) = 0, then B(s) must be zero.

Another physical constraint is that the average of c(x, t) must always have the value N_{AV}.

$$\frac{1}{\Lambda}\int_0^{\Lambda} c(x,t)dx = N_{AV} \tag{4.20}$$

where the average has been taken over one period.

Taking the Laplace transform of both sides of Equation 4.20 yields:

$$\frac{1}{\Lambda}\int_0^{\Lambda} C(x,s)dx = \frac{N_{AV}}{s} \tag{4.21}$$

Eliminating B(s) the full solution may now be expressed as:

$$c(x,t) = L^{-1}\left\{A(s)\exp\left[-\sqrt{s/D}\,x\right]\right\} + N_{AV}H(t) - N_0\exp\left\{-D(2\pi/\Lambda)^2 t\right\}\cos\left(\frac{2\pi}{\Lambda}x\right) \tag{4.22}$$

where H(t) is the Heaviside or step function. H(t) = 1 when t > 0, H(t) = 0 when t ≤ 0.

The integral of the particular solution (Equation 4.17) is found to be N_{AV}. Therefore the integral of the remaining general solution must be zero. This will only be true if A(s) = 0.

$$\int_0^{\Lambda} A(s)\exp\left[-\sqrt{s/D}\,x\right]dx = 0 \Rightarrow A(s) = 0 \tag{4.23}$$

therefore the full solution can be concluded to be

$$c(x,t) = N_{AV} - N_0\exp\left[-D(2\pi/\Lambda)^2 t\right]\cos\left(\frac{2\pi}{\Lambda}x\right) \tag{4.24}$$

Experimentally, the diffraction efficiency of an amplitude grating may be measured. When recording ends this diffraction efficiency is found to decay with time. Recall that the diffraction efficiency of an amplitude grating is given by the formula

$$\eta = \exp\left(-\frac{2\alpha d}{\cos\theta}\right)\sinh^2\left(\frac{\alpha_1 d}{2\cos\theta}\right) \tag{4.25}$$

where α_1 is proportional to N_0 and α is proportional to N_{AV}.

In the approximation of small (low) N_0 values and low diffraction efficiency, Equation (4.25) can be re-written as

$$\eta \approx \left[\frac{\alpha_1}{2\cos\theta} d\right]^2 \exp\left[-\frac{2\alpha d}{\cos\theta}\right] \tag{4.26}$$

The natural log of η is then given by

$$\ln[\eta] \approx 2\ln\left[\frac{\alpha_1}{2\cos\theta} d\right] - \frac{2\alpha d}{\cos\theta} = 2\ln[\alpha_1] + 2\ln\left[\frac{d}{2\cos\theta}\right] - \frac{2\alpha d}{\cos\theta} \tag{4.27}$$

Assuming that $\alpha(x,t) \propto c(x,t)$, the absorption modulation equals

$$\alpha_1 = CN_0 \exp\left\{-D(2\pi/\Lambda)^2 t\right\} \tag{4.28}$$

where C is some fixed constant of proportionality.

This is substituted into Equation 4.27 yielding

$$\ln[\eta] \approx 2\ln[CN_0] - 2D\left(\frac{2\pi}{\Lambda}\right)^2 t + 2\ln\left[\frac{d}{2\cos\theta}\right] - \frac{2\alpha d}{\cos\theta} \tag{4.29}$$

If ln[η] is plotted against t, a straight line of slope $-2D(2\pi/\Lambda)^2$ is obtained. A relaxation time τ may be defined as the reciprocal value of this slope. Recalling that the grating period is related to the angle of separation between the recording beams and the wavelengths of the recording beams

$$\Lambda = \frac{\lambda}{2 \sin\left(\theta/2\right)} \tag{4.30}$$

then

$$D = \frac{\lambda^2}{32\ \pi^2 \sin^2(\theta/2)} \frac{1}{\tau}$$

or

$$D = \frac{1}{8\pi^2}\left(\frac{\Lambda^2}{\tau}\right) \tag{4.31}$$

Equation 4.31 may now be used to calculate the diffusion coefficient of dye molecules through amplitude gratings under any specific experimental conditions. In the following section it is used to investigate whether and the extent to which diffusion of dye molecules is responsible for amplitude grating decay.

4.3 Preliminary investigations

There are three factors that could individually or in combination cause a decrease in the diffraction efficiency of amplitude gratings recorded in this material.

(1) The recovery of bleached (non-absorbing) dye molecules into an absorbing state. This would decrease the amplitude of the absorption grating by converting all the bleached molecules in the bright fringe areas back into absorbing molecules, eventually erasing the grating.

(2) Bleaching of absorbing dye molecules by the probe beam that is used to monitor grating decay. As this is a uniform beam this would decrease the number of absorbing dye molecules in the dark fringe regions, leading to total bleaching and destruction of the absorption modulation.

(3) Diffusion of absorbing dye molecules from the dark fringe regions where they are in high concentrations, to bright fringe regions where they are scarce. This would reduce the amplitude of the absorption grating until it eventually disappeared as the concentration of absorbing dye became uniform across the span of the grating.

Each of these factors is now considered.

4.3.1 Establishing the mechanism of amplitude grating decay

The bleaching of the dye molecules has already been discussed so it is understood that a dye molecule can undergo a reaction with a TEA molecule, to enter a colourless or leuco state. Unlike some other dyes that are used in recording materials the methylene blue dye molecules can 'recover' in the presence of oxygen and regain their characteristic blue colour. If the relaxation time of a grating due to diffusion exceeded the time needed for dye recovery then dye recovery alone could account for the decay of diffraction efficiency.

In order to establish that this was not the case, appropriate layers were bleached with a single beam. The transmittance of these layers was monitored periodically as a function of the incident light from a very low intensity probe beam. As the probe laser and the bleaching beam are the same wavelength, the intensity of the probe beam was chosen so as to be less than 1% of the total power of the bleaching laser beam. This was to prevent additional bleaching of the layer.

When the layer was effectively transparent, the bleaching laser was removed and the probe beam continued to periodically monitor the bleached area. The transmittance began to decrease with time and this could only be attributed to recovery of the dye molecules. For a layer comprising PVA and dye with 1ml of TEA solution, it was found that the transmission decreased at a rate of less than 0.1%/s. This recovery is shown in Figure 4.4.

It must also be noted that probing was only done periodically for a minimum interval each time so that the total time the probe laser actually interacted with the grating was in the order of a couple of seconds. Note at this stage that the recovery time here is representative of a grating containing 1ml of TEA in the coating solution. Later it will be shown that in order to monitor decay effectively, it is essential to limit the TEA content to at least half of this concentration. This indicates that the recovery time of gratings recorded containing lower concentrations of TEA would be even longer than those depicted in Figure 4.4.

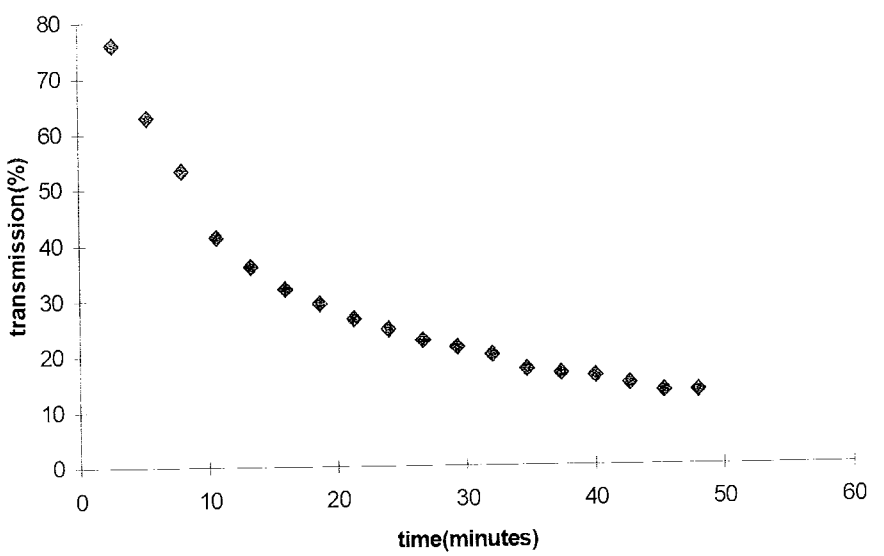

Figure 4.4: The recovery rate of dye molecules. Coating solution comprises PVA, 4mg dye and 1ml TEA.

In Chapter 2 the photochemical process was discussed in detail and it was shown that TEA and dye are essential to one another for the production of free radicals, which is the pre-cursor to polymerisation when monomer is present. It was found that when an amplitude grating was recorded with the amount of TEA that is usually used for the recording of transmission holograms, the grating decay was so rapid that data acquisition was not possible. Using a greatly reduced amount of TEA meant that grating decay was so slow that it could no longer be assumed that bleaching by the probe laser or dye recovery were not contributing to the fall-off in the diffraction efficiency of a grating. Also if the presence of TEA caused refractive index modulation during recording then the resulting grating could not be truly amplitude in nature. Molar refraction theory described by Tomlinson and Chandross[102] was used to calculate an approximate value for any refractive index modulation, which may be attributed to the TEA. Using this theory it was established that the refractive index modulation contribution of the TEA was negligible. The theory and corresponding calculation are both shown in the Appendix.

4.4 Experimental

One of the main advantages of this material is that it may be made sensitive to different regions of the visible spectrum by changing the type of dye used. When recording at a specific wavelength, any analysis should be carried out using a beam of light to which the material is insensitive. The experimental set-up had to be modified to take into account the fact that only 633nm light was available for grating analysis.

4.4.1 Experimental set-up

The experimental set-up shown in Figure 4.7 was arranged so that the probe beam from a low power (1mW) HeNe laser was directed through a beam combiner (7). This beam was then positioned so that the resulting attenuated beam (approximately 0.5% of total recording power when incident on the sample) was oriented along one of the recording beams. This had the advantage of allowing the spatial frequency to be changed by rotating mirrors 5 and 6 without realignment of the reading beam. This also ensures that the probe beam is automatically at the Bragg angle during grating recording.

Two programmable shutters were included in the experimental set-up. One of these was used to control the recording time. When recording ended the first shutter triggered the second, which was directly in front of the smaller probe laser. The second shutter then opened periodically to enable monitoring of the grating by a photodetector. Data from the photodetector passed through an amplifier to a data acquisition unit connected to a PC.

This experimental set-up overcame the problems encountered when probing the gratings at the recording wavelength. The shutter system combined with the very low power used to read the beams meant that analysis could be carried out. In addition, there was no contribution from the reading laser to the decay of the recorded gratings.

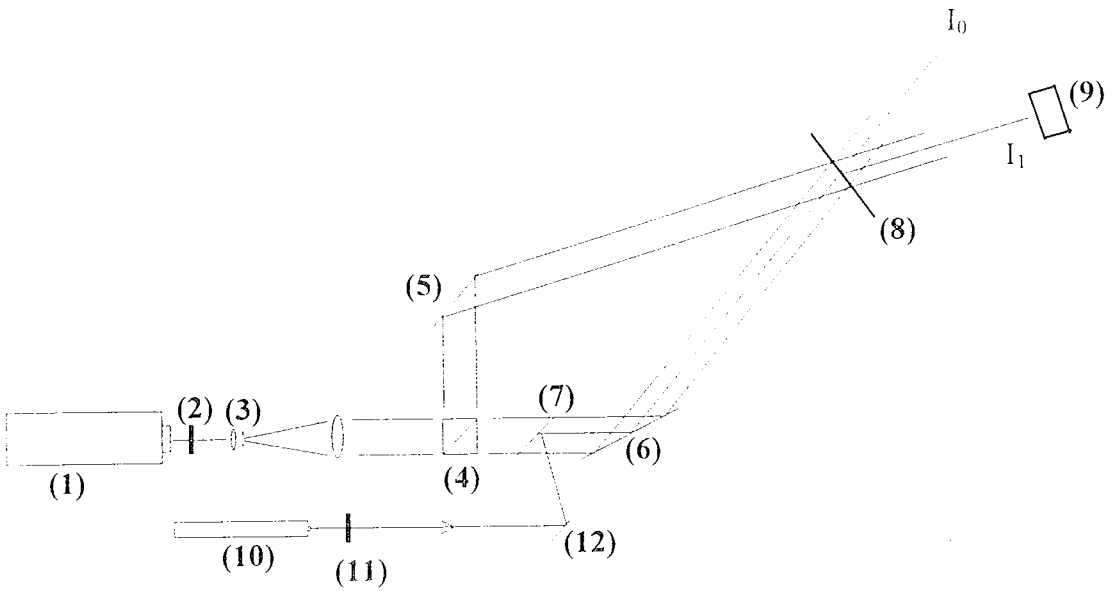

*Figure 4.7 Experimental set-up (1) Recording laser: 35 mW Helium Neon (2) Shutter 1 (3) Spatial filter (25micron pinhole/ *20 objective) (4) 50/50 non polarising beam splitter (5,6) Two mirrors (gimballed mount) (7) 95/5 non polarising beamcombiner , plane mirror (8) Photosensitive sample *(9) Newport power meter (10) Probe laser: 1mW He-Ne (11) Shutter 2 (12) One plane mirror.*

** The Newport power meter is connected to an amplifier which in turn is connected to the acquisition PC unit and a computer, for analysis of data.*

4.4.2 Layer preparation

The PVA (type F unless otherwise stated) had a molecular weight range of 30-200*10^3 with no degree of hydrolysis specified. However, experimental comparisons to other PVAs have shown it to be 99% hydrolysed (Chapter 2). The PVA solution was always 10% w/v (weight per volume) unless otherwise stated. The dye solution contained 1g of dye (w/v).

The sample solution was made up of the appropriate volumes of PVA and dye solution. The TEA concentration was varied from 0ml-0.5ml per 25ml total sample solution.

4.5 Results:

To calculate values for diffusion coefficient (D) Equation 4.26 was used

$$D = \frac{\lambda^2}{32\pi^2 \sin^2\left(\frac{\theta}{2}\right)} \frac{1}{\tau}$$

where $1/\tau$ is the slope resulting from a log plot of diffraction efficiency decrease with time for a particular grating.

4.5.1 Variation of electron donor concentration

Using the experimental technique outlined, amplitude gratings were recorded. When the writing beams were removed the decrease in diffraction efficiency of the gratings was monitored in the first order diffraction direction. This decay process is converted to a linear function of time by converting the values obtained to natural logs. An example is shown in Figure 4.8.

A number of samples, each containing a different concentration of TEA, were exposed to produce gratings of 870lines/mm spatial frequency. The results are shown in Table 4.2 where the relaxation time τ of each grating is included. As can be seen from Table 4.2 there is a definite effect on the diffusion coefficient due to the presence of increased amounts of TEA in the sample layers. It can also be seen that

the results are quite repeatable as different sample layers with the same amount of TEA produced similar relaxation times.

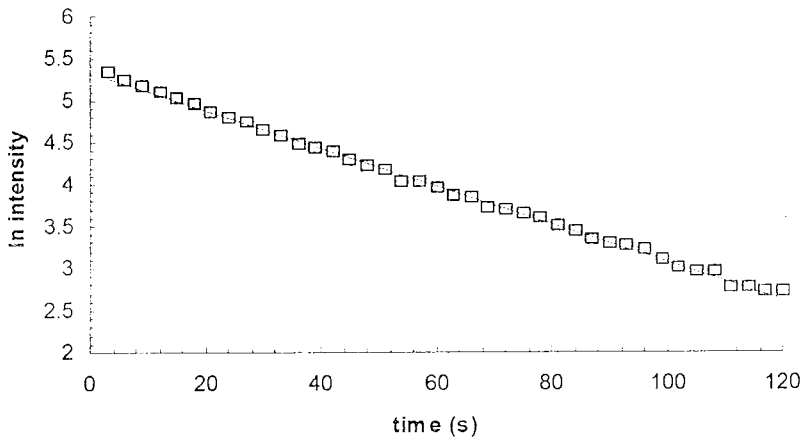

Figure 4.8. Graph of ln intensity vs. time (s). The grating represented was prepared using 0.4ml/25ml of TEA in the coating solution.

TEA concentration/mls (per 25mls sample solution)	Slope *(1/τ)*	***Relaxation time (s) (τ)***	***Diffusion coefficient (cm^2/s)***
0	.00072	1389	1.2E-17
.05	.0006	1667	1.0E-17
.075	.00097	1031	1.6E-17
.1	.0042	238	0.7E-16
.2	.0013	770	2.15E-17
	.0012	847	1.95E-17
.3	.0060	166	1.0E-16
	.0058	172	0.95E-16
.4	.022	45.5	3.7E-16
	.023	42	4.1E-16
.5	.09	12	1.4E-15
	.096	10	1.6E-15

Table 4.2. Calculated diffusion coefficients for varying TEA concentrations for a single fixed spatial frequency. (870lines/mm or 1.1μm fringe spacing)

The slope of a log graph of the type shown in Figure 4.8 has been established from the theory to be $1/\tau$ where τ is the relaxation or decay time for an amplitude grating. The slope for each sample as in Table 4.2 is plotted against concentration of TEA and the result is shown in Figure 4.9.

From Figure 4.9 it can be seen that the relaxation time recorded for transient gratings appears to be exponentially dependent on the TEA content for very low concentrations of TEA. The relation becomes more linear as the concentration of TEA is increased.

Recalling the discussion of plasticisers in chapter 2 it can be said that any component which can cause a reduction in the rigidity of a polymer matrix will affect its mechanical properties. The presence of increasing quantities of TEA seems to cause the PVA matrix to become much more permeable as the diffusion coefficient increases exponentially. A more detailed study was carried out in the concentration region between 0.2ml-0.5ml where this dependence appears to be more pronounced. The results of this study are presented in section 4.5.2.

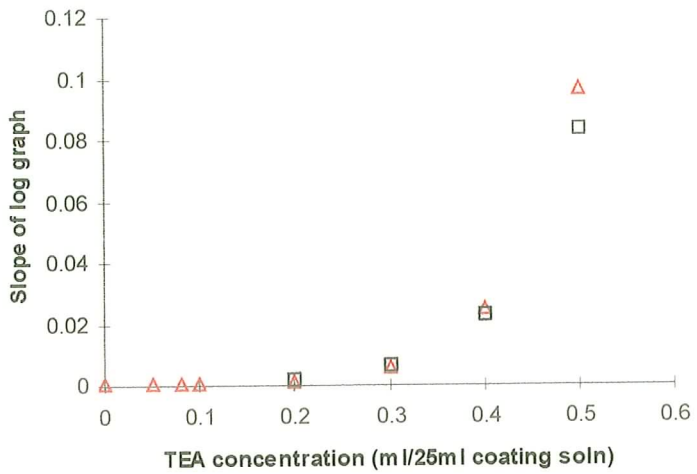

Figure 4.9 Effect of increasing concentration of TEA on the decay rate of amplitude gratings. Spatial frequency was fixed at 870lines/mm.

4.5.2 Dependence of decay rate of gratings on fringe width

The experiments were repeated at the concentrations mentioned above at a lower spatial frequency. It is expected that the decay rate would be slower due to the larger fringe spacing.

Table 4.3 shows the calculated diffusion coefficient of the dye, obtained from experimental data over a fringe spacing of 2.6μm, (spatial frequency 385lines/mm) for each concentration of TEA used in the sample solution.

If the values contained in Tables 4.2 and 4.3 are compared, it can be seen that the calculated diffusion coefficient for the dye in a grating recorded with 385 l/mm is

different from one recorded at 870 l/mm, even though both contained the same amount of TEA.

One of the most fundamental indications that the principal process governing the decay of any grating is the diffusion of the dye molecules, is that a plot of the time constant for the decay of any transient grating against the fringe spacing squared should yield a linear relationship. From the slope of this graph, the diffusion coefficient of the dye may be obtained. This means that although the time constant for the decay of a particular grating may change with varying spatial frequency, the diffusion coefficient should be constant providing the concentration of TEA remains constant. Clearly, this is not the case here. It was thought that variable recording conditions may have been responsible for the inconsistent results.

TEA concentration/mls (per 25mls sample solution)	Slope $(1/\tau x\ 10^{-3})$	***Relaxation time*** (τ/s)	***Diffusion coefficient*** (cm^2/s)
0.1	1.4	714	1.7E-16
	1.5	666	1.3E-16
0.2	1.7	588	1.45E-16
	2.1	476	1.8E-16
0.3	7.1	140	0.6E-15
	4.3	232	3.65E-16
0.4	19.5	51	1.65E-15
	19.0	52	1.6E-15
0.5	18.0	55	1.5E-15

Table 4.3. Calculated diffusion coefficients for varying TEA concentrations at fixed spatial frequency. (385lines/mm)

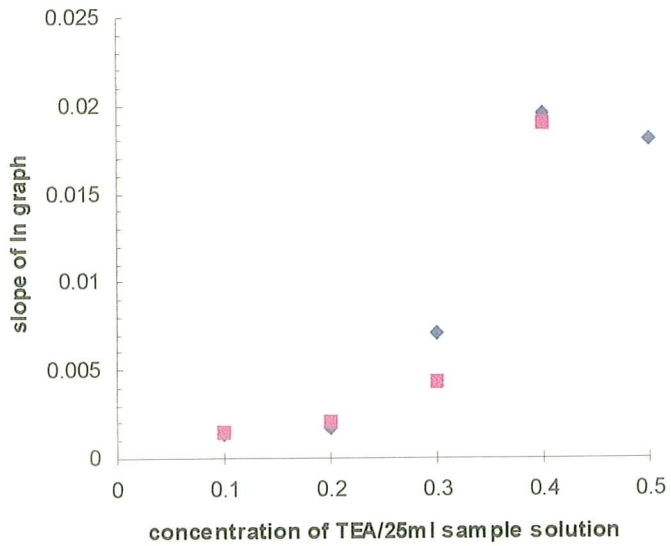

Figure 4.10 Graph of $1/\tau$ vs concentration of TEA contained in grating sample solution for spatial frequency, 385lines/mm. The two sets of points above correspond to the same concentrations of TEA to show repeatability of results.

In order to minimise the effect of fluctuating environmental conditions on diffusion rate through the PVA, it was concluded that a set of experiments should be carried out in such a way that relevant parameters, such as spatial frequency could be varied in a short time. In this way the environmental conditions under which the gratings were recorded would not vary significantly and the results would be much more reproducible.

A concentration of 0.3ml/25mls total solution was chosen as the fixed amount of TEA to be used in the sample solution. This is because gratings recorded at this

concentration exhibited the most conveniently monitored decay time. Relative humidity was 44% and the temperature was 25^0C during grating recording.

Interbeam angle (degrees)	*Spatial frequency (lines/mm)*	*Fringe spacing squared* $\Lambda^2/\mu m^2$	*Relaxation Time* τ*(s)*
9.1	500	4	1428
			1700
12.8	700	2	625
			833
16.55	900	1.2	500
			454
20.4	1100	.82	400
			333
24.3	1300	.59	270
			227

Table 4.4. Some calculated values of relaxation time for grating decay over specific fringe widths.

The results contained in Table 4.4 are plotted in Figure 4.11 along with an extra set of experimental data not included in the table. As can be seen clearly there is a linear relationship between grating decay time and the fringe width of a grating. This is in agreement with the theory in section 4.2.4.

However, there is a small positive intercept if the graph is extrapolated, indicating the presence of another influence on the dye diffusion. This could be attributed to a degree of dye recovery which could occur to some extent over time, especially in the case where decay took approximately 28 minutes.

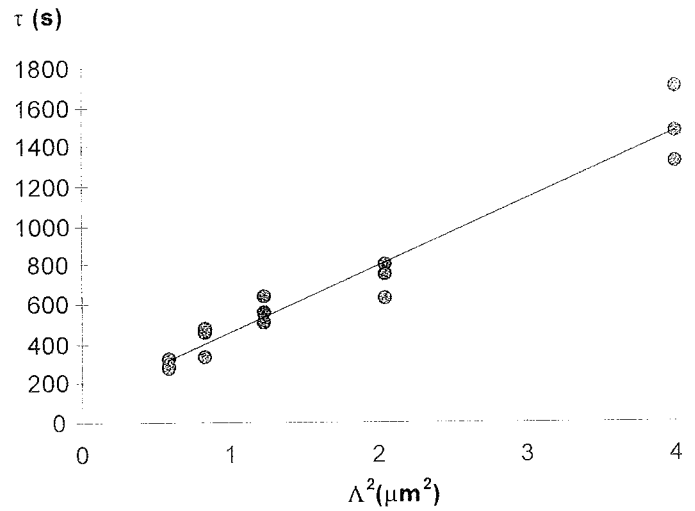

Figure 4.11. Graph illustrating the linear relationship obtained between Λ^2 and τ for transient gratings.

4.6 Influence of binder

In the previous sections the TEA was seen to have an effect on the diffusion rate of dye molecules at a fixed spatial frequency. The binder was also investigated to establish to what extent it contributes to the overall holographic process. Six PVA samples were used in the investigation, each with varying degrees of hydrolysis and molecular weight range.

Amplitude gratings were recorded in material prepared using each of the binders. The HGRT technique was employed as before, to calculate diffusion coefficients for the dye. The experimental conditions under which the material was studied were kept as close as possible to the actual conditions applied for holographic recording.

4.6.1 PVA study

Table 4.5 below contains information, supplied by the manufacturer about each of the PVA samples used. The molecular weight of each of the samples is only quoted as a range of values so the exact percentage of polymer chain lengths was not specified.

PVA Type	*Degree of hydrolysis (%)*	*Molecular weight range ($x10^{-3}$)*
A	80	9-10
B	87-89	13-23
C	98	13-23
D	98-99	124-186
E	99+	50
F	99	30-200

Table 4.5 PVA types and quoted specifications for each.

Transient gratings were recorded and monitored as described in Section 4.4.1. Each grating recorded had a spatial frequency of approximately 900 lines/mm. The relaxation times for a number of transient gratings recorded in each of the six types of binder were determined and an average diffusion coefficient for the dye obtained, as shown in Table 4.6.

PVA	*Degree of hydrolysis (%)*	*Molecular weight range*	*D* $(x10^{-16}cm^2/s)$
D	98-99	124000-186000	0.28
F	99	30000-200000	0.66
E	99+	50000	1.22
C	98	13000-23000	1.25
B	87-89	13000-23000	1.26
A	80	9000-10000	1.58

Table 4.6. Manufacturers specifications and diffusion coefficient for dye in each PVA tested.

From Equation 4.28, it is clear that the smaller the value for diffusion coefficient, the slower the rate of diffusion of the dye molecules. It can be deduced from Table 4.6, that PVA A allows the fastest rate of migrating molecules. This PVA has the narrowest molecular weight range and its polymer chain lengths are small compared to those of other types tested. This could be explained by the greater relative free volume of lower molecular weight samples.

The diffusion coefficient values were plotted as a function of average molecular weight in Figure 4.12.

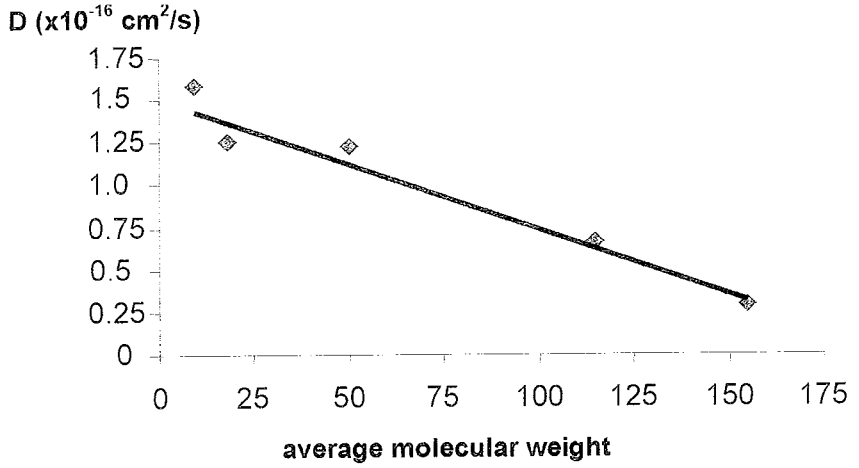

Figure 4.12. Diffusion coefficient for each PVA type plotted as a function of average molecular weight.

It is evident from the graph that the rate of transition of dye molecules through the binder is directly dependent on the molecular weight of the binder. It would appear that the larger the molecular weight of the polymer chains, the less permeable the binder is to migrating molecules. This could have a significant effect on further improving the performance of the material as, if the permeability of the binder could be directly controlled, then the rate of migration of reacting species may also be controlled to some extent.

In order to examine the influence of the binder further, it was necessary to determine the actual molecular weight distribution within the specified range for each PVA.

The PVA samples were sent for analysis by size exclusion chromatography[77], which is a technique that is employed particularly in the area of polymer chemistry for

polymer characterisation by molecular weight distribution. A brief description of the technique is given below.

4.6.2 Exclusion chromatography

Size exclusion chromatography is based on the ability of controlled-porosity substrates to sort and separate sample mixtures according to the size and shape of the sample molecules. The components to be separated are distributed between two mutually immiscible phases that are contained within a column. The stationary phase, which is usually a liquid, is attached to a solid inert material (the support) in the column. The mobile phase, usually a liquid or gas is used to push the injected sample through the stationary phase.

As the mobile phase moves through the stationary phase, the sample components undergo a series of interactions between the two phases. The differences between the chemical and physical properties of the components in the sample govern the degree of interaction thus their rate of migration through the column. Molecules emerge from the column in order of size, the larger molecules being first as they have minimal interaction with the two phases. The retention time (t_R) is the time required by the mobile phase to convey a solute from the point of entering the column, to the detector and is an indication of the extent of interaction.

Table 4.7 below shows the retention times and molecular weight distribution obtained for each PVA.[103] It must be noted that the values of molecular weight distribution are relative to the standard used in the exclusion column. The standard used by the manufacturers to characterise the polymers is unknown so no direct comparison could be made to the experimental results.

PVA	*Retention time (t_R/mins)*	*Peak molecular weight (chromatography)*	*Molecular weight range (manufacturer)*
A	8.69	3303	9000-10000
	8.67	4172	
B	8.21	5726	13000-23000
	8.19	5489	
C	7.96	9978	13000-23000
	7.86	11100	
D	6.98, 8.71	60360, 3314	124000-186000
	4.32, 6.76, 8.76	2097000, 62030, 3210	
E	5.49, 7.26	370400, 33640	50000
	5.53, 7.28, 8.66	369000, 32950, 3326	
F	5.57, 7.76	311700 18480	30000-200000
	4.17, 6.43	2400000 131700	

Table 4.7 Exclusion chromatography results showing retention times and molecular weight distribution for each PVA.

Some relevant details were noted from the chromatography results.

1. Although, PVAs B and C are specified as being in the same molecular weight range, the chromatography results revealed that PVA C has a peak molecular weight of almost twice that for PVA B.

2. PVAs D and F have more than one peak molecular weight and even allowing for the fact that different standards were used to characterise the polymers, from the chromatography results PVAs D and F exhibit peak molecular weights far outside the ranges quoted by the manufacturers.

Point 1 above draws attention to the notion that molecular weight, more so than the degree of hydrolysis is influential to the rate of diffusion through the polymer. This is because the values of diffusion coefficient (Table 4.6) for PVA B and C are almost the same despite a difference of 10% in hydrolysis. However, further work is needed to verify this.

Point 2 suggests that for a truly comprehensive study on the influence of the binder, narrow molecular weight fractions need to be tested to determine what is the optimum range of binder which works best in the material.

4.6.3 Discussion

In Chapter 1, it was noted that during holographic recording, the migration of monomer into light exposed areas, lead to polymerisation in those areas. This diffusion of monomer is thought to be at least partly responsible for refractive index modulation between dark and bright fringe regions. This hypothesis was described by Colburn and Haines[55] who explained the mechanism in more detail as follows:

During holographic recording, the monomer in light exposed regions is polymerised by free radicals, which are produced by the electron donor and dye reaction described in Section 1.1.6. The extent of polymerisation is a function of the incident light intensity and the availability of free-radicals. Monomer concentration gradients, caused by the variation in polymerisation between exposed and unexposed areas, give rise to the diffusion of monomer molecules into exposed areas. When recording is ended, a uniform exposure will polymerise any remaining monomer in unexposed areas. However, an overall refractive index modulation will have taken place due to diffusion of monomer and polymerisation in exposed areas.

It is now evident that dye diffusion also takes place during recording but the rate of dye diffusion will be slower than that of the monomer as the dye molecular structure is larger than that for the monomer. It has also been proven that the molecular weight of the binder can affect the rate of diffusion of dye molecules. These two facts may account for the difference in spatial frequency response between the green and red-sensitised materials.

From the discussion of the difference in the spatial frequency range of both the green and red versions of the material it was noted that whilst the red material had a better response to lower spatial frequencies, the green material responded to a wider range of spatial frequencies. The highest limiting spatial frequency for green was 3000l/mm, whilst for red it was only 2000l/mm.

Considering the size of the two types of dye molecules involved, the smaller methylene blue dye molecules, would diffuse more rapidly than the xanthene molecules. At low spatial frequencies, this would result in more methylene blue molecules being able to travel over wider fringe widths more rapidly than xanthene molecules. As the dye is being depleted in light exposed regions, more dye diffusing into these regions would in turn lead to the production of free-radicals. This would explain the better response of the red-sensitised material at low spatial frequencies, where the fringe widths are much wider than at higher spatial frequencies.

However by the same token, the more rapid diffusion of methylene blue molecules at higher spatial frequencies could lead to polymer chains of higher molecular weight being formed in bright fringe areas or even the migration of initiating species into neighbouring regions. This would cause widening of the polymerised region and less definition between light exposed and unexposed areas, limiting the spatial resolution. This explanation would account for the poor response of the red-sensitised material at high spatial frequencies. The effect would be lessened with the green-sensitised material, as its dye molecules diffuse less rapidly.

This hypothesis would satisfactorily explain the difference between the spatial frequency response of the two materials. Given that the binder has been proven to have some influence on diffusion it may be possible to control the diffusion rate of

both the monomer and the dye molecules by choosing an appropriate binder. If the polymerisation could be controlled as a consequence, it would be possible to contain the polymerised region in the light exposed areas during holographic recording, allowing higher spatial frequencies to be recorded. However, a more extensive comparative study of the materials would need to be conducted, before any definite conclusions can be drawn.

4.7 Conclusions

A mathematical model was developed for the specific case of movement of molecules through a recorded transient grating, leading to the decay of that grating.

Amplitude gratings were recorded in the material to examine diffusion of migrating dye molecules and the role of the PVA binder. It is certain that the dye diffusion takes place very rapidly during recording with the dye molecules almost instantaneously moving into available space in the bright fringe regions. A linear relationship between the relaxation time constant for a particular grating and its fringe width squared has been established thus verifying the predictions set in the model.

It has been shown that the TEA has a definite plasticising effect on the PVA binder, so the concentration of TEA added to the sample solution in turn has an effect on the diffusion coefficient of migrating species within the material. This in itself raised the

question as to what extent the binder affects the photochemical processes in the material.

In addition to the proof of dye diffusion in the material, it has further been shown that the diffusion rate depends on the molecular weight range of the binder. The implications of this are that by controlling binder permeability it may be possible to alter the characteristics of the material.

The following chapter describes the successful application of the material. The material was used to fabricate a variety of Holographic Optical Elements (HOEs). This particular application was chosen as it incorporates all of the material characteristics.

5. Holographic Optical Elements (HOEs)

A Holographic Optical Element (HOE) is the general term used to describe a hologram, which is used to manipulate incident light. Optical components such as beamsplitters and lenses can be fabricated holographically. There are a number of advantages associated with recording optical components in this way. A single element could be used to deflect, filter and focus a beam of light and due to their planar structure, it would be easy to stack individual elements. Several could be recorded on the same plate to perform simultaneous tasks, for example the multiplexing of light from a bundle of optical fibers. In addition HOEs are light, compact and relatively cheap to make.

However, the characteristics of a HOE or diffractive optical element (DOE) depend very much on the material used to record it, as is the case for any application. Many materials have advantages such as reusability, high angular selectivity or very high resolution which make them very suitable for specific holographic applications. [104]

However, most of these materials require post-processing which can distort the fringe planes of the recorded element to some degree. This distortion creates the need for an angular shift of the reconstruction beam when replaying. If the element is required to focus light along its axis, then this distortion will obviously decrease the efficiency at which this may be achieved.

The material presented here has many advantages for the production of diffractive optical elements. No post-exposure processing is required. The high angular selectivity of the material was demonstrated in Chapter 3, which is an important factor as the HOEs described incorporate many spatial frequencies. The spatial resolution of the material will also be discussed in terms of its limitations and how this would affect the HOEs produced.

The results obtained for on and off-axis focusing elements are presented as well as some work on stacked elements.

5.1 Experimental procedure

The photosensitive layers were prepared using the standard formulation described in section 3.2.1, chapter 3.

5.1.1 Experimental set-up

For the recording of on-axis lenses two collimated beams of 633nm light from a Helium Neon laser were aligned so as to combine at a beam splitter (combiner) and illuminate the coated glass plate where the DOE was to be recorded. It was ensured that the beams were parallel and overlapping and then two 20 cm focal length lenses were arranged to bring the beams to their respective foci at points separated by 10 cm.

The support for the recording plate was arranged so that the photosensitive layer was positioned at the midpoint between these foci. This arrangement means that a

diverging beam interferes with a converging beam at the photosensitive plate, and the recorded fringe pattern will therefore bring a similar diverging beam to a focus. The set-up for recording on-axis elements is illustrated in Figure 5.1. The power of the collimated beams illuminating the lenses was usually 3 to 5 mW/cm^2, and the exposure time was controlled by an electronic shutter.

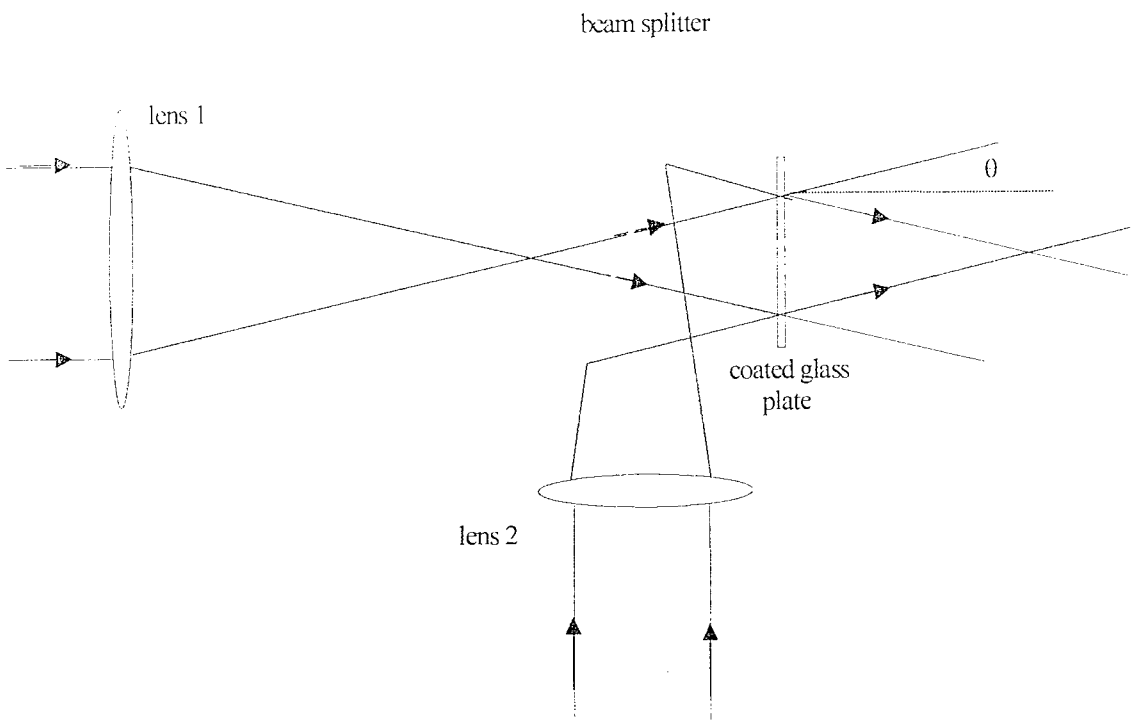

Figure 5.1 Apparatus for the recording of an on-axis DOE

For the recording of off-axis lenses two beams were overlapped at the photosensitive plate (the inter-beam angle was 20°). One beam was collimated and the other was made to converge to a point beyond the photosensitive plate. The distance from the plate to the focus was therefore the focal length of the recorded DOE. For simple gratings two collimated beams were used.

Recorded holograms and DOEs were stored in a low humidity environment (a dessicator containing calcium carbonate) and then covered with a second glass plate and sealed at the edges with epoxy resin.

5.1.2 Types of DOE recorded

Four types of DOE were recorded in this material, as shown in Figures 5.2(a), (b), (c) and (d). Respectively, the four types shown are a DOE which will bring collimated light to a focus on the principal axis, one that will bring diverging light to a focus on-axis, a DOE that will bring collimated light to a focus off-axis and a simple beam-splitter.

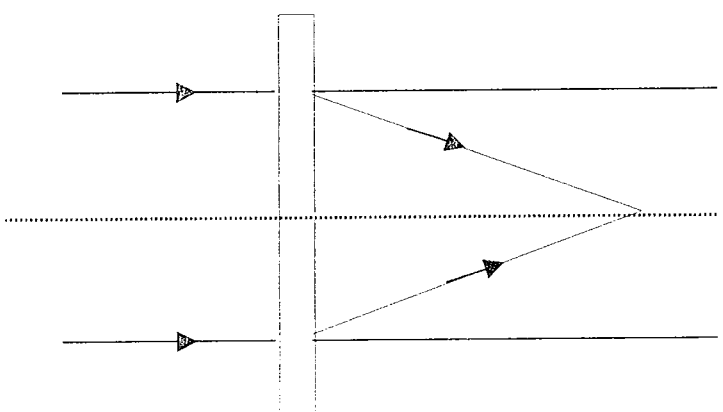

Figure 5.2(a) A DOE which will bring collimated light to a focus on the principal axis

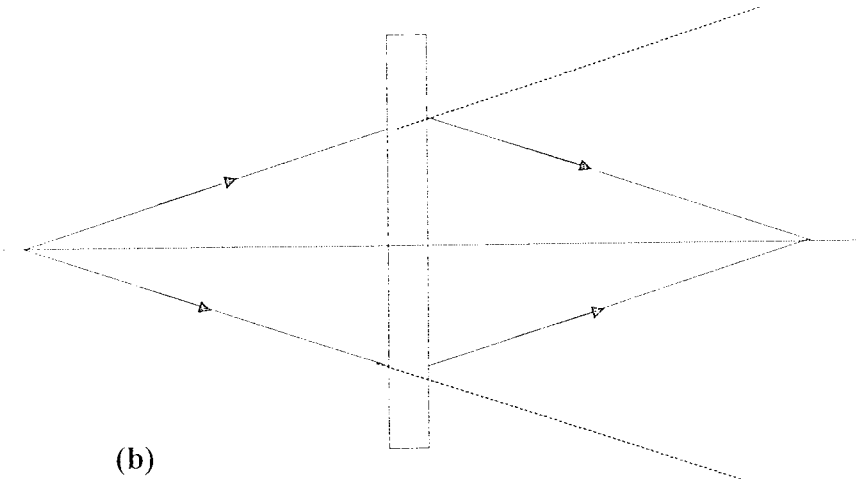

Figure 5.2(b) A DOE which will bring diverging light to a focus on-axis

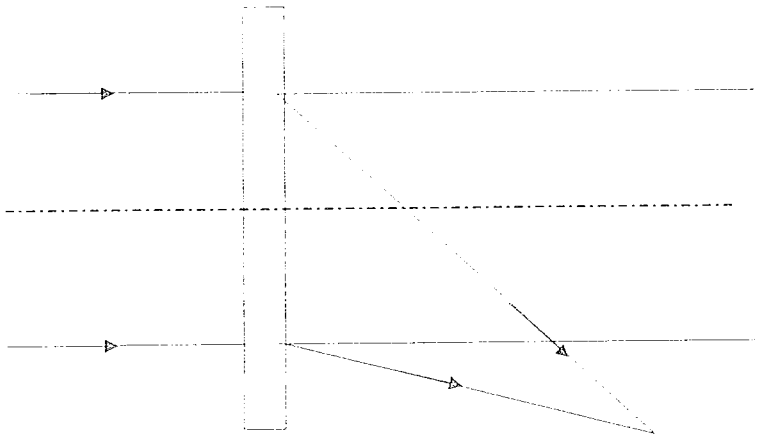

Figure 5.2(c) A DOE that will bring collimated light to a focus off-axis

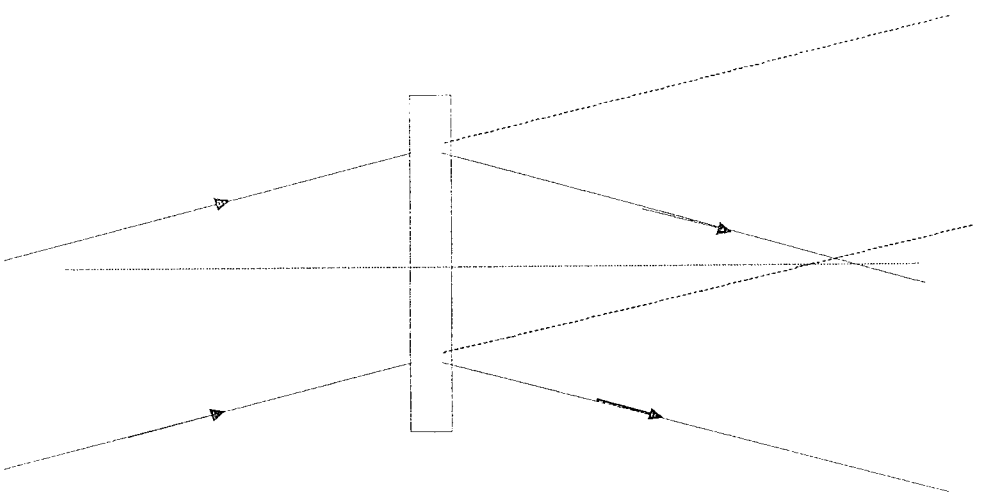

Figure 5.2(d) A simple beam splitter.

5.2 Holographic characteristics of the recording material.

In order for a material to record good quality DOEs with limited laser power, high diffraction efficiencies must be possible with moderate exposure. The spatial resolution range must also be sufficiently broad. Material resolution has already been discussed in detail in chapter 3 but is mentioned again here with relevance to DOE recording limits.

5.2.1 Material resolution

In order to determine the spatial frequency range of the material, the recording angle was varied to record gratings between 300 lines/mm up to 2500 lines/mm.

Referring to the spatial frequency response curve in section 3.7.4 it can be seen that the optimum response is at about 400 lines /mm with the diffraction efficiency dropping to half the maximum value at 350 lines/mm and 1200 lines/mm. The graph indicates that on reconstruction of a typical off-axis transmission hologram the best quality image would be obtained in the angle range between 5.5° (300l/mm) and 42° (1500l/mm) with the reference beam. For short focal length lenses in particular, the upper limit on spatial frequency response limits the effective aperture of a holographically recorded lens.

Taking as an example an on-axis lens which will focus light diverging from a point 5 cm behind the plane of the DOE lens to a point 5 cm in front of it (Figure 5.3), it is clear that the spatial frequency increases from zero as a function of the distance

from the principal axis. The highest spatial frequency recorded will depend on the radius of the illuminated area, and the lowest, in practice will be of the order of one line per millimetre. It follows that in a material whose resolution limit is 2100 lines/mm the largest holographic lens of 5 cm focal length which can be recorded has a radius of 4.5 cm (2100 lines/mm corresponds to a recording angle of 85° between the recording beams). This is more than enough for most applications but it is nonetheless a limitation.

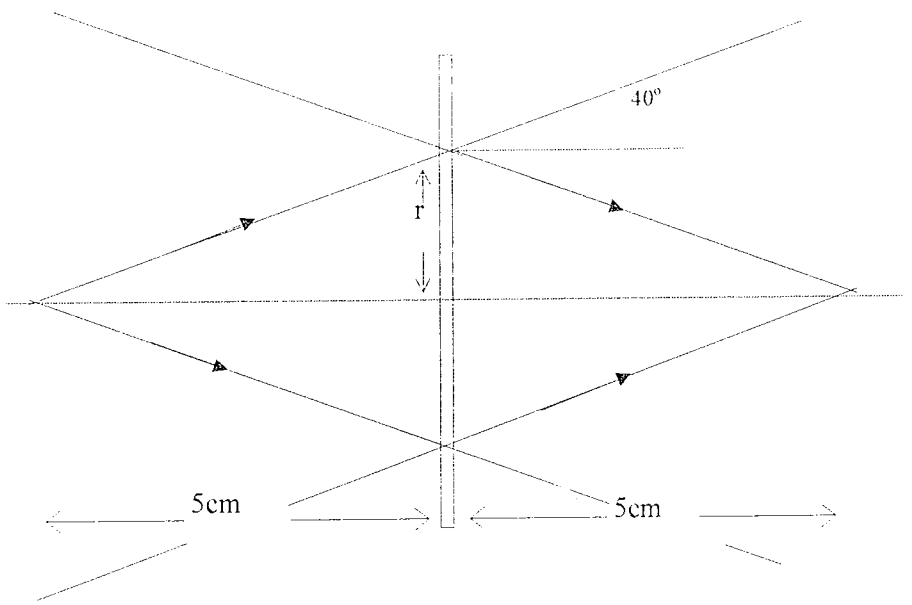

Figure 5.3 Recording a DOE that will bring light diverging from a point 5cm behind it, to a focus 5cm beyond it.

5.2.2 Variation of the grating slant angle.

Slant angle (degrees)	Diffraction efficiency (%) 100 mJ/cm^2 exposure	Diffraction efficiency (%) 120 mJ/cm^2 exposure
0	51	63
10	48	59
20	49	58
30	47	60
40	41	55
50	23	36

Table 5.1 Diffraction efficiencies obtained in gratings recorded at various slant angles. The fringe spacing is 1 μm and the layer thickness is 60μm.

According to coupled wave theory[84] the diffraction efficiency of a lossless grating, illuminated at the Bragg angle should not depend on the slant angle of the fringe planes.

As can be seen from Table 5.1 this photopolymer material can tolerate up to a 40° angle between the grating vector and the plate normal without an appreciable loss of efficiency. (No compensation for the increased reflection losses at high angles of incidence has been included.) This is an important result as some photopolymers perform poorly at high slant angles. The Bragg angle of incidence for maximum diffraction efficiency during reconstruction was the same throughout. This indicates that no shrinkage (or swelling) occurred during recording. This is a particularly important aspect of this material for recording diffractive optical elements as in some materials, the post-processing of recorded DOEs results in the inevitable

distortion of fringe planes. This means that the reconstruction angle has to be adjusted accordingly even if the replay wavelength is the same as that for recording. The nature of a lens dictates that it will always have a varying spatial frequency and slant angle.

5.3 Results

The results are reported below for each of the DOE configurations. Some results are also reported for stacked on-axis lenses.

5.3.1 On-axis lenses

Table 5.2 shows some typical exposure energies and diffraction efficiencies obtained for a set of on-axis DOE lenses. The on-axis lenses depicted in Figure 5.2(b) were recorded in 60 micron thick layers. The best diffraction efficiency recorded was only 17.8%. The fabricated on-axis lenses caused an unacceptable amount of scatter. This is probably due to the surface height modulation which occurs in this material at very low spatial frequencies.[64] This type of surface height modulation can be seen in Figure 5.5, which shows the magnified image of an on-axis lens. The centre of the lens is shown where the surface height modulation is maximum. It is caused by swelling of the layer volume in the polymerised areas and has been observed in similar materials up to spatial frequencies of 45 lines/mm.[9] The amplitude of the surface modulation has been observed to depend linearly on the layer thickness so it follows that the noise due to scatter would be worse in thicker layers. It seems reasonable that when the maximum allowable noise levels for a particular application have been determined, a trade off between scatter levels

and diffraction efficiency will give the maximum achievable diffraction efficiency for on-axis elements. Approximately the same diffraction efficiencies were obtained with type (a) DOEs which focused collimated light to a point 13 cm from the grating.

Exposure time (s)	*Diffraction efficiency (%)*
10	5.2
15	9.8
20	13.7
25	9.5
30	12.7
35	14.4
40	17.8
45	7.6

Table 5.2 Diffraction efficiencies of on-axis DOE (type (b), focal length 5 cm) recorded with increasing exposure times in red sensitive layers approximately 60 microns thick. Total power density was 45-50 mW/cm^2.

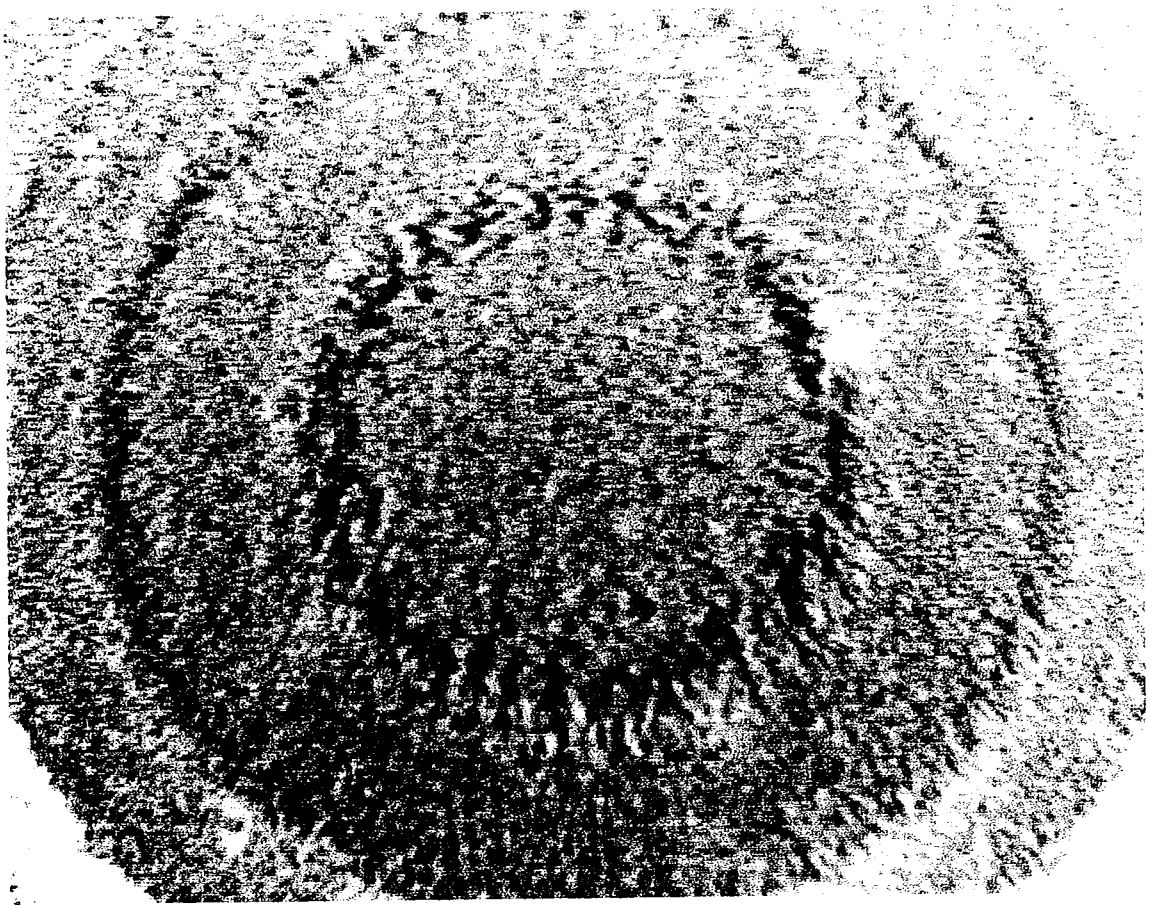

Figure 5.5 The magnified image of the centre of an on-axis lens. The image was taken using the microscope of a Raman spectrometer.

5.3.2 Off-axis lenses

When off-axis lenses were investigated a significant improvement in diffraction efficiency was observed. DOEs were recorded for which up to 97% of the transmitted light (633nm) was diffracted into the focused spot. This corresponded to about 75% of the incident light. The layers were between glass plates for protection from the environment and consequently the reflection losses were large. Losses could be reduced with index matching liquid and coupling prisms. The high diffraction efficiencies obtained above required around 300 mJ/cm^2 exposure.

However a diffraction efficiency of 78% (or 58% of the incident light in the focused spot) was obtained for an exposure of only 100 mJ/cm^2 (10 seconds at 10 mW/cm^2).

The focused beam was off-axis by 20° and the DOE was small in area (6 mm by 6 mm) so the minimum spatial frequency was approximately 550 lines/mm and so surface modulation was not a problem. However taking into consideration the fact that the surface modulation problem disappears at spatial frequencies as low as 45 lines/mm it becomes clear that the holographic lens would only have to be off-axis by approximately 2° to completely avoid this problem.

It may be convenient to use slightly off-axis lenses in order to utilise the high optical quality, high diffraction efficiency and low scatter.

5.3.3 Stacked on-axis DOEs

The possibility of fabricating a high efficiency on-axis DOE from two high efficiency off-axis elements was investigated. This would have the advantage of being less wavelength-sensitive than an ordinary DOE as well as being more desirable for certain applications.

The laser available for recording this DOE was a 633nm Helium Neon of 20mW output power. This power output was significantly lower than that of the laser that is used for normal holographic recording. It was therefore necessary to expose the plates for longer than usual in order to obtain the usual exposure energy. Stability of recording conditions can sometimes be a problem at longer exposure times so it was

necessary to record a series of gratings and DOEs in order to determine the optimum recording conditions.

Figure 5.6 shows the diffraction efficiency dependence on exposure time for layers of standard methylene blue sensitised formulation and 90-100μm layers. The total intensity on the exposed area during recording was 3mW/cm^2. The fringe visibility in the interference pattern would have been approximately 0.98, but this may have varied slightly over the exposed area as the beam splitter used was a variable transmission rotating disc. Under these conditions the best diffraction efficiencies (about 70%) were obtained at about 160 s exposure time (about 500 mJ/cm^2).

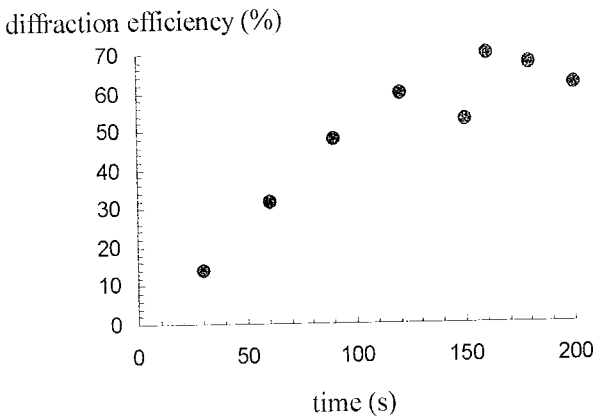

Figure 5.6 Diffraction efficiency as a function of recording time for off-axis (30°) DOEs recorded in methylene blue sensitised layers of approximately 100μm thickness.

Layer 5 which was exposed for 150 seconds must have experienced some vibration during the recording period causing it to have a lower than expected diffraction efficiency.

On-axis elements were successfully produced by combining two off-axis elements of the type shown in Figure 5.7 to make an element which brings a diverging beam to an on-axis focus. Elements of this type recorded on 2" diameter anti reflection coated plates. Diffraction efficiencies were higher than those of on-axis elements recorded in the normal way (20-25%) and these elements are less sensitive to wavelength change as the recording angle has been offset to remove the lower spatial frequencies.

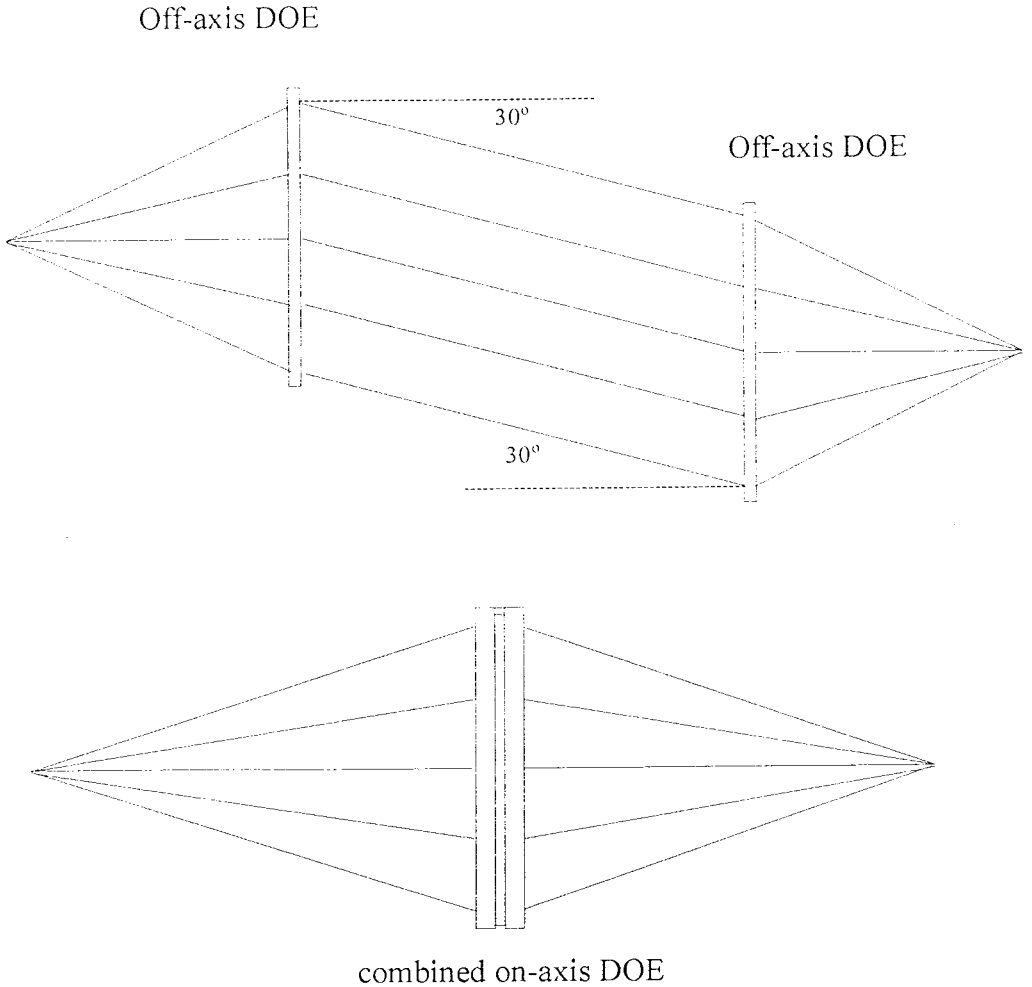

Figure 5.7 Combination of two off-axis DOEs to form an on-axis DOE.

5.3.4 Beam Splitters

Gratings with an inter beam angle of 20° were also recorded with efficiencies up to 95% (400 mJ/cm^2) and these showed negligible drop in diffraction efficiency when illuminated with horizontally polarised light (see Figure 5.8). This demonstrates the ease with which polarisation independent beam splitters of any ratio can be produced with this material.

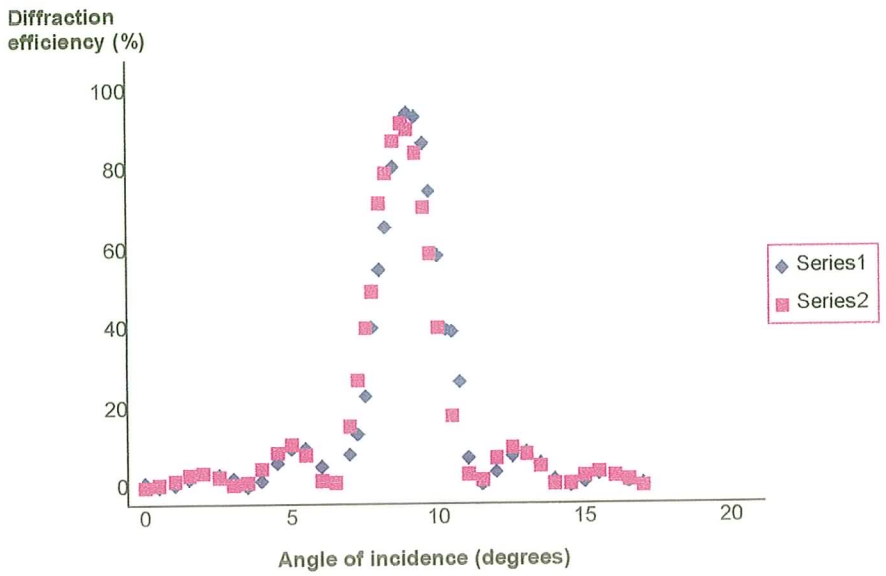

Figure 5.8 Diffraction efficiency as a function of the angle of incidence of the reading beam for a typical grating (approximately 100 microns thick). Series 1 is for a horizontally polarised reading beam, Series 2 is for a vertically polarised reading beam.

5.4 Conclusion

This work shows that it is possible to record good quality, high diffraction efficiency DOEs in this material. Both on and off-axis lenses were recorded, but the efficiencies were much higher for off-axis lenses. With on-axis lenses the main problem was the scatter caused by the surface height modulation produced by the very low spatial frequency components. Near on-axis lenses (offset by a few degrees to remove the problematic lower spatial frequencies) would be expected to give results similar to the off-axis lenses discussed here. Polarisation independent beamsplitters, on-axis lenses of ~15% diffraction efficiency, and off-axis lenses which focus more than 75% of the incident light have also been fabricated.

On-axis elements were successfully produced by combining two high diffraction efficiency off-axis elements. These had higher diffraction efficiencies (~25%) than on-axis elements recorded in the normal way and had the added advantage of reduced sensitivity to wavelength change.

6. Conclusions

The main objective of the research presented was the optimisation and characterisation of a red-sensitive photopolymer holographic recording material, for exposure with low laser power. Some chemical and physical studies of the material were also necessary, in order to improve the understanding of the physical processes that occur in the material both prior to and during exposure.

A review of some photopolymerisable photopolymer materials for holographic recording was presented. The advantages and disadvantages of several materials were discussed. Previous work had highlighted the fact that the green-sensitised version of this material, despite its high diffraction efficiency and self-developing characteristics had limited spatial resolution capabilities. The red-sensitised material studied here was shown to exhibit the same characteristics and in fact had an even lower resolution limit. It was clear that a more complete understanding of the physical and chemical processes that occur in the material during holographic recording were needed before these characteristics could be explained.

The photochemical processes that occur in the material under sensitising illumination were also outlined in order to show the inter-dependence of each of the chemical components. The chemical structure of each of the components was outlined and the chemical characterisation reported. This incorporated the results of a ^{13}carbon and

proton NMR study. This study was conducted to confirm that no chemical interaction occurred between the chemical components prior to exposure under normal circumstances. It was established that this was indeed the case. This is an important result as the extent of polymerisation within light exposed areas during holographic exposure, determines the refractive index modulation, which in turn determines the diffraction efficiency. As each of the three stages of polymerisation are intrinsically linked, if any of the components reacted prior to exposure, this could have an effect on the diffraction efficiency of the final hologram.

The holographic optimisation of the material was then described. It was shown how even small differences in concentrations of, for example, dye had a substantial effect on the final diffraction efficiency. In addition to complete optimisation of the chemical content, some interesting observations were noted. The effect of the electron donor concentration on the permeability of the binder was observed for the first time. It was also noted that the amount of monomer that could be contained in the material without phase separation, varied with different molecular weight binders. This led to the notion that the binder could have had more influence on the material components than was previously thought and to a more complete investigation of its role in the material.

The characterisation of the material was also described in terms of layer thickness, optimum beam intensity and ratio and spatial frequency. The studies undertaken in

characterisation played a vital role in deciding the recording conditions that must be applied for optimum results in practical applications. During the characterisation of the spatial frequency response of the material it was observed that the spatial frequency range of the red-sensitised material differed from that of the green-sensitised version. Since the main difference between each of these materials is the dye, this prompted a study of the possibility of dye diffusion during recording. If this phenomenon could be proven, then it would aid the understanding of the physical processes that occur in the material during recording, which contribute to refractive index modulation.

The dye diffusion study was conducted using a simple mathematical model, which was formulated from a combination of Fick's laws of diffusion and Kogelnik's theory for amplitude holograms. The model is typically used to determine the diffusion coefficient and related characteristics of dyes in various polymers. It was used here, for the first time, in a practical holographic recording material, to investigate the migration of dye molecules through amplitude gratings of various spatial frequencies. Using the model it was proven that diffusion was the underlying mechanism for this migration. The proof that diffusion of dye molecules does occur, was used to help explain the observed difference in spatial frequency response of the two materials.

The difference in spatial frequency response highlighted the fact that a better low spatial frequency response can be obtained with the red-sensitive material but the

limiting spatial frequency was much lower than that of the green-sensitised version. This is thought to be due to the difference in the mobility of each of the dyes. As the methylene blue dye molecules are smaller than the xanthene dye used for green-sensitisation, more rapid diffusion of the molecules would occur. This has two implications: The response of the red-sensitised materials to lower spatial frequencies would be better due to the ability of the dye molecules to diffuse over larger fringe distances, more quickly. However, it would also mean that its response to higher spatial frequencies would result in greater spreading of light exposed areas, due to the higher probability of the presence of dye molecules on the outer regions of the exposed areas. These implications would explain the differences in spatial frequency response of the two materials.

An investigation of the influence of the binder was also conducted. A similar method to that which was used to investigate dye diffusion, was used to determine the diffusion coefficient of the dye through PVA binders of varying molecular weight range. It was proven that the diffusion coefficient of the dye is dependent on the molecular weight of the binder. This is quite a significant result as the binder is usually viewed as an inert medium, in which the photochemical reactions leading to refractive index modulation occur. Although the binder does not contribute significantly in any chemical reactions, it has been shown that its physical properties can influence the physical reactions that occur during holographic recording. If the physical state of the binder affects the diffusion rate of the dye then the diffusion rate

of the monomer must also be affected, as the molecular size of the monomer is significantly smaller than that of the dye. The results of this study imply that the rate of diffusion of the chemical components could be controlled by choosing an appropriate binder molecular weight range.

The successful application of the material to the fabrication of Holographic Optical Elements (HOEs) was also reported. The material presented here has many advantages for the production of (HOEs). No post-exposure processing is required. The high angular selectivity of the material has been demonstrated, which is an important factor as the HOEs described incorporate many spatial frequencies. Stacked elements have also been produced which overcomes some of the problems associated with lower spatial frequencies.

In summary, the successful optimisation and development of the red-sensitised material has been described. It has been shown that the material is capable of high diffraction efficiency with relatively low exposure energy. Some of the physical processes that occur during holographic recording were also investigated. The diffusion of dye molecules and the dependence of the rate of diffusion on the molecular weight of the binder have been proven. This has lead to further ideas on how to improve the spatial frequency response of the material. Although its spatial frequency response is somewhat limited, the material has been used for the fabrication of HOEs demonstrating its usefulness as a practical holographic recording medium.

Further work, arising from the conclusions drawn in this thesis, is being carried out at present. These studies are being conducted by using the holographic grating relaxation technique. The role of the binder is being investigated further by determining the diffusion coefficients of thiazine dye molecules (with varying molecular structure) through various narrow molecular weight fractions of poly(vinylalcohol). The study will be extended to conduct a similar investigation of the green-sensitised material, for comparison.

It is hoped that these studies will further improve the overall understanding of the material, particularly the role of the binder, to the extent that an appropriate molecular weight range may be chosen for specific applications of the material. Through a combination of the dye and binder studies, it is also hoped that the spatial frequency range of the material may be further increased, to extend even further the practical capabilities of the material.

References

1. D. Gabor, "A new microscopic principle", *Nature,* **161,** 777-778, 1948.
2. T. Maimann, "Stimulated optical radiation in ruby ", *Nature,* **187** 493-494, 1960.
3. E. N. Leith, J. Upatneiks, "Reconstructed wavefronts and communication theory", *J. Opt. Soc. Am.* **52,** 1123, 1962.
4. E. N. Leith, J. Upatneiks, "Wavefront reconstruction with continuous tone objects", *J. Opt. Soc. Am.* **53,** 1377, 1963.
5. E. N. Leith, J. Upatneiks, "Wavefront reconstruction with diffused illumination and three-dimensional objects", *J. Opt. Soc. Am.* **54,** 1295, 1964.
6. R. K. Erf, "Holographic non-destructive testing", Academic Press, New York, 1974.
7. R. Jones, C. Wykes, "Holographic and speckle interferometry", 2nd edition, Cambridge Univ. Press, 1889.
8. J. Zhang, C. H Wang, "Application of the laser induced holographic grating relaxation technique to the study of physical aging of an amorphous polymer", *Macromolecules,* **20**, 683-685, 1987.
9. S. H. Lee, "Optical Information Processing", Springer-Verlag, Berlin, 1981.
10. H.J. Zhou, V. Morozov and J. Neff. "Characterization of Dupont photopolymers in infrared light for free-space optical interconnects", Technical note, *Applied Optics*, **34,** 7458, 1995.
11. Y, B. Boiko, V. S. Solovjev, S. Calixto & D. J. Lougnot "Dry photopolymer films for computer-generated infrared radiation focusing elements", *Applied Optics*, **33**, 787-793, 1994.
12. D. W. Swift, "Application of HOEs to head-up displays", Int. Conference on Holographic Systems and Components, 1987.
13. R. J. Collier, C. B. Burckhardt, L. H. Lin, "Optical Holography", Academic Press, New York, 1971.
14. D. Meyerhofer, "Dichromated gelatin in holographic recording materials", *Topics in Applied Optics*, **20**, Springer-Verlag, 209-227, 1977.
15. P. Hariharan, "Optical holography-Principle techniques and Applications", Cambridge Press, 1984.
16. R. T. Ingwall & T. Adams "Hologram: liquid crystal composites", *Computer and Optically Generated Holographic Optics*, **155**, 279-290, 1991.
17. S. Calixto, "Holographic recording and reconstruction of polarized light with dyed plastic", *Applied Optics*, **23,** 4313-4318, 1984.
18. J. M. Moran & I. P. Kaminow "Properties of holographic gratings photoinduced in polymethyl methacylate", *Applied Optics*, **12**, 1964-1970, 1973.

19. Bloom, R. A. Bartolini, P. L. K. Hung & D. L. Ross "Nonpolymeric organic host for recording volume phase holograms", *Applied Physics Letters* , **29**, 483-484, 1976.
20. P.Leclere, Y. Renotte, Y. Lion, "Characterization of DC-PVA films for holographic recording materials", *SPIE, 1507,* Holographic Optics III: Principles and Applications, 339-344, 1991.
21. M. Irie "Advances in photochromatic materials for optical data storage media", *Japanese Journal of Applied Physics*, **28**, 215-219, 1989.
22. K. Matsumoto, T. Kuwayama, M. Matsumoto & N. Taniguchi "Holographic optical elements using polyvinyl carbazole holographic material", *Progress in Holographic Applications*, **600**, 9-13, 1985.
23. Z. Chen, A. Lewis, H. Takei & I. Nebenzahl "Bacteriorhodopsin oriented in polyvinyl alcohol films as an erasable optical storage medium", *Applied Optics*, **30**, 5188-5196, 1991.
24. G. Oster & A. H. Adleman "Long-lived states in photochemical reactions", *Analytical Chemistry*, **25**, 913-916, 1953.
25. G. K. Oster & G. Oster "Photochemical modifications of high polymers by visible light", *Journal of Polymer Science*, **48**, 321-327, 1960.
26. G. Oster & N. L. Yang "Photopolymerization of vinyl monomers", *Chemical Reviews*, **68**, 125-151, 1968.
27. J. D. Margerum, L. J. Miller & J. B. Rust "Photopolymerization studies: II Imaging and optical fixing", *Photographic Science and Engineering*, **12**, 177-184, 1968.
28. D. H. Close, A. D. Jacobson, J. D. Margerum, R. G. Brault & F. J. McClung "Hologram recording on photopolymer materials", *Applied Physics Letters*, **14**, 159-160, 1969.
29. J. A. Jenney "Holographic recording with photopolymers", *Journal of the Optical Society of America*, **60**, 1151-1161, 1970.
30. R. L. Van Renesse, "Photopolymers in holography", *Opt. Laser Tech.*, **4,** p72, 1972.
31. K. Sukegawa, S. Sugawara, K. Murase, "Holographic recording by Fe^{3-}-sensitized photopolymerization", *Electronics and Communications in Japan,* **58-C (11),** 132-138,1975.
32. D. J. Lougnot & C. Turck "Photopolymers for holographic recording: II. Self-developing materials for real-time interferometry" *Pure and Applied Optics*, **1**, 251-268, 1992.
33. D. J. Lougnot & C. Turck "Photopolymers for holographic recording: III. Self-developing materials for real-time interferometry" *Pure and Applied Optics*, **1**, 269-279, 1992.
34. D. J. Lougnot, N. Noiret & C. N. Turck "Photopolymers for holographic recording: IV. New self-processing formulations based on β-hydroxy ethyloxazolidone acrylate", *Pure and Applied Physics*, **2**, 383-392, 1993.

35. Belendez, I. Pascual & A. Fimia "Optimization of reconstruction geometry for maximum diffraction efficiency in HOE: the influence of recording material", *International colloquium on diffractive optical elements*, **1574,** 77-83, 1991

36. A. Fimia, L. Carretero, A. Belendez "Holographic elements recorded on spherical surfaces with photopolymers", *Applied Optics*, **33,** 3633-3634, 1994.

37. C. A. Feely, S. Martin, V. Toal, A. Fimia, F. Mateos "The optimisation of a red sensitive photopolymer holographic recording material", *SPIE proceedings* 1995.

38. A. Fimia, N. Lopez, F. Mateos, R. Sastre, J. Pineda, F. Amat-Guerri, "Elimination of oxygen inhibition in photopolymer systems used a holographic recording materials", *Journal of Modern Optics,* **40,** 699-706, 1993.

39. M. J. Jeudy, J. J. Robbillard, "Spectral sensitization of a variable index material for recording phase holograms with high efficiency", *Opt. Comm.,* **13**, 25, 1975.

40. N. Sadlej, B. Smolinska, "Stable photosensitive polymer layers for holography", *Optics and Laser Technology,* 7, 175, 1975.

41. S. Calixto "Dry photopolymer for holographic recording", *Applied Optics*, **14,** 593, 1987.

42. E. F. Haugh, "Hologram recording in photpolymerizable layers", **U.S. Patent 3658526**, 1972 assigned to E. I. Du Pont de Nemours and Co.

43. J. D. Margerum, A. D. Jacobson, "Method of hologram recording", **U.S. Patent 3694218**, 1972, assigned to Hughes Aircraft Company

44. J. J. A. Robillard, "Process for recording phase holograms using energy activated sensitizer", **U.S. Patent 3989530**, 1976.

45. E. A. Chandross, W. J. Tomlinson, H. P. Weber, "Photopolymerization process and related devices", **U.S. Patent 3993485**, 1976, assigned to Bell Telephone Laboratories.

46. A. Bloom, R. A. Bartolini, "Organic volume phase holographic recording", **U.S. Patent 4049459,** 1977, assigned to RCA corporation.

47. T. Tanaka, K. Nishide, "Hologram and method of production using two solvent treatments, **U.S. Patent 4173474**, 1979, assigned to Canon Kabushiki Kaisha.

48. M. Matsumoto, K. Nishide, "Hologram and method thereof with photo-crosslinkable polymers", **U.S. Patent 4258111,** 1981, assigned to Canon Kabushiki Kaisha.

49. M. Matsumoto, K. Nishide, "Hologram recording material", **U.S. Patent 4287277, 1981**, assigned to Canon Kabushiki Kaisha.

50. H. L. Fielding, R. T. Ingwall, "Stabilization of holograms", **U.S. Patent 4535041,** 1985, assigned to Polaroid Corporation.

51. H. L. Fielding, R. T. Ingwall, "Photopolymerizable compositions used in holograms", **U.S. Patent 4588664,** 1986 assigned to Polaroid Corporation

52. J. J. Cael, "Photopolymerizable composition", **U.S. Patent 4696876**, 1987, assigned to Polaroid Corporation.
53. W. S. Colburn, K. A. Haines, "Volume hologram formation in photopolymer materials", *Applied Optics*, **10**, 1636-1641, 1971.
54. R.H Wopshall, T.R Pampalone, "Dry photopolymer film for recording holograms", *Applied Optics*, **11**, 2096-2097, 1972.
55. B. L. Booth "Photopolymer material for holography", *Applied Optics*, **14**, 593-601, 1975.
56. W. K. Smothers, T. J Trout, A. W. Weber, D. J. Mickish, "Photopolymers for holography", *Practical Holography IV*, SPIE **1212** 20-29, 1990.
57. W. J. Gambogi, A. M. Weber, T. J. Trout, "Advances and applications of DuPont holographic photopolymers", Holographic Imaging and Materials, Proc. SPIE **2043**, 2-13, 1993.
58. B. M. Monroe, W. K. Smothers, D. E. Keys, R. R. Krebs, D. J. Mickish, A. F. Harrington, S. R. Schicker, M. K. Armstrong, D. M. T. Chan & C. I. Weathers "Improved photopolymers for holographic recording I" *IS&T*, 35, 19-25, 1991.
59. B. M. Monroe, "Improved photopolymers for holographic recording II" *IS&T*, **35**, 25-29, 1991.
60. R. T. Ingwall, M. Troll & W. T. Vetterling "Properties of reflection holograms recorded in Polaroid's DMP-128 photopolymer", *Practical Holography II*, **747**, 67-73 1987.
61. R. T. Ingwall & M. Troll "The mechanism of hologram formation in DMP-128 photopolymer", *Holographic Optics: Design and Applications*, **883**, 94-101, 1989.
62. D. H. Whitney & R. T. Ingwall "The fabrication and properties of composite holograms recorded in DMP-128 photopolymer", *Photopolymer Device Physics, Chemistry, and Applications*, **1213**, 18-26, 1990.
63. R. T. Ingwall & H. L. Fielding "Hologram recording with a new Polaroid photopolymer system", *Applications in Holography*, **523**, 306-312, 1985.
64. S. Martin, " *A new photopolymer recording material for holographic applications: photochemical and holographic studies towards an optimized system", Doctoral thesis*, 1996.
65. S. Martin, P. G. Leclere, Y.M Renotte, V. Toal, Y. F. Lion Characterization of an acrylamide-based dry photopolymer holographic recording material", *Optical Engineering*, **22**, 3942-3946, 1994.
66. S. Martin, C. A. Feely, V. Toal, "'Holographic Characteristics of an Acrylamide Based Recording Material", *Applied Optics*, **36**, 5757-5769, 1997.
67. C. Carre & D. J. Lougnot "A photochemical study of the methylene blue/acrylamide system in view of its use for holographic recording under red illumination", *Journal de chimie physique*, **85**, 485-490, 1988.
68. J. B. Birks, "Organic Molecular Photophysics", 2, 153-154, John Wiley and son, N.Y., 1975.

69. A. Zakrzewski and D. C. Neckers "Bleaching products of rose Bengal under reducing conditions", *Tetrahedron*, **43**, 4507-4512, 1987.

70. G. K. Oster and G. Oster, "Photochemical modifications of high polymers by visible light", *Journal of Polymer Science*, **48**, 322, 1960.

71. "Encyclopedia of Polymer Science and Engineering", vol 2, John Wiley and son, N.Y. 1989.

72. H. Tobita & A. E. Hamielec "Crosslinking kinetics in polyacrylamide networks", *Polymer*, **31**, 1546-1552, 1990.

73. C. Brauchle & D. M. Burland "Holographic methods for the investigation of photochemical and photophysical properties of molecules", *Angewandte Chemie: International Edition*, **22**, 582-598, 1983.

74. W. Kemp, "Organic Spectroscopy", 2nd edition, MacMillan, 1986.

75. D.A. Long, "*Raman Spectroscopy*", Mc Graw Hill International Book Co. G. Britain 1977.

76. D. Canet, "NMR: Concepts and methods", J. Wiley and sons, U.K. 1996

77. J. Dean, "Analytical Chemistry Handbook", McGraw and Hill inc. USA, 1995.

78. A. Reiser "Photoreactive polymers: The Science and technology of resists", chapter 4, 135, Wiley Interscience, 1989.

79. F. Bovey, F.H. Winslow, "Macromolecules: An introduction to polymer science", chapter 1, Academic Press, N.Y. 1979.

80. N. G. McCrum, C. P. Buckley, C.B. Bucknall, "Principles of polymer engineering", Oxford University Press, 1988.

81. F. Bovey, F.H. Winslow, "Macromolecules: An introduction to polymer science", chapter 7, Academic Press, N.Y. 1979.

82. G. Oster, N. Wotherspoon, *J. Am. Chem. Soc.* **79**, 4836, 1957.

83. "Encyclopedia of Polymer Science and Engineering", vol 1, John Wiley and son, N.Y. 1989.

84. H. Kogelnik, "Coupled wave theory for thick hologram gratings", *Bell Systems Journal*, **48** 2909-2947, 1969.

85. C. A. Feely, *"A study of a red-sensitive photopolymer holographic recording material", Final year project, DIT, 1994.*

86. H.M. Smith, "Principles of Holography", chapter 2, Wiley-Interscience, N.Y. 1969.

87. L. Solymar, D. J. Cooke, "Volume recordings and volume gratings", Academic Press, New York, 1981.

88. W. R. Klein, "Theoretical efficiency of Bragg devices", *Proc. IEEE*, **54**, 803, 1966.

89. J. O Martins, *"Holographically recorded gratings characterised by Bragg angle analysis", Erasmus project, DIT, 1997.*

90. J. Wilson, J.B. Hawkes, "Optoelectronics", Hemel Hempstead: Prentice Hall, 3rd edition, 1997.

91. G. Manivannan, G. Mailhot, M. Bolte & R. A. Lessard "Xanthene dye sensitized dichromated poly(vinyl alcohol) recording materials: Holographic characterization and ESR spectroscopic study", *Pure and Applied Optics*, **3**, 845-857, 1994.

92. M. J. Bowden, E. A. Chandross & I. P. Kaminow "Mechanism of the photo induced refractive index increase in polymethyl methacrylate", *Applied Optics*, **13**, 112-117, 1974.

93. G. Zhao & P. Mouroulis "Diffusion model of hologram formation in dry photopolymer materials", *Journal of Modern Optics*, **41**, 1929-1939, 1994.

94. V. V. Obukhovskii & T. N. Smirnova "Model of holographic recording on photopolymerizing composites", *Opt. Spektrosk*, **74**, 778-785, 1992.

95. J. Zhang , B. K. Yu & C. H. Wang " Holographic grating relaxation studies of Camphorquinone diffusion in Polystyrene host", *J. Phys. Chem*, **90**, 1299-1301, 1986.

96. J. Zhang, D. Ehlich & C. H. Wang "Investigation of the mass diffusion of Camphorquinone in Amorphous Poly(methyl methacrylate) and Poly (tert - butyl methacrylate) hosts using the holographic grating relaxation technique", *Macromolecules*, **19**,1390-1394, 1986.

97. C. H. Wang , J. L. Xia & L. Yu "Dye diffusion in polycarbonate in the presence of additives" , *Macromolecules* , **24**, 3638-3644, 1991.

98. P. W. Atkins, "Physical Chemistry", 4th edition , Oxford University Press, Great Britain, 1992.

99. R. J. Collier, C. B. Burckhardt, L. H. Lin, "Optical Holography", chapter 9, Academic Press, New York, 1971.

100. J. M. Spencer, "Engineering Mathematics", Van Nostrand Reinhold Co. Britain, 1981.

101. S. Gradshteyn, I. M. Ryzhik, "Table of integrals, series and products", Academic Press, California, 1980.

102. W. J. Tomlinson & E. A. Chandross "Organic photochemical refractive-index image recording systems", *Advanced Photochemistry*, **12**, 201-280, 1980.

103. F. Coyle, J French, *"Technical report: Molecular weight determination of polyvinylalcohols", Polymer Development Centre 1998.*

104. G. Manivannan, R. A. Lessard "Trends in holographic recording materials" *Trends in polymer science* , **2**, No. 8, 282-290, 1994

Appendix

Molar refraction theory

For an isotropic material the refractive index may be expressed by the Lorentz-Lorenz relation as

$$\frac{n^2-1}{n^2+2}=\frac{4}{3}\pi P$$

where P is the optical polarisability per unit volume. For a pure substance total polarisability is equal to the polarisability per molecule, p, times the number density of the molecules so

$$\frac{n^2-1}{n^2+2}=\frac{4\pi\rho Np}{3M}=\frac{\rho R}{M}$$

where M is the molecular weight, ρ is the density, N is Avagadro's number and R is the molar refraction.

The molar refraction of a material is independent of temperature or the physical state of the material. The sum of the contribution of the molar refractions in a substance contributes to that substance's refractive index. It is dependent only on the wavelength of the light travelling through the material. For the following analysis the light is considered monochromatic.

For an ideal mixture

$$\frac{n^2-1}{n^2+2}=\sum_i\frac{\rho_i R_i}{M_i}$$

ρ_i being the density of the ith component in the mixture, whilst R_i and M_i are its molar refraction and molecular weight respectively.

To alter the refractive index of a material, the above three parameters must be somehow altered within a material. There are three basic ways in which this can occur.

1. A change in molecular structure of one or more of the components of a material will result in a change in overall molar refraction. Molar refraction is based on the type and number of the different bonds within a material. Removal or addition of material is not necessary in order to cause this change.
2. The density of a material may be altered without changing its basic chemical composition. This also requires no removal or addition of material.
3. The relative concentrations of each component within a material may be altered, leaving the overall density of the material unchanged. This requires both the addition and removal of material.

In the formulation of the material used to record the gratings described in this chapter, only two of the usual four active components are present. Both of these components, dye and electron donor (TEA) undergo a chemical change. Dye is bleached by the provision of hydrogen atoms from TEA molecules. The theory described above is

used to calculate any contribution from TEA molecules towards a refractive index modulation in the material used in its typical formulation i.e. to record phase holograms. The TEA content in the formulation used to record absorption grating is reduced by at least a factor of ten so if the contribution of refractive index is negligible for the case calculated here then this will hold for the case of the amplitude grating. The calculation will be based upon established values of bond refraction.

In order to calculate the total molar refraction of TEA before and after a holographic grating is recorded, the number and type of bonds contained in one molecule of TEA must be known. How those bonds react during recording must also be known. In Chapter 2, the reaction a TEA molecule undergoes during a typical recording has been illustrated. Table 1 shows the relevant bonds and their respective bond refraction values, contained in a TEA molecule, either before or after recording.

Bond	**Refraction value**
C-O	1.51
O-H	1.73
C-H	1.69
C-C	1.25
C-N	1.54
C=0	3.38

Table 1 Calculated bond refraction values.

During the TEA/dye reaction, one C-H bond and one C-OH bond are replaced by one C=O bond. Using the above values, the total bond refraction before and after a reaction has taken place was calculated to be 38.37 and 36.82 respectively.

The density of TEA present in a layer (substrate dimensions 5 x 4 inches) 140μm thick is 9.7×10^{-5} g/cc. The molecular weight of TEA before and after recording is 149g and 147g respectively.

Using the ideal mixture equation above it is possible to rearrange it in order to deal specifically with the TEA molecules before and after they react with the dye.

$$\Delta n\,(TEA) = \left(\frac{n^2-1}{n^2+2}\right)_{before} - \left(\frac{n^2-1}{n^2+2}\right)_{after} = \left(\frac{\rho_{TEA} R_{TEA}}{M_{TEA}}\right)_{before} - \left(\frac{\rho_{TEA} R_{TEA}}{M_{TEA}}\right)_{after}$$

when the sum of the contributions of the other components remain constant.

Substituting the values calculated above for the density, molar refraction and mass of the TEA both before and after recording, a value of 6.83×10^{-7} is obtained. In the case of the recording of transient gratings the amount of TEA used is reduced even further by a factor of 10 so it may concluded that negligible refractive index of the material occurs due to TEA.